INTERNATIONAL ATOMIC ENERGY AGENCY
UNITED NATIONS EDUCATIONAL, SCIENTIFIC AND CULTURAL ORGANIZATION
INTERNATIONAL CENTRE FOR THEORETICAL PHYSICS
I.C.T.P., P.O. BOX 586, 34100 TRIESTE, ITALY. CABLE: CENTRATOM TRIESTE

SMR.380/8

COLLEGE ON THEORETICAL AND EXPERIMENTAL RADIOPROPAGATION SCIENCE

6 - 24 February 1989

LOW LATITUDE IONOSPHERIC PHENOMENA

J.O. OYINLOYE

University of Horin, Dept. of Physics, Horin, Nigeria

TABLE OF CONTENT

1. INTRODUCTION

1.1. The low latitude region

The low latitude D and E-regions have strong geographic control while the F region has strong electromagnetic controls. It is therefore not unusual to describe low latitude ionospheric phenomena in terms of both geographic and magnetic latitudes (or geogmagnetic latitudes). The latter are more commonly used than the former because most distinguishing features of the low latitude ionospheric phenomena such as the equatorial anomaly equatorial sporadic E, spread F and F-region irregularities etc. (see sections 2.3, 3.1 and 3.2), are influenced by electric field per se or/and electromagnetic forces. Figure 1 illustrates the relative positions of the geographic, magnetic dip and geomagnetic dip equators. The magnetic dip equator refers to the earth's real magnetic field while the geomagnetic dip equator refers to the dipole representation of the earth's magnetic field. The magnetic dip I is related to the magnetic latitude by the equation:

$$\tan I = \frac{Z}{H} = 2 \tan \Phi \qquad (1)$$

where Z and H are the vertical and horizontal components of the real field. Equation (1) is also valid for the geomagnetic dip angle, the geomagnetic latitude Φ' and the corresponding dipole field vertical and horizontal components. The latitude Φ' and the geomagnetic longitude Λ' are given in terms of geographic latitude ϕ and longitude λ (by Davies, 1965) as :

$$\sin \Phi' = \sin\phi \sin\phi_0 + \cos\phi \cos\phi_0 \cos(\lambda - \lambda_0) \qquad (2)$$

$$\sin \Lambda' = \frac{\cos\phi \sin(\lambda - \lambda_0)}{\cos \Phi'} \qquad (3)$$

where ϕ_0 and λ_0 are the geographic latitude and longitude of the north dipole pole ($\phi_0 = 78.3^\circ N$, $\lambda_0 = 291.0^\circ E$). It is seen from Fig. 1 that the three equators do not coincide, neither do their corresponding latitudes (as illustrated in Fig. 2 for magnetic and geographic latitudes). It is considered pragmatic in the course of these lectures to regard the low latitude ionospheric region as that

lying within about magnetic dip I = ± 35° (see Fig. 2) as practically all the distinguishing features of the low latitude ionosphere are found within this region. It should nonetheless be emphasized that these boundaries are not sharp and may depend on solar activity, season and longitude. Table 1 gives an indication of various low latitude ionospheric stations, lying within dip I = ± 35°. A knowledge of the low latitude earth's magnetic field, the equatorial electrojet and the associated electric field is basic to the understanding of the low latitude ionosphere and these topics are discussed briefly below.

1.2. The earth's magnetic field

The total magnetic intensity F of the earth's magnetic field is given by:

$$F^2 = Z^2 + H^2 \qquad \ldots \quad \ldots \quad \ldots \quad (4)$$

The vertical component Z is positive downwards and the horizontal component H is further specified by the northward component X, eastward component Y and the angle of declination D between H and the geographic north. As such,

$$H^2 = X^2 + Y^2 \qquad \ldots \quad \ldots \quad \ldots \quad (5)$$

$$\tan D = Y/X \qquad \ldots \quad \ldots \quad \ldots \quad (6)$$

Figure 3 shows the world map of F in Gauss. In terms of the magnetic flux density B, 10^4G = 1 Wm^{-2}. It is seen that the magnitude of F on the magnetic dip equator is about half that at the poles; the equatorial value of F also increases from about 0.29G over Peru to about 0.39G over India with an intermediate value of about 0.32G over Nigeria. The rate of change of magnetic dip angle with latitude also varies from about 1.9 over Peru to 2.5 over India (Gupta, 1973) with an intermediate value of 2.4 over Nigeria (Onwumechilli, 1967). These may cause longitudinal differences in some ionospheric phenomena. The total field F at low latitudes is mainly horizontal and approximately northward. It should be noted that F decreases as the cube of the distance from the earth's centre.

Magnetic field variations are known to be superimposed on the main field. These variations are ascribed in part to internal origin arising from current induced in the earth and principally to external origin arising from currents flowing in the ionosphere, particularly in the E region.

1.3. Equatorial electrojet

The equatorial electrojet is an intense current flowing in the E region of the equatorial ionosphere in a narrow latitudinal belt, centred about the magnetic equator. It is regarded as part of the worldwide ionospheric E-region current known as the Sq (quiet daily variation) current system. Ionospheric currents have been explained by the atmospheric dynamo theory. According to this theory, electrons and ions driven by neutral wind across the earth's magnetic field, constitute a moving conductor, which in the presence of the earth's magnetic main field, generates an induced e.m.f. The current set up passes through a narrow belt centred about the magnetic equator where conductivity is very high thereby giving rise to a belt of enhanced current flow known as the equatorial electrojet. The horizontal current is contained within an ionospheric sheet. As current flow perpendicular to the boundaries is inhibited, polarisation charges appear on the boundaries such that the current divergence relation (div $\underline{j} = 0$) is satisfied where $\underline{j}$ is the current density. The polarisation charges modify existing conductivity and electric field and the resulting horizontal current density $\underline{j} = \hat{\sigma}\underline{E}$, where $\hat{\sigma}$ is a conductivity tensor given by:

$$\hat{\sigma} = \begin{pmatrix} \sigma_{xx} & \sigma_{xy} \\ -\sigma_{xy} & \sigma_{yy} \end{pmatrix} \qquad (7)$$

so that:

$$j_x = \sigma_{xx} E_x + \sigma_{xy} E_y$$

$$j_y = -\sigma_{xy} E_x + \sigma_{yy} E_y \qquad (8)$$

In equations (7) and (8), z is in the vertical upward direction, the earth's magnetic main field is in xy plane making angle I with ox (i.e. x is southward positive and y is eastward positive).

$$\sigma_{xx} = \frac{\sigma_0 \sigma_1}{\sigma_0 \sin^2 I + \sigma_1 \cos^2 I} \qquad (9)$$

$$\sigma_{yy} = \sigma_1 - \frac{\sigma_2^2 \cos^2 I}{\sigma_2 \sin^2 I + \sigma_1 \cos^2 I} \qquad (10)$$

$$\sigma_{xy} = \frac{\sigma_o \sigma_2 \sin I}{\sigma_o \sin^2 I + \sigma_1 \cos^2 I} \qquad (11)$$

where σ_o is the component of the conductivity parallel to the magnetic field $\underline{B}$ and is known as the direct or longitudinal conductivity, σ_1 is the component parallel to the electric field $\underline{E}$ but perpendicular to $\underline{B}$ and it is known as the transverse or Pedersen conductivity while σ_2 is the component perpendicular to both $\underline{E}$ and $\underline{B}$ and is known as the Hall conductivity. The expression for σ_o, σ_1, σ_2 are given in the appendix. At the magnetic equator $\sigma_{xx} = \sigma_o$, $\sigma_{xy} = 0$ and $\sigma_{yy} = \sigma_1 + \frac{\sigma_2^2}{\sigma_1} = \sigma_3$ and σ_3 is known as the Cowling conductivity. Figure 4a shows model σ_o, σ_1, σ_2 and σ_3 as a function of height for the equatorial situation, based on the vertical profiles of positive ion composition shown as Fig. 4b. The expressions for the various types of collision frequencies are also given in the appendix. It is seen from Fig. 4a that σ_o is much greater than either σ_2 or σ_1, and that σ_3 is confined to a limited height range with its peak value at about 100km; also σ_3 is greater than σ_2 or σ_1 near 100km. The enhancement of σ_3 is what gives rise to the enhanced current density associated with the equatorial electrojet. Figure 5 compares measured current density with measured electron density and computed σ_3. The vertical profiles of σ_3 and the current density j are similar in shape though the peak of j occurs at a higher altitude.
In the region of interest, $w_e \gg \nu_e$, $\nu_i \gg w_i$, $\sigma_3 \approx \frac{\sigma_2^2}{\sigma_1} \approx \frac{m_i \nu_i}{B^2} N_e$.

where w_e, w_i are electron and ion gyrofrequencies respectively, ν_e, ν_i, electron and ion collision frequencies, m_i ionic mass and N_e, electron density. This suggests that current density in the electrojet will be stronger where the main magnetic field B is weaker. Theory further predicts a half width of about 3^o in latitude (Baker and Martyn 1953).

Experimentally, the main characteristics of the equatorial electrojet have been deduced from the magnetic field changes it produces on the ground (Fig. 6) or as detectedb by rocket borne magnetometers. The experimental results obtained have largely confirmed basic theoretical predictions. The equatorial electrojet occupies a height range of about 90–130km (Singer et al., 1951; Onwumechilli, 1959 a,b), a latitudinal belt of about 600km (Egedal, 1947, 1948; Davis et al. 1967), and has a peak current density of the order of 10^{-5} Am^{-2} (Davis et al., 1967). These features are illustrated in Fig. 7. An asymmetry about the dip equator is also exhibited in Fig. 7. The electrojet intensity and width vary with longitude, being strongest and widest over Peru where B is lowest and weakest and narrowest over India where B is highest (Rastogi, 1962; Gupta, 1973). The longitude variation in the width may also be due partially to the longitude variation in the rate of change of I with latitude. There is a high day-to-day variability in the electrojet intensity (Ogbuehi and Onwumechilli, 1964; Hutton, 1967; Kane, 1974), and also in the width of the belt (Ogbuechi and Onwumechilli, 1964; Davis et al., 1967; Burrows, 1970), while the current axis itself may undergo seasonal movements (Price and Wilkins, 1951; Onwumechilli, 1959a and b;). The intensity has equinoctial peaks on the average.

The equatorial electrojet normally flows eastward during the daytime but on some occasions it reverses its direction and flows westwards; the reversal has been called the counter electrojet phenomenon (Gouin and Mayaud, 1967) Counter electrojet often occurs during early morning and (or) the afternoon (Hutton and Oyinloye, 1970; Fambitakoye et al. 1973) and it has been reported that on the yearly average, the occurrence is about 6% in the morning (6–8hr.), 14% in the afternoon (14–18hr.) and about 1 per year at noon (Rastogi, 1974). There is a tendency for a higher occurrence during low than during high solar activity (Hutton and Oyinloye, 1970). The counter electrojet phenomenon has not been satisfactorily explained.

In contrast to the daytime electrojet, only a very small ionospheric current, opposite in direction to the eastward daytime current has been detected at night (Davis et al., 1967). Meridional currents flowing between 100 and 200km at about 380km from the electrojet axis have been reported also. (Musmann and Seiler, 1978).

1.4. Electric fields

The total electric field $\underline{E}$ is made up of two components, the polarization field $\underline{G}$ and the dynamo induced field $\underline{u} \times \underline{B}$ such that:

$$E = G + U \times B \qquad (12)$$

Near the magnetic equator, the contribution of the induced field to the total E-region horizontal field is negligible as both $\underline{U}$ and $\underline{B}$ are nearly horizontal. The horizontal electric field E_y associated with the equatorial electrojet is therefore primarily the polarization field; at the magnetic equator $E_y = j_y / \sigma_{yy}$ where complete inhibition of vertical current flow is assumed. Horizontal electric field in the electrojet region has been deduced from the extensive measurement of the horizontal velocity of a certain type of electron irregularities known as the type II irregularities which are also associated with equatorial sporadic E traces on vertical incidence ionograms. The irregularities are embedded in the electrojet and their velocity V_e is approximately proportional to the electric field E_y. From the analysis of radar echoes returned from the irregularities at Jicarmaca the relation $E_y = -6 \times 10^{-6}$ Ve (volts per metre) was found (Balsley and Woodman, 1971). The composite velocities (and hence electric field) for the period 1967 - 1970 is shown as Fig. 8 (Balsley and Woodman, 1971; Balsley, 1973). The velocity (electric field) is westward (eastward) during the daytime and eastward (westward) during the nighttime; the morning reversal occurs between about 06hr and 08hr and the evening reversal occurs between about 19hr and 21hr. There is the post-sunset peak particularly during the equinoctial period and there is also a high day-to-day variability. The electric field attains a value of up to 0.5mV m^{-1}. Estimate of the daytime electric field has also been made for Ibadan from the measurement of electron drift velocity of the electrojet irregularities using the spaced receiver technique, (Oyinloye and Akinrimisi, 1976). The results are as shown in Fig. 9; the relationship $E_y = -2.9V_e \times 10^6 V_m^{-1}$ was obtained suggesting a longitude effect. Day-to-day variability has also been found in the electric field (e.g. see Fig. 8), just as has been observed in the electrojet itself. Theory suggests that such variability can be linked with variability in the neutral winds (e.g. Richmond, 1973a, b; Fanibitakoye et. al. 1976), and Fig. 10 illustrate obtainable similarity in the time variations of inferred electric field at Jicarmaca and neutral winds at Thumba and Ibadan (Oyinloye and Onolaja, 1978).

The E-region electric field is known to be coupled to the F-region through the highly conducting magnetic field lines (with very high values of σ_o). This is illustrated by Fig. 11 which shows a single day comparison between E- and F- drift velocities. A high degree of correlation between E-region horizontal drift velocity and F-region vertical drift velocity ($\frac{\underline{E} \times \underline{B}}{B^2}$) at Jicarmaca is evident. The hourly variations of the seasonal values of the F-region vertical drift shown as Fig. 12 (Woodman, 1970) also exhibit striking temporal correlation with E-region horizontal drift of Fig. 8. The vertical velocities are upward during the day with typical values of the order of 20m/s, corresponding to east-west electric fields of the order of 0.5mV/m; the night velocities are downwards but with the same order of magnitude as during the day. While the velocities are approximately height independent in the 300-400km range, they show a high day-to-day variability at any one time. The post-sunset rise in the value is evident in Fig. 12.

Comprehensive reviews on the equatorial electrojet have been given by Onwumechilli (1967) and Forbes (1981).

1.5. Low latitude ionospheric measurements

Table 1 gives an indication of ionospheric measurements undertaken at low latitude stations. Of the stations listed, about 75% have operated the vertical incidence ionosonde at one time or the other; about 15% have had ionospheric scintillation and total electron content recordings from satellites, about 10%, vertical incidence A1 absorption measurement, ionospheric drifts and radio noise and fewer than 10% for other types of measurements. The figures for the stations currently operating are much lower. For instance only four of the stations are listed in the WDC C1 catalogue of ionospheric vertical sounding data as having contributed ionogram data during the period January 1985 to December 1988. It is also doubtful if any station is currently making noise measurements while field strength measurements are rare. Thus, while vertical incidence ionosonde data have been accumulated over the years, other types of measurements are few and current measurements are fewer still. Nevertheless the incoherent scatter operation at Jicarmaca and rocket measurements in India and Peru are worth mentioning as they have contributed a lot to low latitude ionospheric data and understanding.

TABLE 1: LOW LATITUDE IONOSPHERIC STATIONS WITHIN ± DIP 30°

STATION	Geographic Lat.	Geographic Long.	Mag dip	Type of Observation
Tamanrasset	23N	06E	28	B1
Ahmedabad	23N	73E	32	B1 B7 B8 B10
Kauai	22N	160W		B2
Kourou	22N	13E		B2
HongKong	22N	114E	30	B1
Macau	22N	114E	30	B1
Bombay	19N	73E	24	B1
Waltair	18N	83E	20	+B6 B10
Hydarabad	17N	78E	19	B1 +B11
•Baguio	16N	121E	18	B1
Dakar	15N	17W	17	B1
Manila	15N	121E	14	B1 +B11
Bangkok	14N	101E	10	B1
+Bangalore	13N	78E		+B11
Madras	13N	80E	09	B1
+Guam	12N	147E		+B11
Kano	12N	09E		B2
Ougadougou	12 N	01W	06	B1, B2
•Djibouti	11N	43E	06	B1
+Ootacamund	11N	77E	04	+B6
Tiruchirapalli	11N	79E	04	B1
Togo	11N	0E	02	B1
Zaria	11N	7E	03	+B1 +B6
Kodaikanal	10N	77E	02	B1
+Adis Ababa	09N	39E	00	B3 +B6
Fort-Archambault	09N	18E	-03	B1
Altair	09N	167E		B2
Thumba	09N	77E	-01	B1
+Ilorin	08N	04E	-03	B1 B9
•Trivandrum	08N		-02	B1

Table 1 (contd)

STATION	Geographic Lat.	Geographic Long.	Mag dip.	Type of Observation
•Colombo	07N	80E	-06	B1 B7 B14
+Ibadan	07N	04E	-06	B1 +B6 B7 B10 B14
Paramaribo	06N	55W	31	B1
+Lagos	06N	03E	-07	B9
Legon(Accra)	06N	00W	-10	B8 +B11 B14
•Bangui	05N	19E	-15	B1 B7
Bogota	05N	74W	32	B1
Bunia	02N	30E	-21	B1
•Sigapore	01N	104E	-18	B1 B2 B7 B10 B14
Nairobi	01S	37E	-26	B1 +B6
Lwiro	02S	29E	-29	B1 B7
Hollandia	03S	141E	-21	B1
Vanimo	03S	141E	-21	B1
Kinshasha-Binza	04S	15E	-35	B1
•Talara	05S	81W	13	B1
Natal	06S	35W	-07	B1 +B11
•Chiclayo	07S	80W	10	B1
•Chimbote	09S	79W	06	B1
+Ascension Island	08S	14W	33	B2 B6 B11
+Ancon	12S	77W	01	+B10 +B11 B12
Huancayo	12S	75W	01	B1 B8 +B11 B12
Lima	12S	77W		B2
Jicarmaca	12S	77W	01	B1 +B3 B10 B12
•Juliaca	15S	70W	-04	B1
•La Paz	16S	68W	-05	B1
Ilo	17S	71W	-07	B1
Tahiti	18S	149W	-30	B1
La Quiaca	22S	66W	-15	B1
San Jose	23S	46W	-24	+B6 B8 +B11 +B13 B1
•Sao Paulo	23S	46W	-24	B1 B14
Tucuman	27S	65W	-22	B1 +B6 +B11 +B13
Buenos Aires	34S	58W	-32	B1

Except for items marked +, source is World Data Centre C1 (WDC C1) 28th Catalogue of data issued March 1984, Rutherford Appleton Laboratory England. Items marked + are obtained from a variety of sources. Asterik • indicates that the station has closed down its vertical incidence ionosonde.

Table 1 (contd)

Types of Observation:

B1 Ionosphere vertical soundings

B2 Topside soundings

B3 Incoherent scatter soundings

B4 Oblique incidence soundings

B6 Total electron, content - satellite beacons

B7 Absorption - method A1 (Pulse echo)

B8 Absorption - method A2 (riometer)

B9 Absorption - method A3 (CW field strength)

B10 Ionospheric drifts

B11 Ionospheric scintillations from beacon satellites

B13 Whistlers and VLF emissions

B14 Atmospheric radio noise.

APPENDIX

Conductivity Equations

Direct conductivity σ_o, Pedersen conductivity σ_1 and Hall conductivity σ_2 are given by the following equations:

$$\sigma_o = \left(\frac{n_e}{m_e \nu_e} + \frac{n_i}{m_i \nu_i} \right) e^2$$

$$\sigma_1 = \left[\frac{n_e}{m_e \nu_e} \left(\frac{\nu_e^2}{\nu_e^2 + w_e^2} \right) + \frac{n_i}{m_i \nu_i} \left(\frac{\nu_i^2}{\nu_i^2 + w_i^2} \right) \right] e^2$$

$$\sigma_2 = \left[\frac{n_e}{m_e \nu_e} \left(\frac{w_e \nu_e}{\nu_e^2 + w_e^2} \right) - \frac{n_i}{m_i \nu_i} \left(\frac{w_i \nu_i}{\nu_i^2 + w_i^2} \right) \right] e^2$$

where e is the electronic charge, m, n, mass and number density respectively,

ν, w, collision frequency and gyrofrequency respectively,

and subscripts e and i stand for electron and ion respectively.

Collision Frequencies

Expressions for ion-neutral collision frequencies in MKS units are given by Richmond (1972) as:

$$\nu_{1n} = \{ (1.07 [N_2] + 1.06 [O_2]) (T/500)^{-0.16} + 0.60 [O] (T/500)^{-0.19} \} 10^{-22} w_1/B$$

$$\nu_{2n} = \{ 1.08 [N_2] (T/500)^{-0.17} + 2.02 [O_2] (T/500)^{0.37} + 0.61 [O] (T/500)^{-0.019} \} 10^{-22} w_2/B$$

$$\nu_{3n} = \{ 0.89 [N_2] (T/500)^{-0.20} + 1.16 [O_2] (T/500)^{0.05} + 0.89 [O] (T/500)^{0.36} \} 10^{-22} w_3/B$$

Subscripts 1, 2, and 3 refer to NO^+, O_2^+ and O^+ respectively. The square bracket [ ] denotes number density of neutral particles, T is the temperature; w, the gyrofrequency and B the earth's magnetic field.

The electron-neutral collision frequencies as given by Richmond (1972) and corrected by Gagnepain et al (1977) are:

$$\nu_{en} = \{ 4.11 \, [N_2] \, (T_e/300)^{0.95} + 2.95 \, [O_2] \, (T_e/300)^{0.79} + 1.09 \, [O] \, (T_e/300)^{0.85} \} 10^{-26} \, w_e/B$$

where subscript e refers to electrons while the electron ion collision frequency is given by Nicolet (1953) as

$$\nu_{ei} = [e] \{ 59.0 + 4.18 \log_{10} (T^6 / [e]) \} 10^{-6} \, T^{-3/2}$$

MKS units.

Electron-ion collisions are negligible in the lower E region but ν_{ei} becomes comparable with ν_{en} above about 140km.

References

Baker, W.G. and Martyn D.F. (1953); Electric currents in the ionosphere,I Conductivity. Phil. Trans. Roy. Soc. London, Series A, 246, 281-294.

Balsley, B.B. (1973); Electric fields in the equatorial ionosphere: A review of techniques and measurements. J. Atmos. Terr. Phys., 35, 1035 - 1044.

Balsley, B.B. and Woodman, R.F. (1971); Ionospheric drift velocity measurements at Jicarmaca, Peru (July 1967 - March 1970) Upper Atmos Geophys. Rep. UAG-17, NOAA World Data Centre A, Boulder Colorado.

Burrows, K. (1970). The day-to-day variability of the equatorial electrojet in Peru. J. Geophys. Res., 75, 1319-1323.

Cain, J.C. and Neilon, J.R. (1963). Automatic mapping of the geomagnetic field. J. Geophys. Res., 68, 4684-4698.

Davies, K. (1965). 'The earth's magnetic field' in "Ionospheric Radio Propagation", Section 1.5, NBS Monograph 80, pp. 19-35.

Davis, T.N., Burrows, and Stolarik, J. D. (1967). A latitude survey of the equatorial electrojet with rocket-borne magnetometers. J. Geophys. Res., 72, 1845-1861.

Egedal, J. (1947). The magnetic diurnal variation of the horizontal force near the magnetic equator. J. Geophys. Res., 52, 449-451.

Egedal, J. (1948). Daily variation of the horizontal magnetic force at the magnetic equator, Nature, 161, 443-444.

Fambitakoye, O., Mayaud, P.N. and Richmond, A.D. (1976). Equatorial electrojet and regular daily variation S_R III, comparison of observations with a physical model. J. Atmos. Terr. Phys., 38, 113 - 121.

Fambitakoye, O., Rastogi, R.G., Tabbagh, J. and Vila, P. (1973). Counter electrojet and Esq. disappearance J. Atmos. Terr. Phys., 35, 1119-1126.

Forbes, J.M. (1975). Atmospheric solar tides and their electrodynamic effects. Ph.D. Thesis, Hayard Univ. Cambridge Mass.

Forbes, J.M. (1981). The equatorial electrojet. Reviews Geophys. and Space Phys., 19, 469-504.

Forbes, J. M. and Lindzen, R.S. (1976). Atmospheric solar tides and their electrodynamic effects, I, The global Sq current system. J.Atmos.Terr. Phys., 38, 897-910.

Gagnepain, J., Crochet, M. and Richmond, A.D. (1977). Comparison of electrojet models. J. Atmos. Terr. Phys., 39, 1119-1124.

Gouin, P. and Mayaud P.N. (1967). A propos de L'existence possible dun "contre electrojet" aux latitudes magnetiques equiatoriales. Ann Geophys., 23, 41-43.

Gupta, J.C. (1973). On solar and lunar equatorial electrojets. Ann Geophys. 29, 49-60.

Hutton, R. (1967). Sq currents in the American equatorial zone during the IGY-II Day to day variability. J. Atmos. Terr. Phys., 29, 1429-1442.

Hutton, R. and Oyinloye, J. O. (1970). The counter-electrojet in Nigeria. Ann. Geophys. 26, 921-926.

Kane, R.P. (1974). Relation between the strength of the Sq current system and its focus position. Proc. Indian Academy of Sciences, vol. LXXX, Sec. 'A', 17-25.

Musmann, G. and Seiler, E. (1978). Determination of moridional currents in the equatorial ionosphere. J. Geophys., 44, 357-372.

Nicolet, M. (1953). The collision frequency of electrons in the ionosphere. J. Atmos. Terr. Phys., 3, 200-211.

Ogbehi, P.O. and Onwumechilli, C.A. (1964). Daily and seasonal changes in the equatorial electrojet in Nigeria. J. Atmos. Terr. Phys., 26, 889-898.

Ogbuehi, P.O. and Onwumechilli, A. (1965). Seasonal studies of the equatorial electrojet during low solar activity. J. Geophys., Res., 70, 4909-4919.

Onwumechilli, C.A. (1959a) A study of the equatorial electrojet-I An experimental study. J. Atmos. Terr. Phys., 13, 222-234.

Onwumechilli, C.A. (1959b). A study of the equatorial electrojet-II A model electrojet that fits H-observations. J. Atmos. Terr Phys. 13, 235-257.

Onwumechilli, A. (1967). Geomagnetic variations in the equatorial zone in "Physics of Geomagnetic phenomena", ed. S. Matsushita and W.H. Campbell, pp. 425-507, Academic, New York.

Oyinloye, J. O. and Akinrimisi, J. (1976). Sporadic-E velocity measurement - interpretation and application to ionospheric E-region electric field determination. J. Atmos. Terr. Phys., 38, 149-154

Oyinloye, J. O. and Onolaja, G.B. (1978). E-region drift at Ibadan. J. Atmos. Terr. Phys., 40, 1001-1010.

Price, A.T. and Wilkins, G.A. (1951). The daily magnetic variations in equatorial regions. J. Geophys., Res., 56, 259-263.

Rastogi, R.G., (1962). Longitudinal variation in the equatorial electrojet, J. Atmos. Terr. Phys., 24, 1031-1041.

Rastogi, R.G. (1974). Counterelectrojet during daytime hours. J. Geophys., Res., 79, 1503-1512.

Richmond, A.D. (1972). Numerical model of the equatorial electrojet. Rep. AFCRL-72-0668, ERP 421, Air Force Cambridge Res. Lab. Hanscom AFB, Bedford Mass.

Richmond, A.D. (1973a). Equatorial electrojet, I, Development of a model including winds and instabilities. J. Atmos. Terr. Phys., 35, 1083-1103.

Richmond, A.D. (1973b). Equatorial electrojet, II, Use of the model to study the equatorial ionosphere. J. Atmos. Terr. Phys., 35,1105-1118.

Singer, S.F. Maple, E. and Bowen, W.A. Jr. (1951). Evidence for ionospheric current from rocket experiments near the geomagnetic equator. J. Geophys. Res., 56, 265-281.

Subbaraya, B.H., Muralikrishna, P., Sastry T.S.G. and Prakash, S. (1972). A study of the structure of electrical conductivities and the electrostatic field within the equatorial electrojet. Planet space Sci., 20, 47-52.

Woodman, R.F. (1970). Vertical drift velocities and east-west electric fields at the magnetic equator. J. Geophys. Res., 75, 6249-6259.

Figure Captions

Fig. 1. Location of the geographic, geomagnetic and dip equators. (After Gupta, 1973).

Fig. 2. World map of magnetic dip angle I (After Cain and Neilon, 1963).

Fig. 3. World map of total magnetic intensity F (After Cain and Neilon, 1963).

Fig. 4 (a) Vertical profiles of direct (σ_0), Pedersen (σ_1), Hall (σ_2) and Cowling conductivities under noontime, equatorial equinox and average solar conditions (After Forbes and Lindzen, 1976).

(b) Vertical profiles of positive ion composition for noontime equatorial equinox conditions and average solar activity. (After Forbes, 1975).

Fig. 5. Comparison of computed vertical profiles of σ_3 and σ_2/σ_1 with measured eastward current densities j and electron concentrations N_e for a rocket flights over Thumba (After Subbaraya et el., 1972).

Fig. 6. Variation of the daily range of the ground northward magnetic component with latitude from the mean equator midway between the dip and geographic equators on international quiet days during September and October 1958. (After Ogbuehi and Onwumechilli, 1965).

Fig. 7. Cross-sectional profile of the equatorial electrojet obtained from nine rocket flights off the coast of Peru in 1965, normalized to yield $\Delta H = 100\gamma$ at Huancayo. Circles indicate locations of data points used to obtain the contours of current density in microamps per square meter. The right-hand portions of the contours are dashed to indicate uncertainty associated with the relative lack of data from this portion of the diagram (After Davis et al., 1967).

Fig. 8. Composite of type II drift velocities obtained at Jicarmaca during the period 1967 - 1970 (After Balsley, 1973).

Fig. 9. Daytime variations of (a) observed westward velosity of Esq. irregularities at Ibadan, (b) computed corresponding mean eastward electric field $\bar{E}_y$, (c) computed corresponding height integrated current density, J and (d) observed magnetic field deviation ΔH at Ibadan. The variations are for the period 18 - 22 October. 1966. (After Oyinloye and Akinrimisi, 1976).

Fig.10. Hourly variation of the eastward components of E-region velocities at (a) Ibadan (b) Thumba and (c) Jicarmaca; (a) and (b) are for neutral winds while (c) is for type II electrojet irregularities. (After Oyinloye and Onolaja, 1978).

Fig.11. Single-day comparison between E region (horizontal) drifts and F region (vertical) drift velocities at Jicarmaca for March 5, 1968. (After Balsley, 1973).

Fig. 12. Composite vertical ionospheric drifts observed at Jicarmaca for different seasons during the period 1968-1970. (After Woodman, 1970). Dotted lines correspond to periods with $k_p \geq 5$.

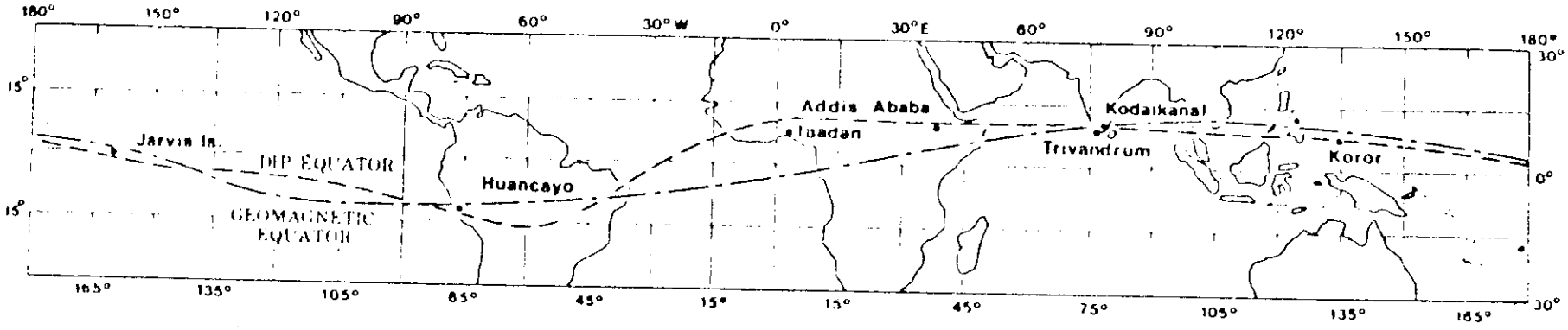
180°
150°
120°
90°
60°
30° W
0°
30° E
60°
90°
120°
150°
180°
30°
15°
0°
15°
Jarvis Is.
DIP EQUATOR
GEOMAGNETIC EQUATOR
Huancayo
Addis Ababa
Ibadan
Trivandrum
Kodaikanal
Koror
165°
135°
105°
85°
45°
15°
15°
45°
75°
105°
135°
165°
30°

Fig. 1

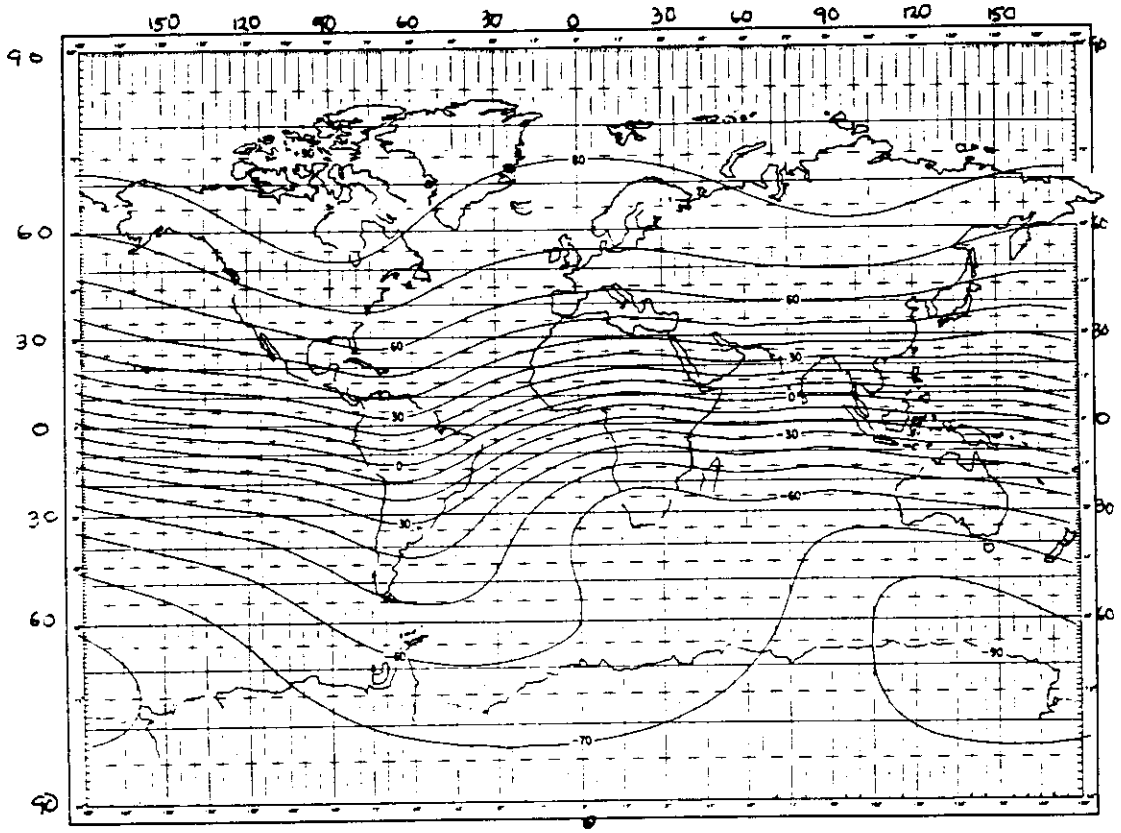
150 120 90 60 30 0 30 60 90 120 150
90
60
30
0
30
60
90
-60
-70

Fig. 2

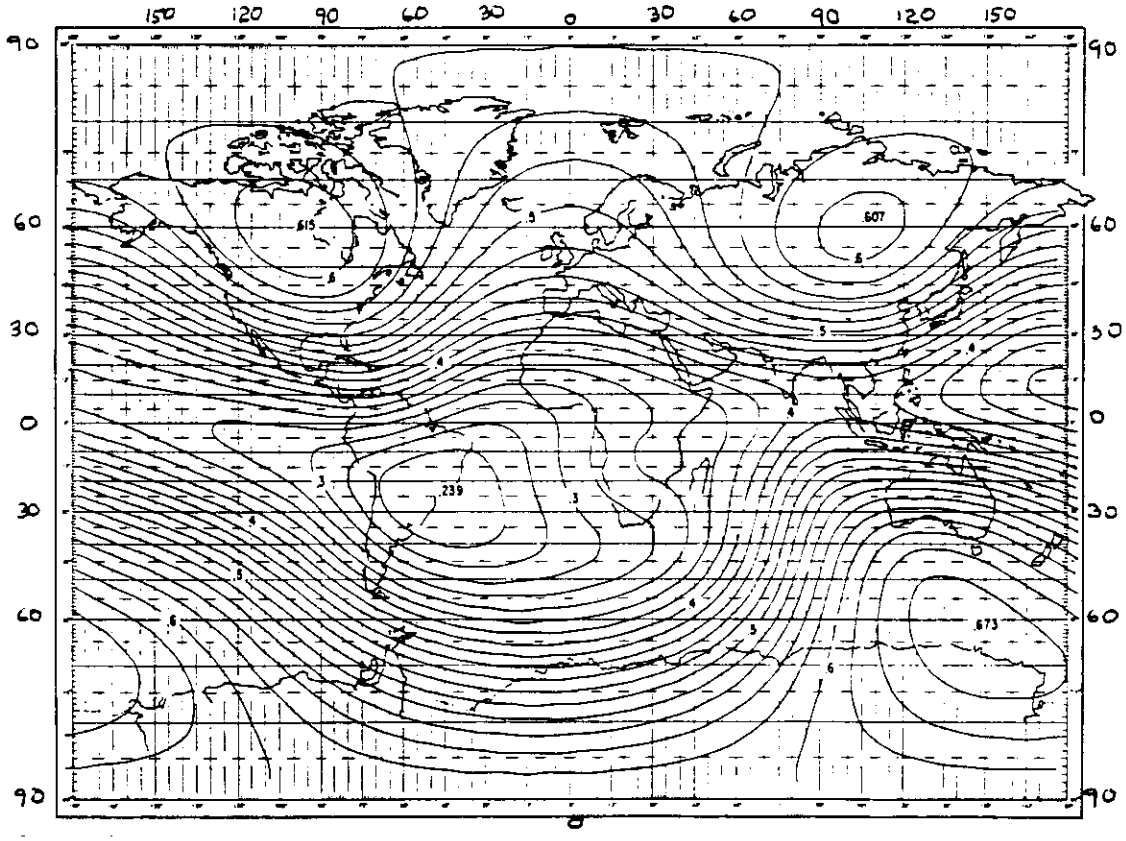
150 120 90 60 30 0 30 60 90 120 150
90
60
30
0
30
60
90
615
607
239
673

Fig. 3

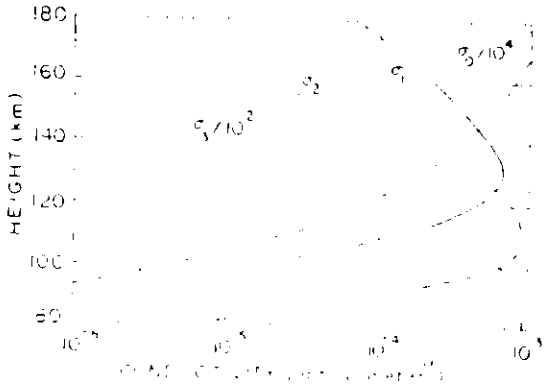

Fig. 4a

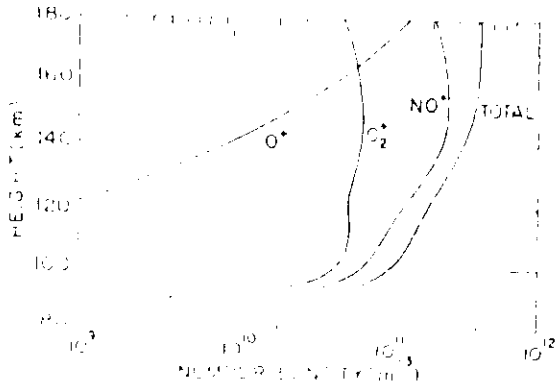

Fig. 4b

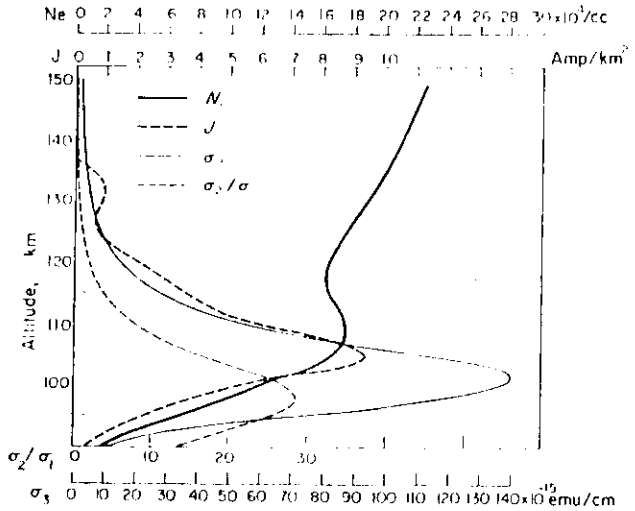

FIG. 4. σ_2/σ_1 AND THE EFFECTIVE CONDUCTIVITY σ_3 COMPUTED FROM THE ELECTRON DENSITY PROFILE OF FLIGHT 10.37 (28 JAN. 1971 1040 hr IST) SHOWN ALONG WITH THE ELECTROJET CURRENTS MEASURED ON FLIGHT 20.06 (29 AUG. 1968 1108 hr IST).
The electron density profile used in the computation is also shown in figure.

Fig. 5

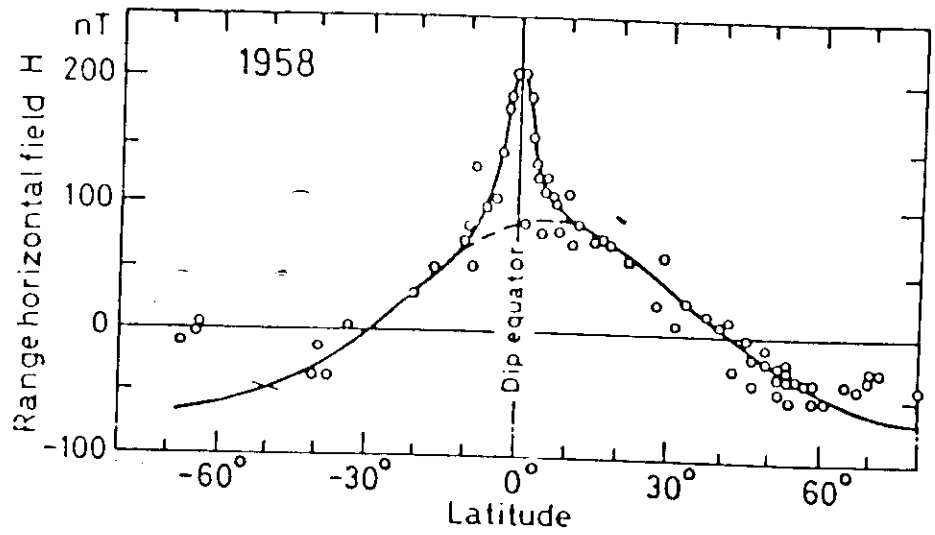

Fig. 6

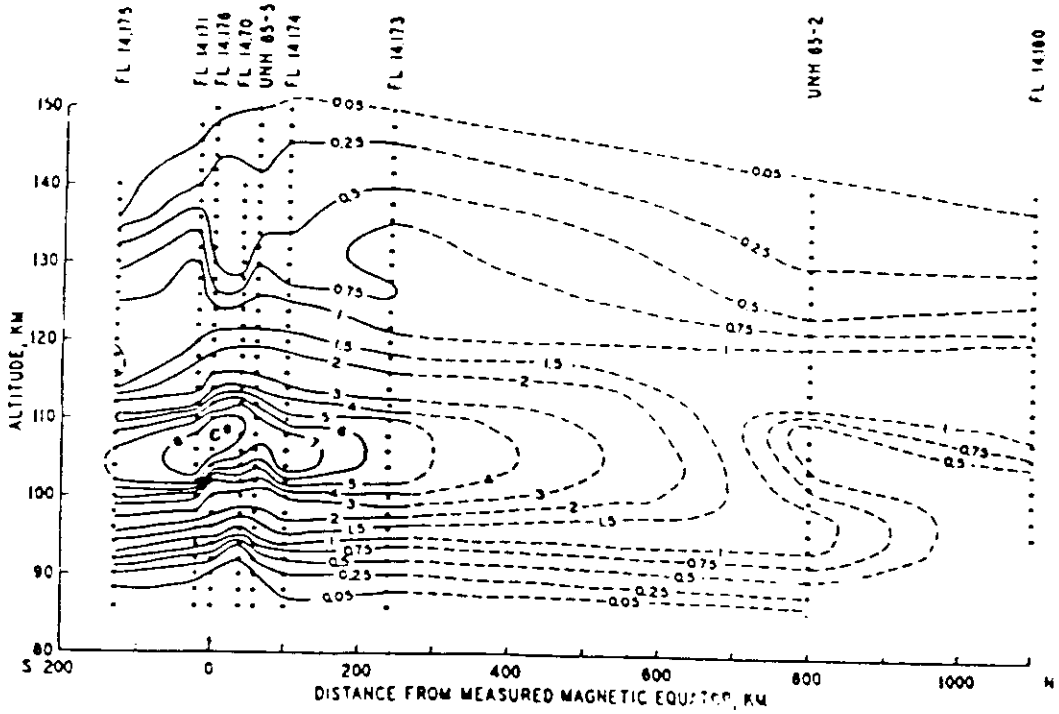

Cross-sectional profile of the equatorial electrojet obtained from nine rocket flights off the coast of Peru in 1965, normalized to yield $\Delta H = 100\ \gamma$ at Huancayo. Circles indicate locations of data points used to obtain the contours of current density in microamps per square meter. The right-hand portions of the contours are dashed to indicate uncertainty associated with the relative lack of data for this portion of the diagram (Figure is from *Davis et al.* [1967])

Fig. 7

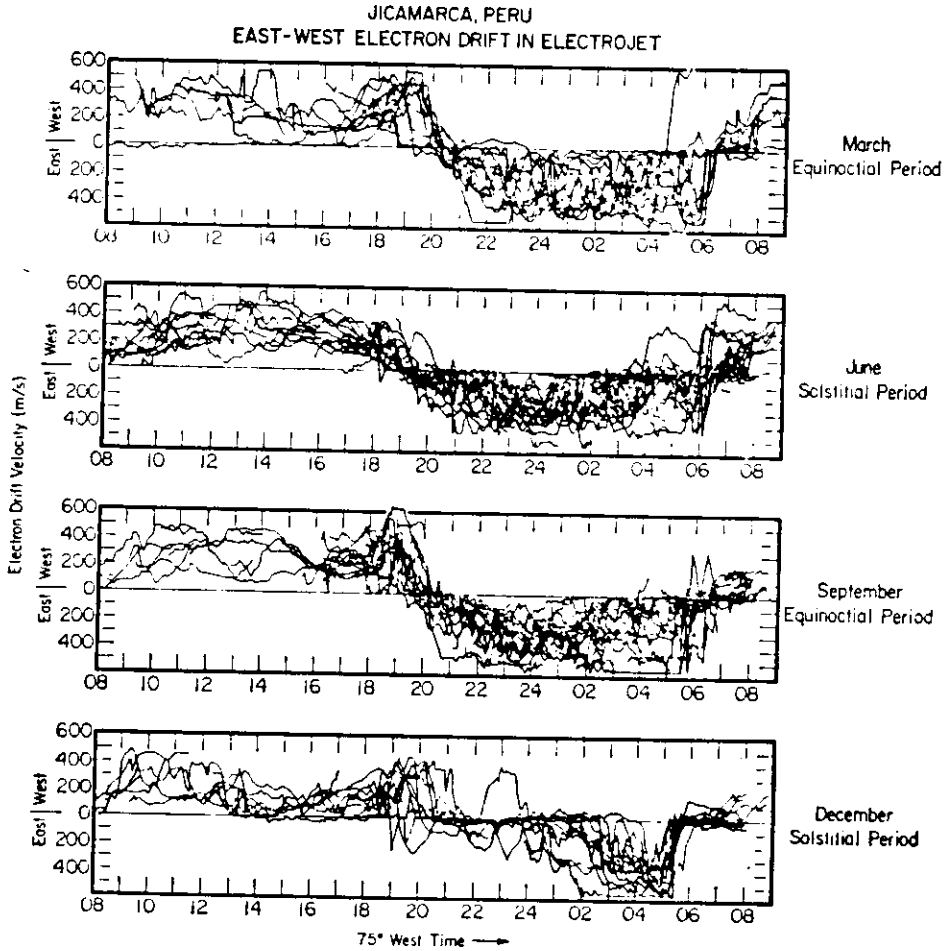

~~Fig. 2~~. A composite of the type II drift velocities obtained at Jicamarca during the period 1967–1970. Note in particular the following features: (1) the westward drifts during daytime periods (≃0700–2000 hr); (2) the eastward drifts during the nighttime periods (≃2000–0700 hr); (3) the prereversal enhancement, prior to the evening reversal, that is most pronounced in the September solstitial data; and (4) the day-to-day variability of the velocities for any given period.

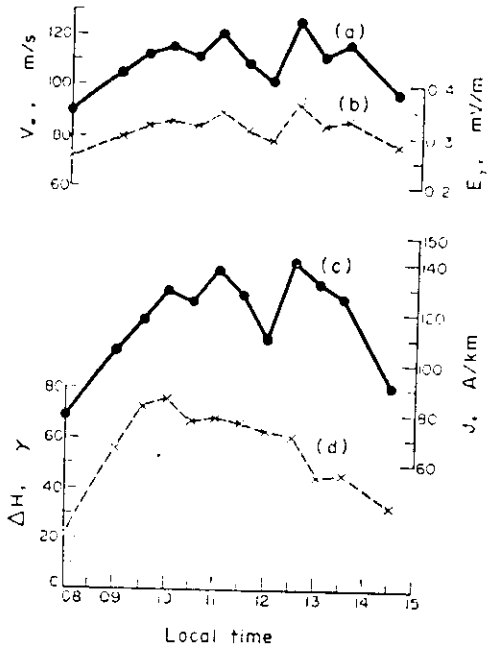
(a)
(b)
(c)
(d)
V, m/s
E, mV/m
ΔH, Y
J, A/km
Local time

Fig. 9

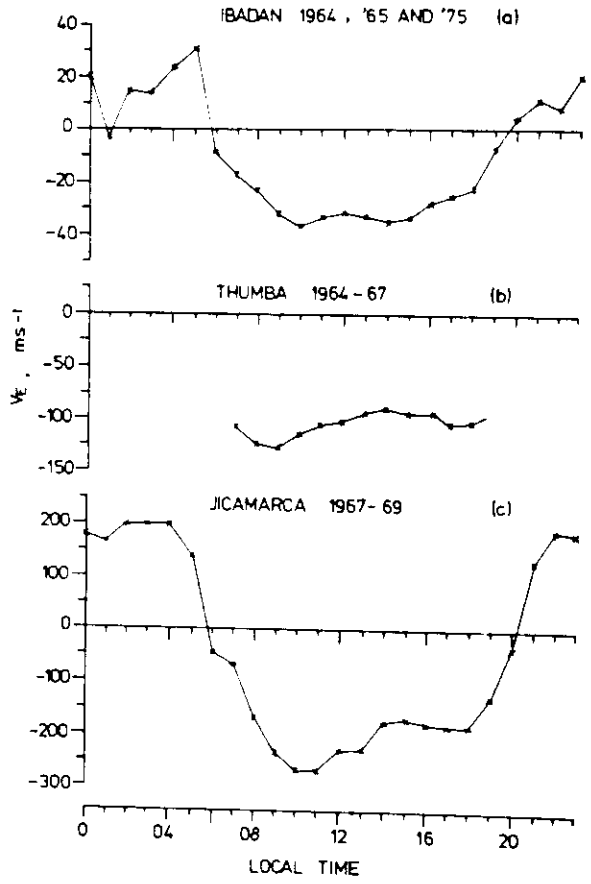
IBADAN 1964 , '65 AND '75 (a)
THUMBA 1964 - 67 (b)
JICAMARCA 1967 - 69 (c)
Vε, ms-1
LOCAL TIME

Fig. 10

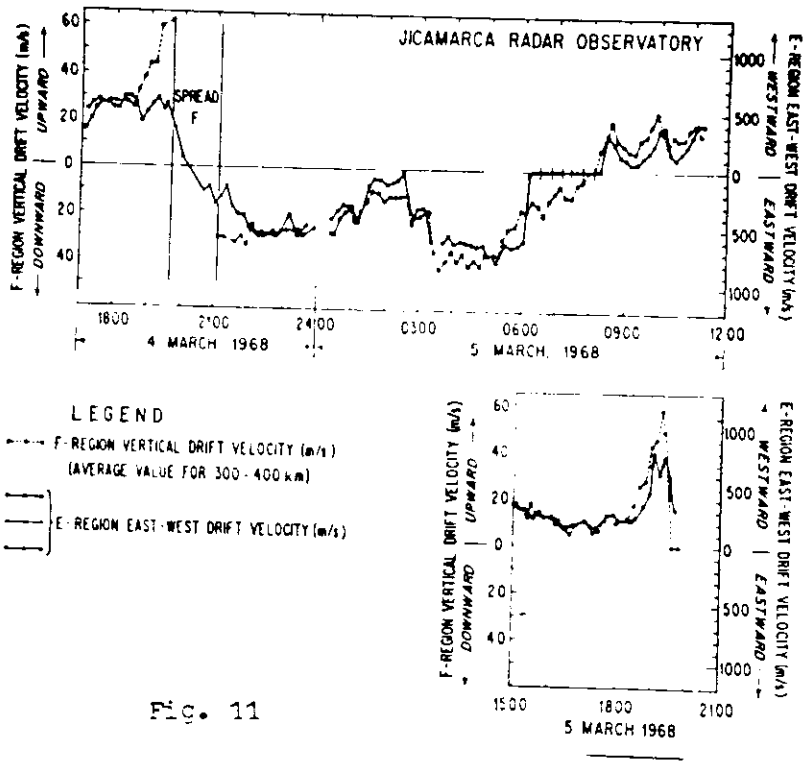
JICAMARCA RADAR OBSERVATORY
SPREAD F
F-REGION VERTICAL DRIFT VELOCITY (m/s)
UPWARD
DOWNWARD
E-REGION EAST-WEST DRIFT VELOCITY (m/s)
WESTWARD
EASTWARD
1800
2100
2400
0300
0600
0900
1200
4 MARCH 1968
5 MARCH, 1968
LEGEND
F-REGION VERTICAL DRIFT VELOCITY (m/s)
(AVERAGE VALUE FOR 300 - 400 km)
E-REGION EAST-WEST DRIFT VELOCITY (m/s)
1500
1800
2100
5 MARCH 1968

Fig. 11

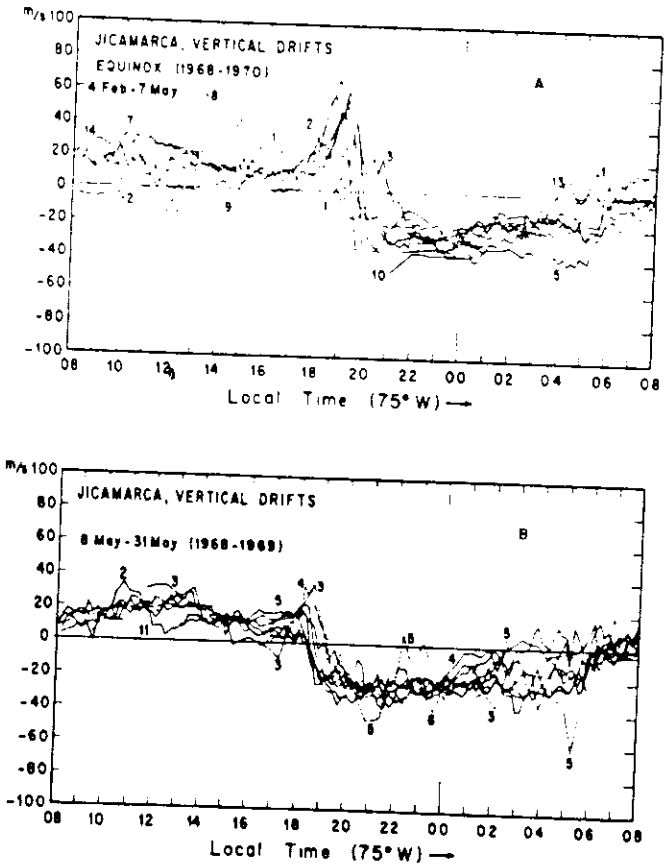
JICAMARCA, VERTICAL DRIFTS
EQUINOX (1968-1970)
4 Feb - 7 May
A
JICAMARCA, VERTICAL DRIFTS
8 May - 31 May (1968-1969)
B
m/s
Local Time (75° W)

Fig. 12

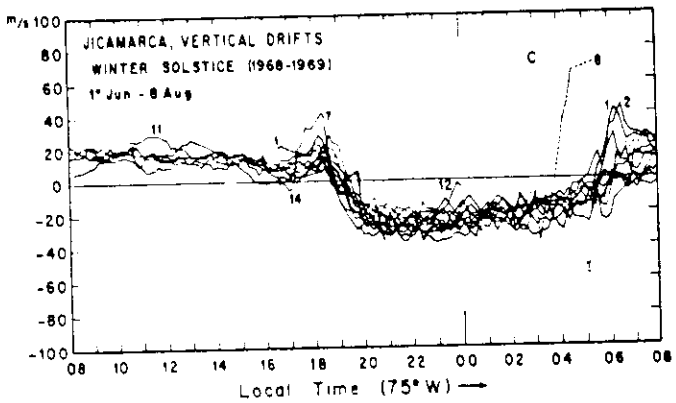
m/s 100
JICAMARCA, VERTICAL DRIFTS
WINTER SOLSTICE (1968-1969)
1° Jun - 8 Aug
C
80
60
40
20
0
-20
-40
-60
-80
-100
08 10 12 14 16 18 20 22 00 02 04 06 08
Local Time (75° W) ⟶

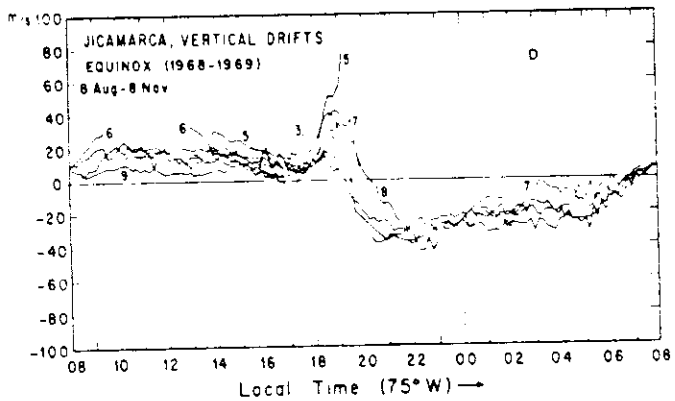
m/s 100
JICAMARCA, VERTICAL DRIFTS
EQUINOX (1968-1969)
8 Aug - 8 Nov
D
80
60
40
20
0
-20
-40
-60
-80
-100
08 10 12 14 16 18 20 22 00 02 04 06 08
Local Time (75° W) ⟶

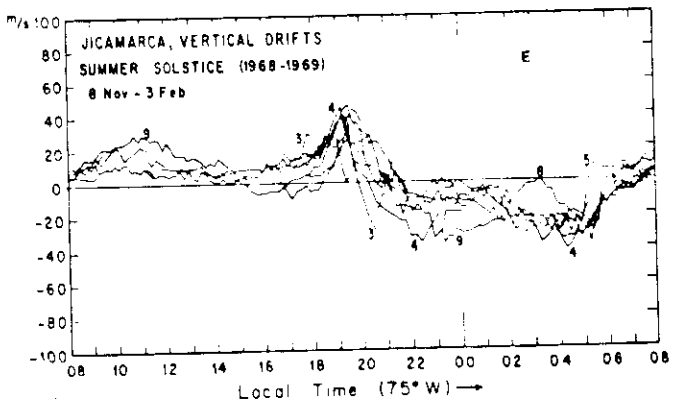
m/s 100
JICAMARCA, VERTICAL DRIFTS
SUMMER SOLSTICE (1968-1969)
8 Nov - 3 Feb
E
80
60
40
20
0
-20
-40
-60
-80
-100
08 10 12 14 16 18 20 22 00 02 04 06 08
Local Time (75° W) ⟶

Fig. 12 (contd)

ICTP COLLEGE ON THEORETICAL AND EXPERIMENTAL RADIO PROPAGATION PHYSICS, FEBRUARY 6-24, 1989

LOW LATITUDE IONOSPHERIC PHENOMENA - ELECTRON CONCENTRATION AND IONOSPHERIC IRREGULARITIES.

J. O. OYINLOYE
DEPARTMENT OF PHYSICS
UNIVERSITY OF ILORIN
ILORIN, NIGERIA.

2.1. D Region

The D region of the ionosphere occupies a height range of about 50-90km. The major sources of ionization under quiet conditions are the solar Lyman - alpha line (102.6nm), 3-4nm X rays, 0.1 - 1nm X rays and galatic cosmic rays (Ratnasiri, 1977). Ly -α ionizes NO and is most effective between about 62 and 85km (Ratnasiri, 1977), it is the dominant source of electrons in the 70-85km altitude range (Gnanalingam, 1974); 3 - 4nm X rays, ionising N_2 and O_2 become the most important above about 85km while galactic cosmic rays become the most important below about 62km (Ratnasiri, 1977). Under quiet conditions, 0.1 - 1.0 nm X rays are only a minor source with the production function vanishing completely below about 70km, though under disturbed conditions, their ionization could dominate the entire D region with values sometimes increasing by more than 100 fold. X-rays increase from sunspot minimum to sunspot maximum; Ly - is nearly constant with solar activity but NO increases with solar activity while cosmic rays decrease with solar activity. In effect electron concentration is expected to increase with solar activity in the upper D region and decrease with increasing solar activity in the lower D region, the solar activity reversal in N_e being below about 70km (Mitra and Rowe, 1974). A gradual loss of solar control in the diurnal variations of electron concentfation is also expected below about 70km (Mitra and Rowe, 1974).

Direct measurements of the properties of the D region are scarce and only a few rocket measurements, made primarily in Peru and India, are available for the low latitude region.

Figure 1 shows a mass plot of the electron densities obtained from twelve daytime rocket experiments conducted at Thumba during the the period 1966 to 1978 (Subbaraya et al., 1983, 1985). The diagram shows an electron density of about 10 per cc at 60km increasing gradually to about 250 per cc at 70km and having a value of about 500-600 per cc in the altitude region of 75-80km. There is a sharp increase in slope at about 82 km, beyond which the electron density increases rapidly with altitude, attaining a value of about 1.0×10^4 electrons per cc at about 90km. Figures 2a-d which display rocket measurements of electron and positive ion density altitude distributions over

Thumba on March 19, 1970 illustrate some interesting features of the equatorial D-region (Akin et al. 1972). Figures 2a and 2b show that positive ions could be significantly larger than electrons at altitudes below 75km thereby indicating a high (negative ion/electron) density ratio for this height region during the daytime; a steep gradient of electron density above 85km is evident in all the figures while Fig. 2d indicates a diurnal asymmetry such that a much larger change is observed between χ = 50° and 28° (in the morning) than between χ = 28° and 48° (in the afternoon) below 100 km; also solar control of the region with higher values of electron density for lower values of χ is consistently exhibited for the height range 70 - 90km.

Sometimes, attempts are made to deduce information on the properties of the D region from HF absorption measurement. Figures 3,a4a and 5 illustrate diurnal, seasonal and solar-cycle variations in equatorial vertical incidence ionospheric absorption on 2.2 MHz. In the diurnal variation, there is a delay of 20-30 minutes between the time of minimum solar zenith angle χ and the time of maximum absorption which gives rise to a diurnal asymmetry such that absorption for a given value of χ is greater in the afternoon than in the morning. The seasonal variation is semi-annual with equnoctial peaks and there are unusually low values of absorption during the June solstial months of May, June and July. The solar-cycle variation shows an increase with solar activity. While variations in collision frequencies may contribute to the observed diurnal and seasonal variations, similar variations in electron density in the D region above 70km and the lower E-region are mainly responsible for the diurnal asymmetry (Fig.2) and the observed seasonal variation (Fig. 4a and b). Also, the solar cycle variation can be attributed to a similar variation in electron density in view of the fact that collision frequencies for heights below about 100km are independent of solar activity (Thrane and Piggott, 1966). A major difference between the observed absorption in the equatorial region and in the middle latitudes is in respect of the 'winter anomaly' which refers to greatly enhanced absorption on some days in winter relative to summer values. It is present in middle latitude absorption (Thomas, 1962) but absent in equatorial absorption (Diemeonger et al., 1967). This is evident in the seasonal patterns of the latitudinal variation in the 2.2MHz absorption (Fig. 6) which is independent of season for dip

angles $|I| \lesssim 20^{\circ}$ whereas there is winter enhancement at greater dips. Midlatitude winter anomaly is attributed to enhanced D-region electron density and it is associated with stratospheric warming and mesospheric circulation (Shapley and Beynon, 1965; Rose et al., 1972). On the other hand, seasonal variation of absorption in the equatorial regions is not associated with either temperature changes in lower atmosphere or winds variation in the meteor zone (Oyinloye, 1978).

2.2. E Region

The E region occupies a height range of about 90 - 150 km. Typical equatorial E-region electron density profile near noon is also illustrated by Fig. 1. Electron density n_e increases from a value of about $1.0 \times 10^4 cm^{-3}$ at 90km to $1.5 \times 10^5 cm^{-3}$ at about 110km and then further increases very slowly with altitude reaching a value of about $2.7 \times 10^5 cm^{-3}$ at 160km. There is very little day-to-day variability in E region electron density profiles and over distances 0-150km from the magnetic equator (Aikin and Blumle, 1968). Figure 6 illustrates the situation at nighttime. There is absence of ionisation at altitudes below 85km, rapid rise in electron density in the altitude range of 85 to 95km reaching values of about 1000 electrons per cc aroung 95km and the existence of pronounced structures in the profiles, in form of layers of ionisation on many of the occasions (Subbaraya et al., 1983, 1985). The daytime electron concentration is about an order of magnitude higher than that of the nighttime. While the daytime ionisation may be attributed to photochemical processes, the nighttime structures represent redistribution of the ambient ionisation due to dynamical processes.

The daytime maximum ionisation N_mE and the corresponding height h_mE have been studied extensively from ionograms (Fig. 8), $N_mE = 1.24 \times 10^{-2} \times (foE)^2$ where NmE is in m^{-3}, foE is in Hz and it is the E-region O-wave critical frequency or the maximum frequency of the ordinary wave that can be reflected from the E region at vertical incidence.

The variation with time t of NmE satisfies the equation:

$$\frac{d(N_mE)}{dt} = q_o \cos\chi - \alpha (N_mE)^2. \qquad (1)$$

where q_o is the maximum electron production rate per unit volume for overhead sun ($\chi = 0$), and α is the recombination coefficient assumed constant. If the layer conditions are completely stationary:

$$(N_mE)^2 = \frac{q_o}{\alpha} \cos\chi \qquad (2)$$

or
$$(foE)^4 = K \cos\chi \qquad (3)$$

$$K = \frac{q_o}{\alpha} \frac{1}{(1.24 \times 10^{-2})^2} \qquad (4)$$

and $$\cos\chi = \sin\phi \sin\delta + \cos\phi \cos\delta \cos\omega t \qquad (5)$$

where ϕ is the geographic latitude, δ, the solar declination, ωt the local hour angle. From the above equations, it is seen that the variations of N_mE or foE will depend on solar activity, season, time of th day and latitude.

On a global basis the dependence of N_mE on solar activity has been given in terms of sunspot number R by Muggleton (1971) as:

$$N_mE \propto (foE)^2 \propto (1 + 0.00334R). \qquad (6)$$

and in terms of solar radio-noise flux S (in units of $10^{-22} Wm^{-2} Hz^{-1}$) by Kouris (1971) as:

$$(N_mE)^2 \propto (foE)^4 \propto (1 + 0.0094S). \qquad (7)$$

Figure 8 illustrates the long-term variation of $(foE)^2$ with S and R at a low latitude station.

For the diurnal observation, it has been found that the expression:

$$(foE)^4 \propto (\cos\chi)^p \qquad (8)$$

fits the data. Kouris and Muggleton (1973a) have found that for stations within the latitude zone of about 12° on either side of the Equator, $p = 1.31$ which differs slightly but systematically from the overall

averaged value of 1.20 for other stations in the tropical region and in the middle latitudes.

The seasonal variation can be obtained by studying $(foE)^4$ at several stations under conditions of constant solar activity, cos χ and Sun-Earth distance. Kouris and Muggleton (1973b) have plotted a parameter A which is the monthly value of $(foE)^4$, normalized to $\chi = 0$ and $S = 0$ to give the seasonal variation. (Fig.10). The parameter A can also be expressed by the function:

$$A = B \ (\cos\chi_{noon})^m \qquad (9)$$

where the latitude variations of B and m are shown as Figs 11a and b respectively. The seasonal variations are dependent on both latitude and longitude. Apart from the fact that the parameter B increases towards the equator, it is striking from Fig. 10 and equation (9) coupled with Figs. 11a and b that seasonal variation in FoE or N_mE is not significant at the low latitude stations. However where seasonal variation is found, the value of A is much less in local summer than in local winter in both hemispheres, a result that is called the Appleton E-layer seasonal anormaly. There is also the interesting aspect that the seasonal variation may be linked with that of the Sq-current system (Kouris and Muggleton 1973b). For instance Fig. 11 shows an enhancement of m in the northern hemisphere over that for a given latitude in the southern hemisphere and the zone centred on the meridian 75°W exihibits the lowest equatorial value of m. Correspondingly, current intensity of the sq. current system for equinoctial months and the yearly average has been found to be about 1.2 times larger in the northern than in the southern hemisphere and the intensity of the equatorial electrojet is greatest in the American zone. Arguments have been advanced that the seasonal changes could be explained by changes in the E-region vertical drift velocity and its gradient, caused by seasonal variation in the Sq current system.

In general, foE is well represented globally by the prediction formula of Muggleton (1975) given in the form

$$(foE)^4 = CDEF \qquad (10)$$

where C, D, E, and F represent respectively the factors for solar activity, season, latitude and time of day. Equation (10) is a composite form of equations (7) (8) and (9). In particular, the equation:

$$N_mE = 1.46 \times 10^{11} (1 + 0.0091R)^{\frac{1}{2}} (\cos \ )^{0.65} \qquad (11)$$

$$foE = 3.55 (1 + 0.009IR)^{\frac{1}{4}} (\cos \ )^{0.315} \qquad (12)$$

given by Aremu and Oyinloye (1988), predicts foE and N_mE for equatorial stations within |(geographic latitude)| $\leq$ 12° with a high degree of accuracy better than 5%. (Fig. 12).

The height h_mE corresponding to foE can be estimated from the expression obtained for the middle latitudes by Piggott and Thrane (1966) and given as:

$$hmE = h_o + 7.5 \ln (\sec\chi) \qquad (13)$$

where hmE is in km and h_o = 105km and 108km for high and low solar activities respectively. A comparison with experimental data for low latitude stations indicates that equation (13) is also applicable to low latitude stations.

2.3. F Region

(a) Equatorial anomaly

A distinct feature of the F-region at low latitudes is the equatorial anomaly which is the latitude variation of F-region electron concentration with a trough centred about the geomagnetic equator and with peaks appearing at about magnetic latitude $\pm$ 15° - 20°. The anomaly first appears in the morning and this could be as early as 10 hr., becomes prominent late in the afternoon or towards sunset and decays about midnight (Lyon and Thomas, 1963; Rastogi, 1959b; Walker and Chan 1976). The exact time of appearance, the development of the anomaly, the time of decay and eventual disappearance depend on solar activity (Rush et al., 1969) and longitude. There is also considerable variability on a day-to-day basis (Vila, 1971; Rush et al., 1972). Studies of electron density at fixed heights below (Croom et al., 1959) and above (King et al., 1964, 1967) the F2 peak have shown that the anomaly can be found within a height range of about 160-800 km, though there is a tendency for the

anomaly to get narrower as altitude increases or during magnetic storm. The main features of the equatorial anomaly are illustrated in Fig. 13. The enhancement of electron concentration in the northern hemisphere over that in the southerns hemisphere is worth noting.

It is believed that the anomaly is due to a "fountain effect" caused by the electrodynamic vertical lifting of the plasma over the equator which then diffuses along field lines to subtropical latitudes. The two effects lead to the observed "trough" and "crest" of ionization. It has been theoretically demonstrated by Hanson and Moffett (1966) that an upward vertical drift of the order of 10 ms^{-1} could be adequate to produce both the depth of trough $\{(N_mF2)_{max}/(N_mF2)_{eq} \simeq 2\}$ and latitude of the maximum value of NmF2 (Fig. 14). The fountain effect that would result from a vertical drift of 10 ms^{-1} for sunspot maximum conditions is illustrated by Fig. 15. Conversely, a downward drift leads to an "inverted fountain" effect whereby ionization from higher latitude flows up the field lines and is eventually recombined at low latitudes in the peak formed near the equator.

(b) Temporal variations

The characteristic frequency foF1 for the F1 region fits well the Chapman model and foF1 can be expressed as :

$$foF1 = f_s \cos^n \chi \quad \text{for} \quad \chi \leq \chi_m \qquad (14)$$

where χ_m is the maximum solar zenith angle for which foF1 is observed and both f_s and n are empirically derivable parameters which depend on geomagnetic latitude ϕ' and solar activity (Ducharme et al., 1971, 1973). For equatorial stations foF1 may be obtained, with an accuracy better than 5% from (14) and the relationship given by Aremu (1987) as:

$$f_s = 4.438 + 0.0041\phi' + 0.0077R \qquad (15a)$$

and

$$n = 0.085 + 0.002\phi' + 0.002R \qquad (15b)$$

The characteristic frequency f_oF2 is the most important factor for radio propagation by ionospheric reflection and it determines the maximum usable frequency. Its diurnal ard seasonal variations at low latitudes are influenced by the eqatorial anomaly resulting in large departures from variations predicted by a Chapman model.

The peak in the diurnal variation f_oF2 occurs outside local noon. A single pre-noon peak occurring typically between 08 and 10 hr is common. At sunspot minimum two peaks are common,one occurring before noon and the other in the afternoon thereby giving rise to a noon bite-out instead of a noon peak (Olatunji, 1966; Adeniyi, 1980). It has also been found that on about 10 percent of the time during sunspot maximum, midnight median values of f_oF2 at low latitude stations are equal or greater than corresponding noon values (Awe, 1975). Large local time variations of f_oF2 especially during sunrise hours have been observed at low-latitude stations. Lakshmi et al. (1980) have reported normalized percentage changes in f_oF2 that were sometimes higher than 300 percent at 5.00 a.m. for Kodaikanal (Geomagnetic Latitude 0.5^oN) during low solar activity compared with changes of about 50 percent for Brisbane (Geomagnetic latitude 35.7^oS). (Fig. 16). The changes have been found to gradually decrease with increasing geomagnetic latitude reaching very marginal values at latitude of about 30^o and above.

Anomalous seasonal variations in f_oF2 have also been observed at low latitude stations. Using midnight median f_oF2 data for Ibadan for about two solar cycles (1954-1973), Awe (1980) has found that values of f_oF2 at midnight are much lower during June solstice (Local summer) than December solstice (Local winter) as shown in Fig. 17. For noon f_oF2, the seasonal anomaly is favoured at sunspot maximum but not at sunspot minimum (Lyon, 1965). It is unlikely that the anomaly is consistently present in the daytime f_oF2 for stations within about 10^o magnetic latitude of the magnetic equator (Olatunji, 1967).

Such a complex variation in the F2 region does not readily lend itself to a simple representation in terms of cos . Instead, several attempts have been made to represent the variations by a variety of mathematical functions of varying degrees of complexity (Jones and Gallet, 1963 , 1962; Yonezewa, 1971; Chiu, 1975). In order to obtain f_oF2 and hmF2, resort is usually made to numerical maps of the parameters f_oF2 and the propagation factor for a distance of 4000km, M(4000)F2, that are presented in CCIR reports (1983) for solar index values R_{12} = 0 and 100, for each month and for different univeral times. The variation of

f_oF2 with sunspot number for $R_{12} \leq 100$ can be represented approximately by a linear relationship between R_{12} and f_oF2. For $R_{12} > 100$, the relationship can be extrapolated to give:

$$f_oF2 = f_o + 0.01(f_{100} - f_o)\, R_{12} \qquad (16)$$

where f_o is the value of f_oF2 for $R_{12} = 0$ and f_{100} is the value of f_oF2 for $R_{12} = 100$. Similar relationships are applicable to hmF2. For example, using the annual values of f_oF2 and hmF2 averaged over 09, 12 and 15 hr for the years 1952-1964, Lyon (1965) has obtained for Ibadan the empirical relations:

$$f_oF2 = 6.96(1 + 8.50 \times 10^{-3} R)\ \text{MHz} \qquad (17)$$

$$hmF2 = 325(1 + 2.06 \times 10^{-3} R)\ \text{km} \qquad (18)$$

where the unsmoothed sunspot number $R \leq 100$.
Long-term and seasonal variations of hmF2 for Ibadan are shown in Fig. 17.
More generally, hmF2, can be estimated from the formula given by Bradley and Dudeney (1973):

$$hmF2 = \frac{1490}{M(3000)F2 + M} - 176\text{km} \qquad (19)$$

with

$$\Delta M = \frac{0.18}{x - 1.4} + \frac{0.096(R_{12} - 25)}{150} \qquad (20)$$

where $x = f_oF2/f_oE$ or 1.7, whichever is the larger. M(3000)F2 is related to M(4000)F2 by the equation:

$$M(4000)F2 = 1.1 \times M(3000)F2 \qquad (21)$$

2.4. Total Electron Content

Total elcolumnar electron content (TEC) has been estimated mainly from measurements of Faraday rotation which applies up to altitudes of about 1000 -2000 km encompassing the major portion of the ionosphere. TEC for this altitude range is usually denoted by N_I to distinguish it from TEC measured to the height of geostationary satellite which is denoted by N_T. Very high values of N_I in the world occur in the low latitude region with the highest values occurring at the crest of the equatorial anomaly. This is

easily seen by considering the latitudinal values at a given longitude in Fig. 18. Figure 18 further indicates that N_I at low latitudes is of the order of 10^7 el/m^2.

Measurements of N_I at low latitudes have been reported by several authors, for instance by Skinner (1966) and Olatunji (1967) in Nigeria, Hunter and Webster (1966) in Kenya, Grimolizzi et al. (1978) and Ortiz de Adler and Ezquer (1987) in South America and Somayajulu (1983) in India. In general, the diurnal and seasonal variations are similar to those in NmF2. Near the equator, the daytime maximum value occurs in the afternoon and it is of the order of 3×10^7 el/m^2 close to sunspot minimum conditions. Measurements at Ibadan (dip 6°S) by Olatunji (1967) illustrate the diurnal pattern during low solar activity (Fig. 19), and the top side/bottom side electron content ratio for N_I which depends on time of the day with a maximum of about 3.5 occuring at about 03 h and a minimum of about 0.4 occurring about 06 h. The seasonal variation of N_I is semi-annual with equinoctial peaks and a minimum in local summer. N_I also exhibits the equatorial anomaly such that near the peak of the anomaly, the daytime maximum value is about twice that observed near the trough (Ma and Walker, 1983). Figure 20 which shows the diurnal and seasonal variations of N_I for Ascension Island (Geographic 8°S 14°N and mag dip 31°S), illustrates the patterns near the anomaly crest for sunspot maximum conditions. Maximum values during the day could reach values as high as 12×10^{17} el/m^2, there are also post sunset very high values and high day-to-day variability as well. On the average, equinoctial values are higher than solstial values. Similar results have been reported by Ortiz de Alder and Ezquer (1987) for Tucuman which is near the crest of the anomaly in South America. Several features of the diurnal and seasonal variations in N_I can be explained by corresponding features of the equatorial electrojet strength: the day-to-day variability during the solar minimum conditions (Klobuchar, 1983), the post sunset high values (Anderson and Klobuchar, 1983) and the latitude of the crest of the anomaly which is wide on days of strong electrojet and absent on days of no electrojet or counter electrojet (Rao et al., 1983)

The variation of N_I with solar activity is of the type

$$N_I = N_o(1 + a(S-b)) \qquad (22)$$

where S is the smoothed 10.7cm solar flux. N_o is the value of N_I at S = b and a and b are constants. Usually the value of b ≃ 70 and 80 have been used a and N_o depend on season, latitude and longitude. Equation (22) is illustrated by the results obtained at Ibadan by Onwukwe (1973) over 11-16 hr, which are described by the following equations:

$$\begin{aligned} \text{Spring } N_I &= 2.78(1 + 0.026(S - 80)) \times 10^{17}\ m^{-2} \\ \text{Autumn } N_I &= 2.68(1 + 0.21(S - 80)) \times 10^{17}\ m^{-2} \\ \text{Summer } N_I &= 2.17(1 + 0.019\ (S - 80)) \times 10^{17}\ m^{-2} \\ \text{Winter } N_I &= 2.15(1 + 0.028\ (S - 80)) \times 10^{17}\ m^{-2} \end{aligned} \qquad (23)$$

Fig. 21 shows recent measurements of N_I during a sunspot minimum period (October 1975 - January 1976) at Ootacamund (dip 6°) in India (Donelly et al., 1979). The measurements were made using the Earth-space signal time delay technique (Davies, 1982).

The difference:

$$N_p = N_T - N_I \qquad (24)$$

is regarded as the total electron content N_p in the protonosphere. A comparison of Fig. 21 with Fig. 19 suggests that N_T and N_I have similar diurnal variations. As suspected, if the variations on N_T are due to those in N_I, it is not unlikely that N_p is essentially independent of the hours of the day at low latitudes similar to what has been found at middle latitudes. It is however not reliable to estimate N_p at low latitudes from Figs 21 and 19 as the two results refer to different seasons and longitudes and the measurements at Ootacamund were for slant paths.

3. IONOSPHERIC IRREGULARITIES

Prominent ionospheric irregularities at low latitudes are those associated with sporadic E and spread F observed on vertical incidence ionograms (Fig. 8).

3.1. Sporadic E and E region Irregularities

Sporadic E refers to abnormal E-region ionisation, typically in excess of the normal values and it is an entirely different phenomenon from the normal E-region ionisation which is jointly controlled by the intensity of emissions of solar ultra-violet light and sun's zenith distance (Appleton and Naismith, 1937, 1940). Sporadic E traces on

ionograms are considered as transparent when reflections from greater altitudes are obtained in addition to those from the associated E-region irregularities (Fig. 8). Such traces are indicative of the presence of blebs of ionisation or fluctuations in electron density which are only a few percentages over the ambient ionisation. On the other hand, sporadic E traces are considered as blanketing when reflections from greater altitudes are "blanketed" off (Fig. 8). They are typically indicative of the presence of a thin layer of ionisation which is much enhanced over the ambient.

A comprehensive review of sporadic E has been given by Fejer and Kelley (1980). There are three major sporadic E zones characterised by broadly different properties of Es. These are equatorial zone which is centred on the magnetic equator and about ± 6° dip on both sides (Knecht and McDuffe, 1962; Matsushita 1953; Wright and Hibberd, 1967), the auroral zone which extends beyond about 60° geomagnetic latitude and the temperate zone which is found between the equatorial and auroral zones.

In the auroral zone, sporadic E is mainly a night-time occurrence and would appear to originate from either the auroral electrojet or the precipitation of particles. As sporadic E in the equatorial and temperate zones are those that are of direct interest to low latitudes, no further consideration will be given to the auroral zone.

Sporadic E studies in the equatorial region have been made from ionosonde measurements, radar measurements on 16.25, 49.92 and 146.25 MHz at Jicamarca (e.g. Bowles et al., 1962; 1962; Bowles and Cohen, 1962; Cohen and Bowles, 1967; Balsley and Farley, 1971; Fejer et al., 1975, 1976) and on 7.3, 14.2, 21.3, 29.0 at Addis Ababa (Crochet, 1977; Manuise and Crochet, 1977) as well as from rocket measurements in Thumba (Prakash et al., 1970, 1971a, 1971b) and Punta Lobos in Peru (Pfaff et al., 1985). Ionosonde measurements provide information on morphology; radar measurements on accurate determination of height of returned echoes, threshold velocity conditions, wave number (or irregularity) spectra, relative echo power (etc) while rocket measurements provide additionally, information on the irregularities in the E-region electron density profiles.

In the equatorial zone, daytime occurrence of sporadic-E is predominantly of the equatorial type (Es-q) though a few other types including blanketing Es may be found. Es-q is transparent on vertical - incidence ionograms. From ionogram studies conducted for South American

stations (Bandyopadhyay and Montes, 1963) and Nigerian Stations (Oyinloye, 1969) it is found that near the equator, Es - q is nearly always present over several hours centred about noon. On the contrary, a minimum may be observed around midday for stations with dip angles greater than 6^{o} (Fig. 22). Though there is no significance seasonal variation in the occurrence frequency, there is a tendency of equinoctial peaks for stations close to dip equator and solstial peaks for stations a few degrees from it.

A strong association also exists between equatorial sporadic E irregularities and the equatorial electrojet; these occupy about the same altitude region and latitudinal belt, they exhibit similar temporal variations (Fig. 23), and a reversal of the equatorial electrojet tends to give rise to a disappearance of equatorial sporadic E. The observation by Giraldez et al. (1981) that the width of equatorial sporadic E belt varies slightly with season is a consequence of the fact that the width of the electrojet itself undergoes temporal variations, it is minimum around noon (Agu and Onwumechili, 1981), it tends to be wider during summer solstice than the equinoctial months (Onwumechili and Ogbuechi, 1967) and during low than high solar activity (Agu and Onwumechili, 1981).

Radar studies have shown that equatorial sporadic E irregularities are indeed embedded in the equatorial electrojet and form part of the equatorial electrojet irregularities which are found both during the daytime and nighttime. The irregularities are field aligned in the sense that correlation distance is much greater along the magnetic field than across it and they are aspect sensitive in the sense that echoes are observed only when the wave vector is nearly perpendicular to the earth's magnetic field Radar echoes are typically generated between 93 and 113 km during daytime with the power profile peaking at about 103 km. while the echo region extends over a wider range of altitudes (from 90 to 130 km) during nighttime than it does during daytime (Fig. 24).

The electrojet irregularities have been classified into two types according to the linear instability process responsible for their generation (Balsley, 1969). The type 1 irregularities are thought to be due to a two-stream plasma instability (Buneman, 1963; Farley, 1963, 1965). The plasma becomes unstable and the irregularities are generated when the component of the relative electron-ion drift velocity in the direction of the wave exceeds the ion-acoustic velocity C_s (which is about 360 m/s in

the electrojet region). The phase velocity of the wave is independent of the zenith angle but increases with decreasing wavelength, slightly at VHF and significantly at HF. The type 1 irregularities are associated with strong electrojet and they dominate the small scale irregularities down to 1m wavelength sizes. The type 2 irregularities are considered to be due to a gradient drift instability (Maeda et al., 1963; Rogister and D'Angelo, 1970) which generates modes at wavelengths greater than about 10m. The gradient drift instability operates in a plasma with a gradient in ionization density and with different electron and ion drifts perpendicular to the density gradient. In the electrojet region the different drifts occur since the ions are collision dominated while the electrons move through an essentially collisionless magnetized plasma. Depending on the time of observation, electron density gradient of a given sign promotes the generation of the type 2 irregularities while gradient of the opposite sign inhibits them. In the daytime when the horizontal electric field is eastwards, the vertical Hall polarization field which is set up in the presence of the earth's magnetic field is upwards and the condition for the generation of type 2 irregularities is that the electron density height gradient be positive. In the nighttime when the horizontal electric field is westwards, the vertical Hall polarization field is downwards and the condition for the generation of type 2 irregularities is that the electron density height gradient be negative. This is illustrated by Figs 25 and 26. During an evening twilight flight over Thumba (Flight 10.13 at 1856h IST on February 2, 1968), type 2 irregularities were observed in the positive electron density gradients whereas during a near midnight flight (Flight 20.08 at 2300h IST on August 29, 1968), the irregularities were observed in the negative electron density gradients (Prakash et al., 1971b). The gradient instability is also known as the cross field instability. The type 2 irregularities are observed at weak electrojet relative to the electrojet stength for the type 1 irregularities. They therefore occur regularly at night except during counter electrojet conditions. Type 2 irregularities are observed at very small electron drift velocities and hence must need only very small threshold electron drift velocities, if any at all, for their generation. The average phase velocity of the irregularities is smaller than the ion-acoustic velocity and it is proporational to

the sine of the zenith angle - a fact which suggests that the type 2 irregularities move with the electrojet drift velocity. Type 2 irregularities are associated with equatorial sporadic E (Es - q) on ionograms.

Irregularity sizes observed during the daytime are different from those observed during the nighttime. During daytime flights over Thumba (Flights Nike Apache 10.37 and 10.38 at 10.40h IST and 11.10h IST respectively on January 28, 1971.), large scale irregularities in electron density in the scale sizes 30 - 150m and with amplitudes of about 10% were limited to the 87 - 98 km height region while only small scale irregularities in the scale sizes 1-15m with peak irregularity amplitude of about 1% were observed about 100km (Fig. 27). The daytime peak 1-15m irregularity amplitude occured at about 105km (Prakash et al., 1971a). On the other hand the large scale irregularities with scale sizes 30 - 150m of 5-30% span the height range of about 90 - 130km at night. (Fig. 26). Sporadic E traces on ionograms, corresponding to the type 2 electrojet irregularities are transparent.

The occurrence frequency of blanketing Es in the equatorial belt is much less than at temperate latitude and it decreases rapidly as the dip equator is approached. Knecht and Mcduffie (1962) noted that in South America, blanketing sporadic E was at last fifteen times less prevalent at two locations within 2.5° of the dip equator than at stations having dips of 5° or more and this led them to conclude that the occurrence of blanketing Es is inhibited close to the dip equator. This pattern of latitude variation is evident in the diurnal curves for the occurrence of daytime blanketing Es (Fig. 28) obtained by Oyinloye (1971) for equatorial stations. The occurrence frequency tends towards peak values in the evening and it is consistently a maximum for all stations during equinoctial periods and a minimum during the June solstice while it increases with decreasing solar activity (Oyinloye, 1969). The monthly mean hourly occurrence probability p of blanketing Es for fbEs $\geq f_o$ at equatorial stations has been found by Oyinloye (1973) to satisfy the logarithmic relation:

$$\log_e p = \frac{f_2 - f_o}{f_1} \qquad (25)$$

where f_2 and f_1 are constants for a given location and time. The corresponding mean blanketing frequency is then given by:

$$fbEs = f \qquad (26)$$

The values of the plasma frequency above which occurrence probability is less than one percent are about 7 MHz and 3 MHz during the day and nighttim respectively. These values are not strongly dependent on solar activity.

Though the mechanism for generating blanketing sporadic E in the equatorial region is obscure, it seems that conditions which inhibit the occurrence of equatorial type sporadic E tend to favour the occurrence of blanketing sporadic E in the region (Oyinloye, 1969). As such, blanketing Es occurs often during the counter electrojet phenomenon (Hutton and Oyinloye, 1970) and the presence of sporadic E in the electron-density profile over Thumba during counter electrojet conditions is illustrated in Fig. 29.

In the temperate zone, sporadic E is characterized by a summer maximum. Its occurrence probability, based on the Es top frequency f_oEs a observed on ionograms has been studied extensively (Smith 1957; Smith, 1978 and occurrence probability curves are contained in Annex I to recommendati 534-I of CCIR (1986). Intense Sporadic E in the temperate zone is often associated with a thin layer observable in rocket measurements of E-region electron density (Smith and Mechthy 1972) and the theory of a wind-shear mechanism for its production (Dungey, 1959; Axford, 1963) has gained wide acceptance.

More recently, Giraldez (1980) has proposed a prediction formula for fbEs which is found to give a good fit to observed fbEs data for geographic latitude 20° to 40° in both hemispheres. According to his formula:

$$fbEs(Mhz) = 3.8440\,(1 + 1.7374 \times 10^{-3}R) \times (\cos\chi)^{0.25} \times \exp\frac{(|lat| - \phi)^2}{52.26^\circ}(\cos\chi)^{0.73} \qquad (27)$$

and

$$\phi = 150.0^\circ(\cos\chi - \frac{\cos^2\chi + \cos^3\chi}{9}) + 7^\circ$$

where R and χ are sunspot number and solar zenith angle respectively.

Oyinloye (1973) has found that equations (25) and (26) fit the observed data for Port Stanley which is in the temperate zone. It will be

interesting to compare with the observed, the values of fbEs predicted by equations (25) and (26) on one hand and equation (27) on the other hand for stations in the temperate zone.

3. Spread F and F region irregularities

Ionosonde observation of spread F was first reported by Booker and Wells (1938). It appears on vertical incidence ionograms as diffuse echoes from the F region. Two types have been identified (Calvart and Cohen, 1961; Cohen and Bowles, 1961). It is known as the range type if echo-spread occurs at the lower end of the F trace but a clean reflection is found at the higher frequency; sometimes, echoes are received at low frequencies from several distinct layer heights simultaneously. It is the frequency type if the echo spread occurs near the F-layer critical frequency and the trace is clean at low frequencies. Both types of spread F are illustrated on the ionograms for Ibadan (Fig. 8) and Huancayo (Fig. 30). In Fig. 8e, the bottom of the F layer is indicated by the flat part of the F race at the lower frequency and its altitude is given approximately by h'F which is the minimum virtual height of the F trace.

In the vicinity of the magnetic equator, the onset of spread F is usually associated with the post-sunset rise in the height of the F layer (Osborne, 1952; Wright, 1959; Lyon et al., 1961). Figure 31 illustrates the association of percentage occurrence of spread F at Singapore with both h'F and its rate of increase with time. The equatorial belt in spread F lies approximately between 20° north and south of the magnetic equator (Fig. 32) and is nearly always present near the magnetic equator between 20h and 05h during quiet days with a peak in intensity and frequency of occurrence around 2000 - 2100 local time (Lyon et al., 1960, 1961). From a network of low-latitude ionospheric stations in India, it has been found by Rastogi (1983) that during 1965 the peak in the nocturnal occurrence of spread F was around 0000h at Kodaikanal (Geographic lat. 10°N), 0200h at Hyderabad (Geographic lat 17°N), 0230h at Ahmedabad (Geographic lat 23°N) and 0330h at Delhi (Geographic lat. 28°N) thereby suggesting a poleward movement of spread F (Fig. 33).

As seen from Figs. 7 and 30 the echoes for the range type spread F come from a wide range of altitude. Further ionosonde studies have shown that the range type spread F is predominant between the post-sunset and midnight periods, and is more common in high solar epochs with

equinoctial maxima (Skinner and Kelleher, 1971; Chandra and Rastogi, 1972; Rastogi, 1980). Other techniques have also been applied to the study of spread F. These include radar back scatter at HF (Clemesha 1964; Kelley et al., 1986), VHF (Kelleher and Skinner, 1971; McClure and Woodman, 1972; Woodman and LaHoz, 1976) and UHF (Tsunoda et al., 1982) rocket measurements (Szuszczewicz et al., 1980; Kelley et al., 1986) and in-situ satellite measurements (Hanson and Sanatani, 1973; Dyson et al., 1974; McClure et al., 1977; Dyson and Benson, 1978; Aarons et al., 1980). Apart from generally confirming ionosonde spread F results, these studies give insight into the nature and cause of the equatorial spread F irregularities. Premidnight radar echoes at HF, VHF and UHF are associated with the range type spread F on ionograms. The echoes are predominant in the post-sunset to midnight period with equinoctial maxima and solstial minima and there is a tendency to receive more echoes from the west than the east (Clemesha, 1964; Kelleher and Skinnar, 1971; Balsley et al;, 1972). It has in fact been demonstrated by Rastogi (1984) that the altitudes of strong echoes from the 50MHz Jicarmaca radar show excellent correspondence with the altitudes of range spread F on Huancayo ionograms (Fig. 34a) whereas radar echoes do not accompany frequency spread F on ionograms. (Fig. 34b). From the modified ranged-time-intensity radar (MRTI) plot (Fig. 34a) and digital back scatter power maps (Fig. 35) of spread F echoes, it has been found that spread F can occur at altitudes as low as 200km and as high as 1000 km (Woodman and LaHoz, 1976; Kelley et al, 1986). Thus spread F can occur below, at or above the altitude of peak electron density, that is in regions of positive, zero or negative delectron density. The associated equatorial spread F irregularities have scale sizes ranging from some few centimetres to hundreds of kilometres (Fejer and Kelley, 1980; Kelley, 1985) and several orders of magnitude in the spectral intensity $I_n = (\delta n/n)^2$ of the plasma fluctuations. I_n is wave number (K) dependent such that the power spectrum may be represented by $I_n \propto k^{-n}$ where n, in this case is the power spectral index. Values of n from about 1 to 5 have been reported, depending on the size and altitude location of the irregularities. The values have been discussed in several reviews (Fejer and Kelley, 1980; Kelley, 1985; Kelley and McClure, 1981; Kelley et al., 1986). The irregularities are strongly field aligned (Cohen and Bowles, 1961; Kent and Koster, 1967; Dyson and Benson, 1978). They are also highly structured both in altitude

(Woodman and LaHoz, 1976) and horizontally (Tsunoda et al., 1982). Figure 34 illustrates the structuring in altitude. In this case, the phenomenon has as many as 15 layers or blobs separated into two well defined patches, one in the altitude range between 170 and 450 km and the other in the altitude range between 500 and 600 km. (Woodman and LaHoz, 1976). On the other hand, Fig. 36 illustrates horizontal structuring. In that Figure, the scanning Altair radar was able to map out several plumes as well as large modulation of bottomside density (Tsunoda, 1983). The layer also seems tilted with lower heights on the western than eastern sides. Wave like bottom structures in the 200 -1000 km range in the east-west direction have earlier been detected by Rottger (1973) in his off-great-cicle propagation experiment. The development and the features of equatorial spread F irregularities vary from night to night (Woodman and LaHoz , 1976). On a night of weak spread F, such as that of March 26 1974 at Jicarmaca (Fig. 37), the phenomenon starts in a thin layer at the bottom of the F layer, rises to an apogee and then falls in altitude as it decays while maintaining the thin layer form throughout the night. On a night of strong spread F such as that of March 19 1974 at Jicarmaca (Fig; 38) the phenomenon starts as a thin scattering layer at the bottom of the F layer, then rises and broadens, becoming stronger; just after the apogee series of bifurcations of the blobs of ionisation occur and as the layer further decends a large plume-like structure occurs between 2300 and 2400h, capped with a large diffuse region of irregularities with its peak reaching about 750km. The plume has a tilt to the right indicating an east-west asymmetry (Woodman and LaHoz, 1976). Another well developed plume is that of March 6, 1983 at Jicarmaca (Fig. 35). The plume which extends to more than 1000km is preceded by a bifurcated form and a sudden increase in height. Plumes usually evolve from a thin layer of bottom side irregularities. Evidence now abounds that plumes on backscatter radar maps are associated with regions of plasma depletion in the topside ionosphere with biteuts of up to 3 orders of magnitude (McClure et al., 1977; Kelley et al., 1986); this is illustrated by Fig. 39. Ion composition inside the biteouts has actually indicated that they originated at altitudes below the F peak (Hanson and Sanatani, 1971; McClure et al., 1977) and then convects to the topside ionosphere.

Direct measurements of the plasma drift inside the depletions indicate, that with respect to the background, the plasma either moves up vertically or remains stationary (McClure et al., 1977; Hanson and Bamgboye, 1984); the upward movement is usually associated with a westward motion (McClure et al., 1977) while meridional motions, as shown in Fig. 40, have been found to be poleward (Hanson and Bamgboye, 1984). F-region irregularities often produce deep and rapid fluctuations of amplitudes and phase, known as scintillations (Fig. 41) VHF and GHz signals from satellites in their passages through the ionosphere. Such scintillations often accompany plumes on Jicarmaca 3m radar back scatter power maps. The scintillations are usually strong on the GHz signals and even saturated on VHF signals. Figure 42 compares features of the Jicarmaca radar maps with the SI and S_4 scintillation indices of 1.7 GHz satellite signals received at Ancon near Jicarmaca and it is seen that strong scintillations are associated with the 'plumes'. The scintillation index is given by Whitney et al., (1969) as:

$$SI = \frac{P_{max} - P_{min}}{P_{max} + P_{min}} \qquad (28)$$

where P_{max} and P_{min} are the power (dB) corresponding to the third highest peak and the third deepest trough respectively within the same 15 min interval while S_4, due to Briggs and Parkin (1963) is defined as:

$$S_4 = \sqrt{\frac{(p - \bar{p})^2}{\bar{p}}} \qquad (29)$$

where p and $\bar{p}$ are the power and average power respectively. The plasma depletions associated with 'plumes' have often been regarded as plasma 'bubbles' but there are also possibilities that the depletions or holes do not pinch off as in the 'bubble' picture but form wedge shaped regions of depleted density extending into the bottom side (Fejer and Kelley, 1980; Kelley et al, 1986). The range spread F associated irregularities are usually ascribed to the generalized collisional Rayleigh - Taylor (GRT) instability (Dungey, 1956; Ossakow, 1976, Scannapieco and 1981; Fejer and Kelley, 1980; Kelley et al., 1981; Kelley 1985). The generalized Rayleigh - Tayl instability incorporates the roles of electric field and neutral winds in destabilising plasma and the gravitational term. At the magnetic equator, the gravitational term is unstable, whenever the earth's gravitational

acceleration g has a component antiparallel to the plasma density gradient and the local linear growth rate is given by

$$\gamma_g = g/\nu L \qquad (30)$$

where ν is the ion-collision frequency and L is the gradient scale length $(N(-\partial N/\partial z)^{-1})$. The electric field term is unstable when $\underline{E} \times \underline{B}$ is parallel to n and the local linear growth rate is given by

$$\gamma_E = E/BL \qquad (31)$$

An eastward electric field seems important in destabilising the bottomside F layer as in the commencement of Spread F (Fejer and Kelley, 1980), and as in the electric field reversals at night (Rastogi and Woodman, 1978b). The gravitational term is considered important in the 'plume' processes (Kelley et al., 1986), the westward tilt being explained by Ott (1978) and Burke et al. (1979) in terms of an effective gravitational force:

$$\underline{g}' = \underline{g} - \nu \underline{U} \qquad (32)$$

where ν is the ion-neutral collision frequency and $\underline{U}$ is the neutral wind velocity in the plasma frame. There are arguments in favour of gravity waves being responsible for the seeding of large scale irregularities, about 20km or greater (Booker, 1979; Fejer and Kelley, 1980; Kelley, 1981) and velocity shear playing an important role in determining plume spacings (Kelley et al., 1986).

The frequency type spread F and associated F region irregularities have been less intensively studied. The frequency type spread F is more common between midnight and sunrise. It is also more common in sunspot minimum in the June solstice months at Nairobi, and Thumba but in the December solstice months in Huancayo (Skinner and Kelleher, 1971; Chandra and Rastogi, 1972), Rastogi, 1980). A strong association between frequency type spread F and patches of irregularities in the bottom side F region known as bottomside (BSS) irregularities has been reported (Valladares etal., 1983). Based on the analysis of the data from the retarding potential analyzer (RPA) and the ion drift meter (IDM) on the Atmosphere Explorer Satellites AE-C and AE-E over 1977 - 1980, they have found that the BSS irregularities are inherently a nighttime phenomena, occurring from after local sunset to about 6.00 a.m., with peaks near midnight and a seasonal variation, with maxima at the

solstices; 87 per cent of the BSS events were found to occur between the limit of $\pm$ 10° dip latitude and were never seen at dip latitudes greater than $\pm$ 15° compared to other equatorial irregularities found at up to about $\pm$ 20°, BSS irregularities can coexist with "bubbles" or be found on their own. Unlike the range spread F associated irregularities, the BSS irregularities could extend over several thousand kilometres in the east-west direction and are associated with VHF but not GHz scintillations (Basu and Basu, 1985). It is also plausible that the generalized Rayleigh - Taylor instability would explain the BSS irregularities (Valladares et al., 1983).

4. IONOSPHERIC DISTURBANCES AND STORMS

4.1. General Consideration

The primary sources of ionization for the 'quiet' ionosphere is radiation from the sun. In like manner, ionospheric disturbances and storms are associated with occurrence of solar flares during 'active sun' conditions. A flare is a sudden short-lived brightening of the solar surface in the neighbourhood of a sunspot and is most easily observed in the H light, = 656.3nm (Friedman, 1960). Flares may be classified primarily as 1, 2 or 3 in order of its increasing size and importance. Average duration of class 1 flare is about 20 minutes while that of class 3^+ is about 180 min. The occurrence of a flare is often accompanied by sudden increase in the solar emission of radio waves, X radiation and ultraviolet radiation as well as the emission of relativistic cosmic ray particles and highly energetic particles. The schematic diagram of Fig. 43 (Davies, 1965) clearly illustrates the effects of solar emissions during a solar flare on the ionosphere and the earth's magnetic field.

The enhanced electromagnetic radiation which travels with the speed of light in free space gives rise to sudden enhanced ionisation in the D region leading to what is usually called 'Sudden Ionospheric Disturbances' or SID. These disturbances are usually observed only in the sunlit hemisphere and may last between about 20 to 90 minutes. The effects that may be listed under SID are sudden short-wave fade out or SWF of radio transmissions as a result of enhanced D region absorption,

sudden cosmic noise strong absorption SNA, sudden phase anomalies or SPA in the phase difference between ground and ionospheric waves of very long waves reflected from the base of the ionosphere due to the lowering of the altitude of the base, sudden enhancement of atmospherics or SEA at 27 kHz and magnetic crochet which is sudden enhancement of the earth's magnetic field associated with strong flares, typically of class 3 types.

The cosmic particles and the stream of energetic particles from the sun take about ½ hr to several hours and 20 to 40 hours respectively to reach the earth (Davies, 1965) and as such impose delayed effects on the ionosphere and the earth's magnetic field. The delayed disturbance of the ionosphere is called an ionospheric storm while the accompanying disturbance of the magnetic field is called a magnetic storm.

The D- and F region but not the E region are strongly effected by ionospheric storms. During an ionospheric storm, incoming protons produce visible aurora while very energetic electrons ionize the D region and hence cause increase in D region absorption which may lead to total disappearance of high frequency signals in the polar regions, a phenomenon known as polar blackout or PCA. Worldwide, ionospheric storm is most easily observed in the F region. An increase in the height of the F layer is observed and depending on the latitude, an increase or decrease in foF2 may be observed. From the statistical average of the effects of 51 strong storms and 58 weak storms that occurred over the period 1946 to 1955, Matsushita (1959) found that severe depressions in NmF2 (and hence foF2) occurred in geomagnetic latitudes of 45^{0} and higher, only mild depressions occurred in intermediate latitudes while an increase occurred in equatorial regions. The detailed results are illustrated in Fig. 44.

A statistical relationship between sunspot number R and the number of class of flares F is known to exist (Friedman, 1960). This is given as follows:

$$\begin{aligned} F &= 0.044\,R \text{ for Class 1} \\ &= 0.015R \text{ for class 2} \\ &= 0.002R \text{ for class 3} \end{aligned} \qquad (33)$$

This relationship suggests that ionospheric storms would occur rarely and with a greater number during high solar activity. This is butressed

by the statistics given by Mitra (1982) and shown as Table 1.

A magnetic storm is typically characterized by three phases which are the initial phase (sometimes the sudden commencement), the main phase and the recovery phase (Fig. 45). Relative to a quiet day field variation the initial phase corresponds to an increase in the horizontal component H of the time variations in the earth's magnetic field and it occurs simultaneously all over the world. Storm time is reckoned from the initial phase. The main phase corresponds to a rapid and substantial decrease in H and the recovery phase corresponds to a slow increase in H back to the quiet day value. A magnetic storm may last several days. The degree of a magnetic disturbance may be indicated by such magnetic indices as the planetary 3-hour indices k_p, and the daily values of the world wide indices A_p or C_p. Values of k_p range from 0_o to 9_+, c_p from 0.0 to 2.0 and A_p, given in positive integers, may be as high as 40 or more. Low values of these indices represent quiet magnetic conditions while very high values represent magnetic storm conditions. Magnetic storms are ascribed to a complexity of disturbance currents which are superimpose on the normal queit current system sq and which are caused by the stream of energetic particles from the sun. These currents, which include the disturbance charged flux current (DCF) , the auroral electrojet and the ring current, have been discussed in a review paper by Chapman (1965.).

4.2. Low latitude Effects

Enhancement in short wave ionospheric absorption, associated with sudden ionospheric disturbance or shortwave fade out has been reported for equatorial stations both at vertical incidence (Skinner 1957, Gnanalingam, 1974) and oblique incidence (Shamsi, 1986). These are illustrated by Fig. 46. On the contrary no significant difference has been found on the average values of ionospheric absorption on magnetically quiet and disturbed days (Gnanalingam, 1974).

On the average, the E region is not affected by ionospheric storms. Significant changes in NmE or foE that is associated with magnetic storms have been detected only on very rare occasions. Adeniyi (1980, 1987) compared hourly monthly means of NmE for disturbed days at Ibadan with $k_p \geq 5$ and $A_p \geq 26$ with the average for the five most quiet days over the period 1956 to 1966. No significant difference was found between foE on disturbed and quiet days over the low solar activity

period of 1962 - 1966. During the high solar activity period of 1956-1960 differences were observed only on 19 occasions, 16 decreases and 3 increases were observed on magnetically disturbed days relative to the quiet days (Fig. 47). The decreases occurred on storm days with maximum K_p ranging from 6_o to 9_- while maximum K_p on the days of the increase ranged from 9_- to 9_o.

Ionospheric storms have been most noticeable in the F region. On the average, daytime values of f_oF2 and hmF2 or hF2 are higher during disturbed than quiet days at equatorial stations resulting in the disappearance of the noon bite-out during strong magnetic storms; while these effects are most prominent at high sunspot number, they are present during all phases of the solar cycle (Skinner and Wright, 1955; Kelleher, 1965; Olatunji 1966). Though there are reports of both increases (Skinner and Wright, 1955; Kellher 1965) and decreases (Olatunji, 1966) in night-time f_oF2 on disturbed days relative to the corresponding value on quiet days, the increases occur more frequently (Adeniyi, 1986). Adeniyi has further found that usually, daytime and night-time increases in f_oF2 are associated with the main and early part of recovery phase of magnetic storms while daytime decreases are associated with the initial phase of storms (Fig.47). The equatorial anomaly tends to get narrower or dissapear during magnetic storms. Premidnight scintillation, which is associated with range spread F, is also inhibited by magnetic activity. The storm effects in the F layer can be explained primarily on the basis of the $\underline{E} \times \underline{B}$ force. When the effective electric field is eastward, there is a vertical upward motion of plasma which, leads to a drift of F region ionisation away from the equator while the reverse occurs when the effective electric field is westward. Thus when an eastward electric field is enhanced during a magnetic storm, a decrease in F region ionisation results around the magnetic equator whereas an increase in F region ionisation results when a westward electric field is enhanced or an eastward electric field is depressed. The postsunset rise in the F layer will also be inhibited during the main phase of a magnetic storm thereby retarding the onset of the F region range spread F irregularities that are primarily responsible for the premidnight equatorial scintillations.

5. SUMMARY

The low latitude ionosphere is under the influence of three major factors, geographic, geomagnetic and the electrojet. The region between about 70km to the E region is primarily under geographic control. The altitude of about 70km marks the reversal height of solar activity in electron density. Below this height, ionisation comes primarily from cosmic radiation and electron density increases as solar activity decreases whereas above this height, ionisation comes primarily from solar radiation and electron density increases with solar activity. From about 70km to the E region, the diurnal variation in electron density has a maximum at about noon, though with a little asymmetry such that the value of electron density for a given value of zenith angle is greater in the afternoon than in the morning. There is also little day-to-day variability in the electron density.

The influence of the electrojet per se is manifest primarily in the sporadic E irregularities. The electrojet irregularities are embedded in the electrojet itself and are co-located in space (altitude and width) with the electrojet and have the same temporal variations (diurnal, seasonal, solar-cycle or long term) with the electrojet. They also exhibit high day-to-day variability. The other type of sporadic E of importance is the blanketing type which tends to thrive under conditions that inhibit the occurrence of equatorial type sporadic E. The electrojet influence on sporadic E seems to be confined to a region of about $\pm$ 3 magnetic latitudes beyond which the features of midlatitude sporadic E creap in.

Geomagnetic control takes over in the F region and beyond. The underlying force is the $\underline{E} \times \underline{B}$ force. When the electric field is eastward, there is an upward vertical movement of ionisation which then diffuses along the magnetic field lines, leading to outward flow of plasma from the region centred about the magnetic equator and the occurrence of ionisation peaks about $\pm$ 15^o to 20^o magnetic latitude. When the electric field is westward, there is a downward movement of ionisation and into the region centred about the magnetic equator. This phenomenon accounts, in the main, for the F - region latitude distribution of ionisation known as the equatorial anomaly, the appearance of a trough in the diurnal variation of F region ionisation around noon and the increase (or decrease) in F region ionisation during ionospheric

storms. Spread F irregularities and the occurrence of the associated scintillations in VHF and GHz satellite signals are also influenced by the $\underline{E} \times \underline{B}$ force such that the latitude extent of both seem to coincide with that of the equatorial anomaly. Arising from the high day-to-day variability in the electric field, corresponding high day-to-day variability is also observed in F-region phenomena such as the electron density, the development and features of the equatorial anomaly, equatorial spread F irregularities and scintillations.

A common feature of the seasonal variation in low latitude phenomena is the semiannual variation with equinoctial maxima. This is found in the seasonal variation of short wave ionospheric absorption, incidence of sporadic E, F-region ionisation, total electron content, the incidence of range type spread F equatorial irregularities and associated VHF and GHz scintillations.

REFERENCES

D-Region

Aikin, A.C. and Blumle, L.J. (1968). Rocket measurements of the E-region electron concentration distribution in the vicinity of the geomagnetic equator. J. Geophys. Res., 73, 1617-1626.

Aikin, A.C., Goldberg, R.A., Somayajulu, Y.V. and Avadhanulu, M.B. (1972). Electron and positive ion density altitude distributions in the equatorial D-region. J. Atmos. Terr. Phys., 34, 1483-1490.

Diemenger, W., Rose, G., Schwentek, A. and Widdel, A.U. (1967). The morphology of winter anomaly of absorption; Space Research, VII, 228-239.

Gnanalingam, S. (1974). Equatorial ionospheric absorption during half a solar cycle (1964 - 1970). J. Atmos Terr. Phys., 36, 1335-1354.

Mitra, A.P. and Rowe, J.N. (1974). Ionospheric constraints of mesospheri nitric oxide. J. Atmos. Terr. Phys., 36, 1797-1808.

Oyinloye, J. O. (1978). On the seasonal variation of absorption of radio waves in the equqtorial ionosphere. J. Atmos. Terr. Phys., 40, 793-798.

Ratnasiri, P.A.J. (1977). D-region processes at equatorial latitudes. J Atmos. Terr. Phys., 39, 999-1009

Rose, G., Widdel, H.U., Azcarraga, A. and Sanchez, L. (197). Results of an experimental investigation of correlations between D-region neutral ga winds density changes and short-wave absorption Radio Sci., 7, 181-191.

Shapley, A.H. and Beynon, W.J.G. (1965). Winter anomaly in ionospheric absorption and stratosphere warmings. Nature, London, 206, 1242-1243.

Subbaraya, B.H., Prakash, S. and Gupta, S.P., (1983). Electron densities the equatorial lower ionosphere from the Langmiur probe experiments condu ted at Thumba during the years 1966-1978. Indian Space Research Organizat Bangalore Scientific Report ISRO-PRL-SR-15-83.

Subbaraya, B.H., Prakash, S. and Gupta, S.P. (1985). Structure of the equatorial lower ionosphere from the Thumba Langmiur probe experiments. Adv. Space Res., 5, 35-38.

Thomas, L. (1962). The winter anomaly in ionospheric absorption. J. Atmos. Terr. Phys., 23, 301-317.

Thrane E.V. and Piggott, W.R. (1966). The collision frequency in the E- and D-regions of the ionosphere. J. Atmos. Terr. Phys., 28, 721-737.

E-Region

Aremu, A.O. (1987). Modelling of equatorial ionospheric E- and F1 regions. M.Sc. Thesis Univ. Ilorin.

Aremu, A.O. and Oyinloye, J. O. (1988). Prediction of ionospheric E-layer maximum electron density and critical frequencies at equatorial stations. Paper presented to the 1988 Annual Conference of the Nigerian Union of Planetary and Radio Sciences, Lagos, Nigeria.

Kouris, S.S. (1971). Ph.D. Thesis Edinburgh Univ.

Kouris, S.S. and Muggleton, L.M. (1973)a). Diurnal variation in the E-layer ionization. J. Atmos. Terr. Phys., 35, 133-139.

Kouris, S.S. and Muggleton, L.M. (1973b). World morphology of the Appleton E-layer seasonal anomaly. J. Atmos. Terr. Phys., 35, 141-151.

Muggleton, L.M. (1971). Solar cycle control of NmE. J. Atmos. Terr. Phys., 33, 1307-1310.

Muggleton, L.M. (1975). A method of predicting foE at any time and place. Telecomm. J. 42, 413-418.

Piggott, W.R. and Thrane, E.V. (1966). The electron densities in the E- and D-regions over Kjeller, J. Atmos. Terr. Phys., 28, 467-479.

F-Region

Adeniyi, J.O. (1980). A study of some features of the equatorial ionosphere on magnetically quiet and distrubed days. Ph.D. Thesis Univ. Ibadan.

Awe, O. (1975). Some aspects of the behaviour of nighttime F-layer at low latitudes. J. Atmos. Terr. Phys., 37, 181-183.

Awe, O. (1980). A note on the variation of midnight foF2 at Ibadan Nig. J. Sci., 14, 125-131.

Aremu, A.O. (1987). (As under E-region refernences).

Bradley, P.A. and Dudeney, J.R. (1973). A simple model of the vertical distribution of electron concentration in the ionosphere. J. Atmos. Terr. Phys., 35, 2131-2146.

Chiu, Y.T. (1975). An improved phenomenological model of ionospheric density. J. Atmos. Terr. Phys., 37, 1563-1570.

Croom, S.A., Robins, A.R. and Thomas, J.O. (1959). Two anomalies in the behaviour of the F2 layer of the ionosphere. Nature, 1984, 2003-2004.

Ducharme, E. D., Petric, L.E. and Eyfrig, R. (1971). A method for predicting the F_1 layer critical frequency. Radio Sci., 6, 369-378.

Ducharme, E.D., Petric, L.E. and Eyfrig, R. (1973). A method for predicting the F_1 layer critical frequency based on the Zurich smoothed sunspot number. Radio Sci., 8, 837-839.

Hanson, W.B. and Moffett, R.J. (1966). Ionization transport effects in the equatorial F-region. J. Geophys. Res., 71, 5559-5572.

Jones, W.B. and Gallet, R.M. (1963). The representation of diurnal and geographical variations of ionospheric data by numerical method. Telecomm. J., 29, 129-149 and Radio Sci., 66D, 419-438.

King, J.W., Smith, P.A. Eccles, D., Fooks, G.F. and Helm, H. (1964). Preliminary investigation of the structure of the upper ionosphere as observed by the topside sounder satellite alouette, Proc. Roy. Soc. A281, 469-487.

King, J.W. Reed, K.C., Olatunji, E.O. and Legg, A.J. (1967). The behaviour of the topside ionosphere during storm conditions. J. Atmos. Terr. Phys., 29, 1355-1363.

Lakshmi, D.R., Aggarwal, S., Pasricha, P.K. and Raddy, B.M. (1980). HF communication problems due to steep spatial and temporal gradients. Solar terrestrial predictions proceedings, Vol. 4, ed. R.F. Donnelly, pp. D2-58-D2-64.

Lyon, A.J. (1965). The F2 region at Ibadan over a sunspot cycle. Part-I Solar cycle and annual variation. Proc. Second International Symposium on equatorial aeronomy, ed. F. de Medonca, pp. 129-134.

Lyon, A.J. and Thomas, L. (1963). The F2 region equatorial anomaly. J. Atmos. Terr. Phys., 25, 373-386.

Olatunji, E.O. (1966). Some features of equatorial ionospheric stoms. Ann. Geophys., 22, 485-491.

Olatunji, E.O. (1967). The total columnar electron content of the equatorial ionosphere. J. Atmos. Terr. Phys., 29, 277-285.

Rastogi, R.G. (1959a). Geomagnetic influence on the F1 and F2-regions of the ionosphere-effect of solar activity. J. Atmos. Terr. Phys., 14, 31-40.

Rastogi, R.G. (1959b). The diurnal development of the anomalous equatorial belt in the F-2 region of the ionosphere. J. Geophys. Res., 64, 727-737.

Rush, C.M., Rush, S.V., Lyons, L.R. and Venkateswaran, S.V. (1969). Equatorial anomaly during a period of declining solar activity. Radio Sci. 4, 829-841.

Vila, P. (1971). New dynamic aspects of intertropical F2 ionization. Radio Sci., 6, 945-956.

Walker, G. O. and Chan, C.S. (1976). The duirnal variation of the equatorial anomaly in the topside ionosphere at sunspot maximum. J. Atmos. Terr. Phys., 38, 699-706.

Yonezewa, T. (1971). The solar activity and latitudinal characteristics of the seasonal, non-seasonal and semi-annual variations in the peak electron densities of the F2 layer at noon and at midnight in middle and low latitude. J. Atmos. Terr. Phys;, 33, 889-907.

Total Electron Content

Anderson, D.N. and Klobuchar, J.A. (1983). Modelling the total electron content observations above Ascension Island. Proc. Int. Symp. on "Beacon Satellite Studies of the Earth's Environment" and Workshop "Beacon Techniques and Applications" Radio Sci. Div., National Physical Laboratory, New Delhi, India, Ed. T.R. Tyagi, p.152.

Davies, K. (1982). Earth-space prediction ICTP Autumn-course on geomagnetism, the ionosphere and magnetosphere. SMR/98-39.

Donnelly, R.F., Davies, K. and Anderson, D.N. (1979). The equatorial total electron content and shape factor. J. Geophys. Res., 84, 7359-7364.

Grimolizzi, O.M.L., Lagori, J.F., Manzano, J.R., Rios, V.H. and Lascano, J.V. (1978). Contenido electronico total sobre Tucuman para el periodo equinoccial de 1975 a partir de senales del satellite Int. as at Revista Geofisica, no. 8, 85, IPGH. Mexico.

Hunter, A.N. and Webster, A.R. (1964). Faraday rotation and other measurements on the ionosphere at Nlarobi, Ann. Geophys., 26, 385-392.

Klobuchar, J.A. (1983). Characterstics of TEC results from satellite beacon studies and application to trans-ionospheric ranging systems. Proc. Inter. Symp. on "Beacon satellite studies of the Earth's Environment" and Workshop "Beacon Techniques and Applications", New Delhi, India, ed. T.R. Tyagi, pp. 3-17.

Ma, J.H.K. and Walker, G.O. (1983). The effect of hm values on the electron content - latitude profile obtained from the reduction of Faraday rotation recordings of satellite beacon radio signals. Ibid. pp. 157-161.

Olatunji, E.O. (1967). The total columnar electron content of the equatorial ionosphere J. Atmos. Terr. Phys., 29, 277-285.

Onwukwe, D.N. (1973). Variation of total electron content and slab thickness with solar activity at Ibadan. Proc. 4th Inter. Symp. on Equatorial Aeronomy, Ibadan, Nigeria, ed. E. Oni pp. 744-751.

Ortiz de Adler, N. and Ezquer, R.G. (1987). Recent progress in electron content studies in Argentina. Proc. Biregional Latin American - Africa Workshop on Radio Propagation research and applications, Buenos Aires, Argentina, pp. 61-71.

Rama Rao, P.V.S., DasGupta, A., Klobuchar, J.A. and Rastogi, R.G.(1983). Electrojet control over the equatorial anomaly in TEC and equivalent slab thickness. Proc. Inter. Symp. on "Beacon Satellite Studies of the Earth's Environment and Workshop "Beacon Techniques and Applications", New Delhi, India, ed. T.R. Tyagi, pp. 393-400.

Skinner, N.J. (1966). Measurements of total electron content near the magnetic equator. Planet. Space. Sci., 14, 1123-1129.

Somayajulu, Y.V.(1983). Twenty-five years of satellite beacon studies in India. Proc. Inter. Symp. on "Beacon Satellite studies of the Earth's Environment" and Workshop "Beacon Techniques and Applications", New Delhi, India, ed. T.R. Tyagi, pp. 99-113.

Sporadic E

Agu, C.E. and Onwumechili, C.A. (1981). Temporal variations of POGO equatorial electrojet parameters. J. Atmos. Terr. Phys., 43, 809-816.

Appleton, E.V. and Naismith, R. (1983). Weekly measurements of upper atmospheric ionization. Proc. Phys. Soc., 45, 389-398.

Appleton, E.V. and Naismith R. (1940). Normal and abnormal Region-E ionisation. Proc. Phys. Soc., 52, 402-415.

Axford, W. I. (1963). The formation and vertical measurement of densed ionized layers in the ionosphere due to vertical wind-shear. J. Geophys. Res., 68, 769-779.

Balsley, B.B., (1969). Some characteristics of non-two stream irregularities in the equatorial electrojet. J. Geophys. Res., 74, 2333-2347.

Balsley, B.B. and Farley, D.T. (1971). Radar studies of the equatorial electrojet at three frequencies. J. Geophys. Res., 76, 8341-8351.

Bandyopadhyay, P. and Montes, H. (1983). Some aspects of E_s ionization of the magnetic equatorial region. J. Geophys. Res., 68, 2453-2484.

Bowles, K.L., Balsley, B.B. and Cohen, R. (1963). Field-aligned E-region irregularities identified with acoustic plasma waves J. Geophys. Res., 68, 2485-2501.

Bowles, K.L. and Cohen, R. (1962). A study of radio wave scattering from sporadic E near the magnetic equator. Ionospheric Sporadic-E, ed. E.K. Smith and S. Matsushita, Pergamon Press, London, pp. 51-77

Buneman, O. (1963). Excitation of field aligned sound waves by electron streams. Phys. Rev. Lett., 10, 285-287.

Cohen, R., and Bowles, K. (1967). Secondary irregularities in the equatorial electrojet. J. Geophys. Res., 72, 885-893.

Crochet M., (1977). Radar studies of longitudinal differences in equatorial electrojet? A review. J. Atmos. Terr. Phys., 39, 1103-1117.

Dungey, J.W. (1959). Effect of a magnetic field on turbulence in an ionized gas. J. Geophys. Res., 64, 2188-2191.

Farley, D.T. (1963). A plasma instability resulting in field aligned irregularities in the ionosphere. J. Geophys. Res., 68, 6083-6097.

Farley, D.T. (1985). Theory of equatorial electrojet plasma waves - new development and current status. J. Atmos. Terr. Phys., 47, 729-744.

Fejer, B.G., Farley, D.T., Balsley, B.B. and Woodman, R.F. (1975). Vertical structure of the VHF backscattering region in the equatorial electrojet and the gradient drift instability. J. Geophys. Res., 80, 1313-1324.

Fejer, B.G., Farley, D.T. Balsley, B.B. and Woodman, R.F. (1976) Radar observations of two-dimensional turbulence in the equatorial electrojet, 2. J. Geophys., Res., 81, 130-134.

Fejer, B.G. and Kelley, M.C. (1980). Ionospheric irregularities. Rev. Geophys. and Space Phys., 18, 401-454.

Giraldez, A.E. (1980). Daytime sporadic E blanketing frequency prediction. Solar-terrestrial predictions proceedings, vol.4, ed. R.F. Donnelly, pp. C-87 to C-106.

Giraldez, A.E., Puig, L. and Lama, I. (1981). Variabilidad de la ionizacion Es equatorial Geoacta, vol. XI, 57-64.

Hanuise, C., and Crochet, M. (1977). Multifrequency HF radar studies of plasma instabilities in Africa. J. Atmos. Terr. Physg 39, 1097.

Hutton, R. and Oyinloye, J. O. (1970). The counter-electrojet in Nigeria. Ann. Geophys., 26, 922-926.

Knecht, R.W. and McDuffie, R.E. (1962). On the width of the equatorial Es belt. Ionospheric Sporadic -E, ed. E.K. Smith and S. Matsushita, Pergamon Press, London, pp. 215-218.

Maeda, K., Tsuda, T. and Maeda, H. Theoretical interpretation of the equatorial sporadic-E layers. Phys. Rev. Lett., 11, 406-407.

Matsushita, S. (1953). On the sporadic E.Rpt. Ionosphere Res. Japan, 7, 72-73.

Onwumechilli, C.A. and Ogbuehi, P.O. (1967). Analysis of the magnetic field of the equatorial electrojet. J. Atmos. Terr. Phys, 29, 553-566.

Oyinloye, J. O. (1969). A comparison study of the occurrence of equatorial type Es and daytime blanketing Es in magnetic equatorial zone, Radio Sci;, 4, 765-769.

Oyinloye, J. O. (1971). A study of blanketing sporadic E in the equatorial region. Planet Space Sci., 19, 1131-1139.

Oyinloye, J. O. (1973). An empirical approach to the study of blanketing type Es. Planet Space Sci., 21, 889-898.

Pfaff, R.F.,Kelley, M.C., Fejer, B.G. Maynard, N.C., Brace, L.H., Ledley, B.G., Smith, L.G. and Woodman, R.F. (1985). Comparative in situ studies of the unstable day-time equatorial E-region. J. Atmos. Terr. Phys., 47, 791-811.

Prakash, S., Gupta, S .P. and Subbaraya, B.H. (1970). Nighttime equatorial E region irregularities. Planet. Space Sci., 18, 1307-1318.

Prakash, S., Gupta, S.P., Subbaraya, B.H. and Jain, C.L. (1971a). Electrostatic plasma instabilities in the equatorial electrojet, Nature, 233, 56-58.

Parakash, S., Subbaraya, B.H. and Gupta, S.P. (1971b). Cross field instability and ionization irregularities in the equatorial E region. Nature, 230, 170-171.

Rogister, A. and D'Angelo, N. (1970). Type II irregularities in the equatorial electrojet. J. Geophys. Res., 75, 3879-3887.

Smith, E.K. (1957). Worldwide occurrence of sporadic E. NBS circular 582.

Smith, E.K.(1978). Temperate zone sporadic E maps (FoEs > 7MHz) Radio Sci., 13, 571-575.

Smith, L.O. and Mechthy, E.A. (1972). Rocket observations of sporadic-E layers, Radio Sci., 7, 367-372.

Subbaraya, B.H., Prakash, S. and Gupta, S.P. (1982). (As under D region reference).

Wright, R.W. and Hilberd, P. (1963). Preliminary report on recent measurements to determine the width of the equatorial sporadic-E J. Geophys. Res., 68, 2527-2528.

Spread F and F region Irregularities

Aarons, J., Mullen, J.P. Koster, J.R., da Silva, R.F. Medeiros, J.R., Medeiros, R.T. Bushby, A., Pantoja, J. and Lanat, J. (1980). Seasonal and geomagnetic control of equatorial scintillations in 1° to 2 69°W longitude sectors. J. Atmos. Terr. Phys. 42, 861-896.

Balsley, B.B., Haerendel, B.G. and Greenwald, R.A. (1972). Equatorial spread F: Recent observations and a new interpretation. J. Geophys. Res., 77, 5625-5628.

Basu, S. and Basu, S. (1985). Equatorial scintillations: advances since ISEA-6J. Atmos. Terr. Phys., 47, 753-768.

Basu, S., Basu, S., Labelle, J., Kudeki, E., Fejer, B.G., Kelley, M.C., Whitney, A.E. and Bashby, A. (1986). Gigahertz scintillations and space receiver drift measurements during Project Condor Equatorial F Region Rocket Campaign in Peru. J. Geophys. Res., 91, 5526-5538.

Booker H.G. (1979). The role of acoustic gravity waves in the generation of spread and ionospheric scintillations. J. Atmos. Terr. Phys., 41, 501-515.

Booker, H.G. and Wells, H.W. (1938). Scattering of radio waves by the F region of the ionosphere. Terrest. Mag, 43, 249-256.

Briggs, B.H. and Parkin, I.A. (1963). On the variation of radio star and satellite scintillation with zenith angle. J. Atmos. Terr. Phys., 25, 339-365.

Burke, W.J., Donalelli, D.E., Sagalyn, R.C. and Kelley, M.C. (1979). Observations of low density regions at high altitude in the topside equatorial ionosphere and their interpretation in terms of equatorial spread F. Planet. Space Sci., 27, 593-602.

Calvert, W. and Cohen, R. (1961). The interpretation configurations and synthesis of certain spread-F configurations appearing on equatorial ionograms. J. Geophys. Res., 66, 3125-3140.

Chandra, H. and Rastogi, R.G. (1972). Spread-F at magnetic equatorial station Thumba, Ann. Geophys., 28, 37-44.

Clemesha, B.R. (1964). An investigation of the irregularities in the F-region associated with equatorial type spread-F. J. Atmos. Terr. Phys., 26, 99-112.

Cohen, R. and Bowles, K.L. (1961). On the nature of equatorial spread F. J. Geophys., 66, 1081-1106.

Dungey, J.W. (1956). Convective diffusion in the equatorial F-region. J. Atmos. Terr. Phys., 9, 304-310.

Dyson, P.L. and Benson, R.F. (1978). Topside sounder observations of equatorial bubbles. Geophys. Res. Lett., 5, 795-798.

Dyson, P.L., McClure, J.P. and Hanson, W.B. (1974). In situ measurements of the spectral characteristics of F region ionospheric irregularities. J. Geophys. Res., 79, 1497-1502.

Fejer, B.G. and Kelley, M.C. (1980) (As under sporadic E reference).

Hanson, W.B. and Bamgboye, O.K. (1984). The measured motions inside equatorial plasma bubbles. J. Geophys. Res., 89, 8997-9008.

Hanson, W.B. and Santani, S. (1973). Large Ni gradients below the equatorial F Peak. J. Geophys. Res., 78, 1167-1173.

Keheller, R.F. and Skinner, N.J. (1971). Studies of F-region irregularities at Nairobi II-by direct scatter at 27.8MHz, Ann. Geophys., 27, 195-200.

Kelley, M.C. (1985). Equatorial spread F: recent results and outstanding problems. J. Atmos. Terr. Phys., 47, 745-752.

Kelley, M.C. and McClure, J.P. (1981). Equatorial spread-F: A review of recent experimental results. J. Atmos. Terr. Phys. 43, 427-435.

Kelley, M.C., LaBelle, J., Kudeki, E., Fejer, B.G., Basu, Sa., Basu, Su., Baker, K.D., Hanuise, C., Argo, P., Woodman, R.F., Swartz, W.E., Farley, D.T. and Meriwether, J.W. (1986). The condor equatorial spread F campaign: overview and results of the large-scale measurements. J. Geophys. Res. 91, 5487-5503.

Kent, G.S. and Koster, R.J. (1966). Some studies of the night-time F-layer irregularities at the equator using high frequency signals radiated from earth satellites. Ann. Geophys., 3, 405-417.

Lyon, A.J., Skinner, N.J. and Wright, R.W.H. (1960). The belt of equatorial spread F.J. Atmos. Terr. Phys., 19, 145-149.

Lyon, A.J., Skinner, N.J. and Wright, R.W.H. (1961). Equatorial spread-F at Ibadan, Nigeria.J. Atmos. Terr. Phys., 21, 100-119.

McClure, J.P., Hanson, W.B. and Hoffman, J.H. (1977). Plasma bubbles and irregularities in the equatorial ionosphere. J. Geophys. Res., 82, 2650-26

McClure, J.P. and Woodman, R.F. (1972). Radar observations of equatorial spread F in a region of electrostatic turbulence. J. Geophys. Res., 77, 5617-5621.

Osborne, B.W. (1952). Ionospheric behaviour in the F_2 region at Singapore J. Atmos. Terr. Phys., 2, 66-78.

Ossakow, S.L. (1981). Spread F theories - A review. J. Atmos. Terr. Phys. 43, 437-452.

Ott, E. (1978). Theory of Rayleigh-Taylor bubbles in the equatorial ionosp J. Geophys. Res., 83, 2066-2070.

Rastogi, R. G., Deshpande, M.R., Vats, H., Davies, K., Grubb, R.N. and Jones, J.E. (1977). Amplitude scintillations at ATS-6 radio beacon signal within the equatorial electrojet region (Cotacamund, dip 4° N). Pramana, 8,

Rastogi, R.G. (1980). Seasonal and solar cycle variations of equatorial spread-F in the American zone. J. Atmos. Terr. Phys., 42, 593-596.

Rastogi, R.G. (1983). Tropical spread F. Indian Journal of Radio and Space Physi, 12, 104-113.

Rastogi, R.G. (1984). Study of equatorial ionospheric F-region irregularit by reflection, backscatter and transmission of radio waves. Indian Journal of Radio and Space Phys., 13, 84-93.

Rastogi, R.G. and Woodman, R.F. (1978a). VHF radio wave scattering due to range and frequency types of equatorial spread F. J. Atmos. Terr. Phys., 40, 485-491.

Rastogi, R. G. and Woodman, R.F. (1978b). Spread F in equatorial ionograms associated with reversal of horizontal F region electric field. Ann. Geophys., 34, 31-36.

Roggter, J. (1973). Wave like structures of large scale equatorial spread F irregularities. J. Atmos. Terr. Phys., 35, 1195-1206.

Scannapieco, A.J. and Ossakow, S.L. (1976). Nonlinear equatorial spread F, Geophys. Res. Lett., 3, 451-454.

Skinner, N.J. and Kelleher, R.F. (1971). Studies of F-region irregularities at Nairobi-I from spread F on ionograms 1964-1970. Ann Geophys., 27, 181-194.

Szusczewicz, E.P., Tsunoda, R.T., Narcisi, R. and Holmes, J.C. (1980). Coincident radar and rocket observations of equatorial spread F. Geophys. Res. Lett., 7, 537-540.

Tsunoda, R.T., Livingstone, R.C., McClure, J.P. and Hanson, W.B. (1982) Equatorial plasma bubbles: vertically elongated wedges from the bottomside F layer. J. Geophys. Res.,87, 9171-9180.

Tsunoda, R.T. (1983). On the generation and growth of equatorial backscatter plumes, 2, structuring of the west walls of upwellings. J. Geophys. Res., 88, 4869-4874.

Valladares, C.E., Hanson, W.B., McClure, J.P. and Cragin, B.L. (1983). Bottom side sinusoidal irregularities in the equatorial F region. J. Geophy. Res., 88, 8025-8042.

Whitney, H.E., Aarons, J. and Malik, C. (1969). A proposal index for measuring ionospheric scintillation. Planet Space Sci., 17, 1069-1073.

Woodman, R.F. and LaHoz, C. (1976). Radar observations of F region equatorial irregularities. J. Geophys. Res., 81, 5447-5466.

Wright, R.W.H. (1959). Geomorphology of spread-F and characteristics of equatorial spread-F J. Geophys. Res., 2203-2207.

Ionospheric Disturbances and Storms

Adeniyi, J. O. (1980) (As under F-region references).

Adeniyi, J.O. (1986). Magnetic storm effects on the morphology of the equatorial F2-layer. J. Atmos. Terr. Phys., 48, 695-702.

Adeniyi, J. O. (1987). Magnetic storm effects on the equatorial day-time E layers' Proc. Biregional Latin American-African Workshop on Radio Propagation Research and Applications, Buenos Aires, Argentina, pp. 103-106.

Chapman, S. (1965). Magnetic storms. Proc. Second International Symposium on Equatorial Aeronomy, Sao Paulo, Brasil, ed. F.de Mendonca, pp. 449-451.

Davies, K. (1965). Ionospheric Radio Propagation, NBS Monograph 80, USA. Ch. 6, pp. 257-288.

Friedman, H. (1960). The sun's ionizing radiations in Physics of the Upper Atmosphere, ed. J. A. Ratcliffe, Academic Press, New York and London, ch. 4, pp. 133-218.

Gnanalingam, S. (1974) (As under D-region references).

Kelleher, R.F. (1965). Ionospheric parameters for Nairobi for magnetically disturbed and quiet days. Proc. Seasonal International Symposium on Equatorial Aeronomy, Sao Paulo, Brasil, ed. F. de Mendonca, pp.475-478.

Matsushita, S. (1959). A study of the morphology of ionospheric storms. J. Geophys. Res., 64, 305-321.

Mitra, A.P. (1982). Tropical ionosphere and troposphere. ICTP Autumn Course on Geomagnetism, the Ionosphere and Magnetosphere. SMR/98-50.

Olatunji, E.O. (1966) (As under F region references).

Shamsi, S. (1986). Oblique incidence ionospheric absorption near the magnetic equator. Ph.D. Thesis Univ. Lagos.

Skinner, N.J. (1958). Routine ionospheric measurements at University College, Ibadan, Nigeria, January - December 1957, issued by Physics Dept., University College, Ibadan.

Skinner, N.J. and Wright, R.W.H. (1955). Some magnetic effects in the equatorial F2-region. J. Atmos. Terr. Phys., 6, 177-188.

Table 1 Disturbances

	S.Max	S.Min.	Typical Duration	Long path Phase	VLF Effects Ampl
SID	2/week	2/year	½ hr	5–30 cec	–1 to +5 db
PCA	1/mo	0	3d	40 cec	
Storm (Mag)	26/yr	22/yr	days	10–20 cec	5–10db fade
W.A.	20/yr	20/yr	days	usually phase advance	5–10db fade
Stratwarm	2/yr	2/yr	weeks	unknown	unknown

cec = Centicycles; At 10KHz, 1 cec = 1 ms in time

= 0.1 mile

Source Mitra (1982)

List of Diagrams

Fig. 11. (a) Variation with geographic latitude of m in the equation $A = B(\cos \quad)^m$ for stations centred on the (i) 5°E meridian, (ii) 75°W meridian and (iii) 150°E meridian.

(b) Variation with geographic latitude of B in equation $A = B(\cos \quad)^m$, showing the equatorial enhancement. Both Figs. 11a and 11b are from Kouris and Muggleton (1973b).

Fig. 12. Comparison of predicted and observed values for foE for Ouagadougou, ——— observed foE, - - - - predicted foE using model by Aremu and Oyinloye (1988), ... predicted foE using CCIR formula.

Fig. 13. Equatorial anomaly in the F region in
(a) foF1 (After Rastogi, 1959a)
(b) NmF2 at fixed heights below F2 peak (After GCroom et al. 1959).
(c) NmF2 at fixed heights above F2 peak (After Kim et al., 1967).

Fig. 14. Calculated electron concentration contours for an upward equatorial drift velocity of w_o = 10 ms^{-1} (a) sunspot maximum conditions ( ) (= 3). Peak-to-trough ratio of NmF2 equals 1.55 and (b) sunspot minimum conditions (= 3). Peak-to-trough ratio of NmF2 equals 2.16; = $(T_e + T_i)/T_i$ where T_i is ion temperature and T_e is electron temperature. Both diagrams are from Hanson and Moffett (1966).

Fig. 15. Illustrating fountain effect. A vector plot of electron fluxes that are associated with the electron concentration profiles shown in Fig. 14(a). Magnetic field lines are shown every 200km. (After Hanson and Moffett, 1966).

Fig. 16. A comparison of down increase in foF2 at Kadaikanal (a low latitude station) with that at Brisbane (A mid-latitude station) (After Lakshmi et al., 1980)

Fig. 17. Seasonal and long-term variations in (a) Ibadan noon hmF2 (After Adeniyi, 1980), and (b) Ibadan midnight foF2 (After Awe, 1980).

Fig. 18. Contours of vertical total electron content TEC in units of 10^{16} el/m^2 column for 2000UT, March 1980 (After Klobuchar, 1983).

Fig. 19. (a) Diurnal variation of the Faraday total electron content observed at Ibadan May–June 1962 and
(b) Topside/bottomside Faraday electron content ratio observed at Ibadan, November 1962 – January 1963.
Both diagrams are from Olatunji (1967).

Fig. 20. Monthly overplots of diurnal curves of total electron content in units of 10^{16} el/m^2 for Ascension Island, May 1980–April 1981 (After Klobuchar, 1983).

Fig. 21. Diurnal variations of total electron content N_T at Ootacamund, India (After Donelly et al., 1979).

Fig. 22. Diurnal variations of Es-q occurrence frequency (a) in South American stations (After Bandyopadhay and Montes, 1963) and (b) in Nigerian stations (After Oyinloye, 1969).

Fig. 23. Correlation in the temporal variations of Es-q and electrojet parameters.

Fig. 24. Echo height regions of electrojet irregularities at Jicarmaca from 18–19 February 1971 (After Fejer et al., 1975).

Fig. 25. Type II electrojet irregularities observed at Thumba at 1856h, IST, on February 2, 1968. The irregularities are seen in the height regions 87 to 102 km and 134 to 138 km where the electron density gradient is positive (After Prakash et al., (1971b).

Fig. 26. Type II electrojet irregularities observed at Thumba at 2300h, IST, on August, 29, 1968. The irregularities are seen only in regions of negative electron density gradient (After Prakash et al., 1971b).

Fig. 27. (a) Percentage amplitude of type II electrojet irregularities in the scale sizes 1–15m, observed at Thumba at 1110, IST on January 28, 1971 and (b) corresponding extrapolated electrojet current density

(After Prakash et al., 1971a).

Fig. 28. Diurnal variation of occurrence frequency of Blanketing Es at the equatorial stations of Talara (Ta), Chiclayo (CL), Chimbote (CH), Huancayo (HU), Juliaca (UJU), Ilorin (IL) and Ibadan (IB) (After Oyinloye, 1971).

Fig. 29. Electron density profiles obtained at Thumba showing the presence of a blanketing sporadic E layer during counter electrojet conditions (After Subbaraya et al., 1983, 1985).

Fig. 30. Illustrating (a) Frequency type and (b) range type spread F on Huancayo ionograms (After Booker and Wells, 1938).

Fig. 31. Illustrating the association of incidence of spread F with (a) seasonal rate of increase of the F layer minimum virtual height h'F and (b) post sunset rise in h'F (After Osborne, 1952).

Fig. 32. The belt in equatorial spread F (After Lyon et al; 1960).

Fig. 33. Nocturnal variation of occurrence of spread F at Indian stations, averaged for the year 1965, with an indication of poleward movement in spread F (Rastogi, 1983).

Fig. 34. Illustrating (a) correspondence in the occurrence of spread F echoes on Jicarmaca 3m modified range-time intensity plot (MRTI) with the range type spread F on Huancayo ionogram (After Rastogi, 1984.)

(b) the association of backscatter echoes of 50MHz radar at Jicarmaca with range type spread F (After Rastogi and Woodman, 1978a).

Fig. 35. Illustrating the occurrence of plumes on the 3m back scatter power map of spread F at Jicarmaca. Note that spread F can occur at altitude as low as about 200km and as high as about 1000km. (After Kelley, et al., 1986).

Fig. 36. Altair scanning radar map of irregularities at 0.96m wavelength in Kwajalein Island in the South Pacific, illustrating horizontal structuring in spread F irregularities and an east-west asymmetry in the scattering region altitude (After Tsunoda, 1983).

Fig. 37. The 3m back scatter power map of spread F at Jicarmaca, illustrating a night of weak spread F (After Woodman and LaHoz, 1976).

Fig. 38. The 3m back scatter power map of spread F at Jicarmaca, illustrating a night of strong spread F (After Woodman and LaHoz, 1976).

Fig. 39. Simultaneous in situ plasma density and scanning radar data during equatorial spread F, illustrating the association of plumes on back scatter radar maps over Altair with depletions in ionisation (After Tsinoda et al., 1982).

Fig. 40. Illustrating the poleward movement of north-south horizontal ion motions in plasma bubbles in the near equatorial ionosphere (After Hanson and Bamgboye, 1984).

Fig. 41. (a) Amplitude scintillation of 40, 140 and 360 MHz beacon radio waves from ATS-6 satellite received at Ootacamund (After Rastogi et al., 1977).
(b) Amplitude scintillation of 1694MHz radio waves from geostationary satellite GOES 5 received at Ancon and Their Spectra from Fourier transform technique (FFT) (After Basu et al., 1986).

Fig. 42. Illustrating association of plumes on the 3m Jicarmaca back scatter power map of spread F with strong 1.7GHz scintillation at Ancon using (a) S.I. Scintillation index (After Kelley et al., 1986) and (b) S_4 scintillation index (After Basu et al., 1986).

Fig. 43. The terrestrial effects of a solar flare (After Davies, 1965).

Fig. 44. Storm time variations of maximum electron densities (F2) in different latitudes. Geomagnetic latitudes of the zones are as follows: Zone 1, 60°–55°; zone 2, 55°–50°; zone 3, 50°–45°; zone 4, 45° – 40°; zone 5, 40°–29°; zone 6, 29°–20°; zone 7, 20°–9°; and zone 8, $+9^{\circ}$ to -9° (After Matsushita, 1959).

Fig. 45. Illustrating the association between a magnetic and ionospheric storms as recorded at Ibadan (After Adeniyi, 1986).

Fig. 46. Solar flare X-ray effect on HF absorption at (a) vertical incidence (After Chandlingam, 1974) and (b) oblique incidence (After Chamsi, 1986).

Fig. 47. Ionospheric storm effect on the E region at Ibadan (After

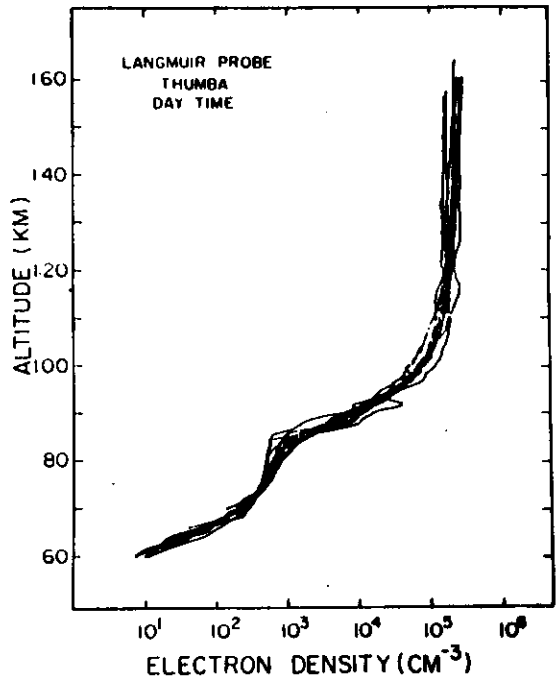

Fig. 1

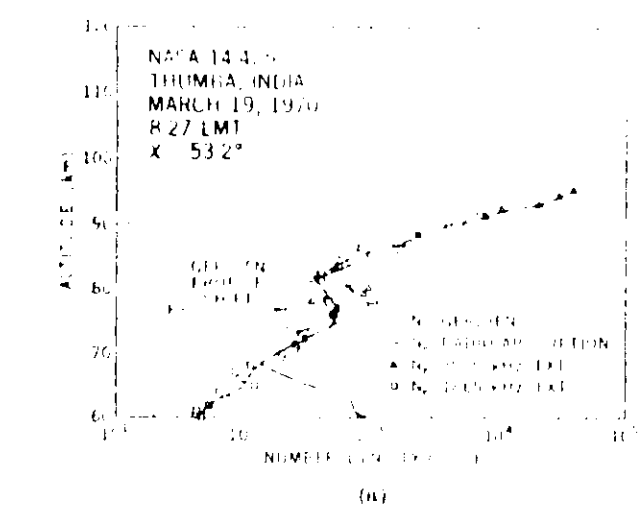
THUMBA, INDIA
MARCH 19, 1970
8 27 LMT
X = 53 2°

(a)

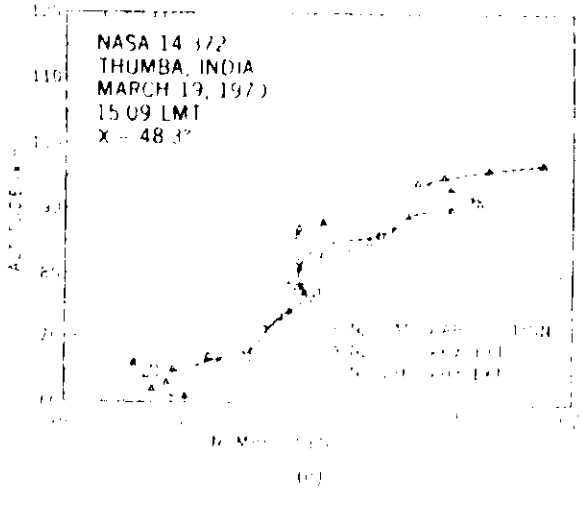
NASA 14 422
THUMBA, INDIA
MARCH 19, 1970
15 09 LMT
X = 48 3°

(c)

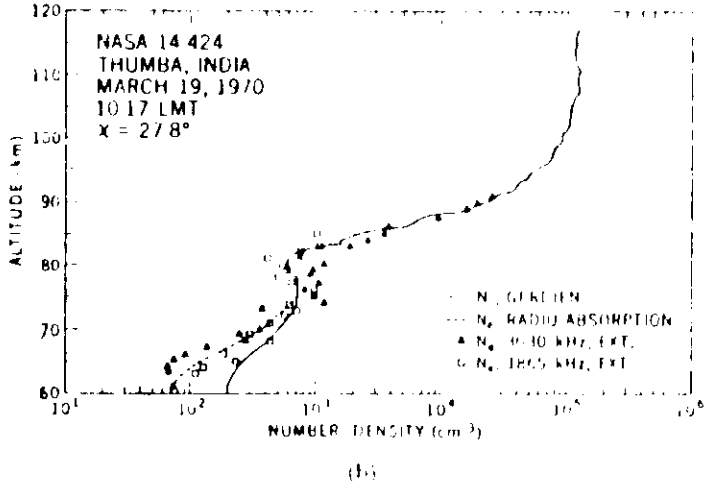
NASA 14 424
THUMBA, INDIA
MARCH 19, 1970
10 17 LMT
X = 27 8°
ALTITUDE (km)
NUMBER DENSITY (cm⁻³)
N, GIDDEN
Ne RADIO ABSORPTION

(b)

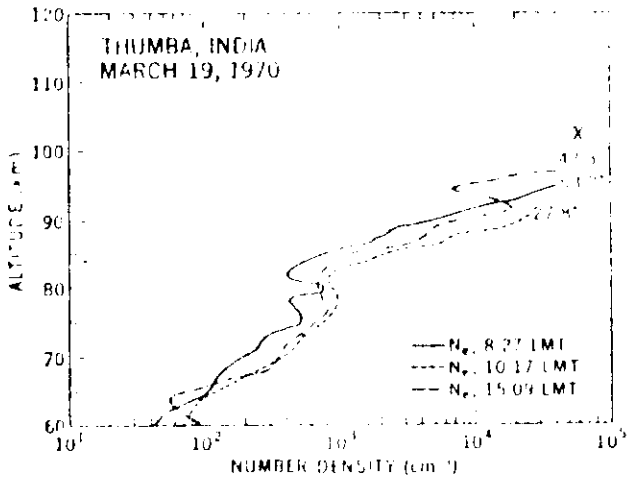
THUMBA, INDIA
MARCH 19, 1970
ALTITUDE (km)
NUMBER DENSITY (cm⁻³)
Ne, 8 27 LMT
Ne, 10 17 LMT
Ne, 15 09 LMT

Fig. 2

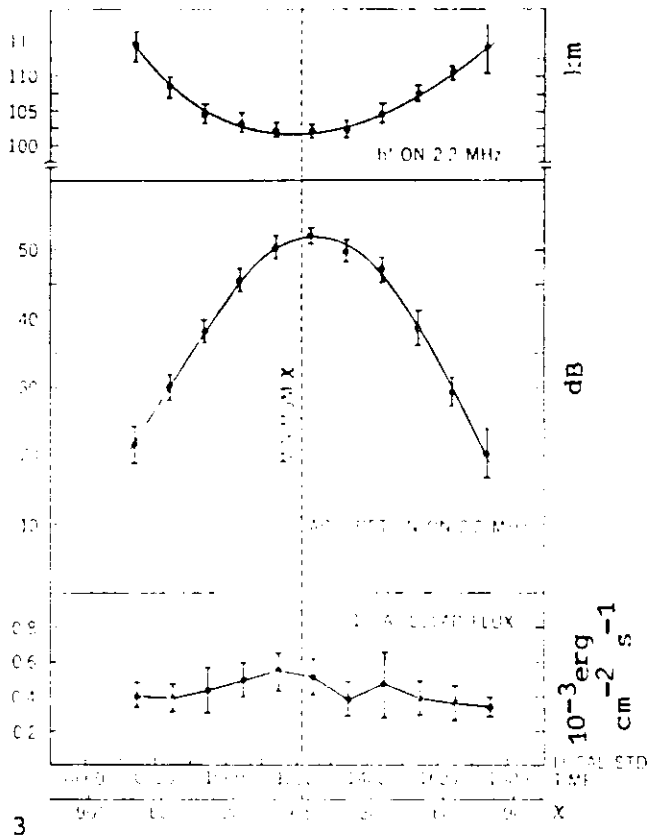

Fig. 3

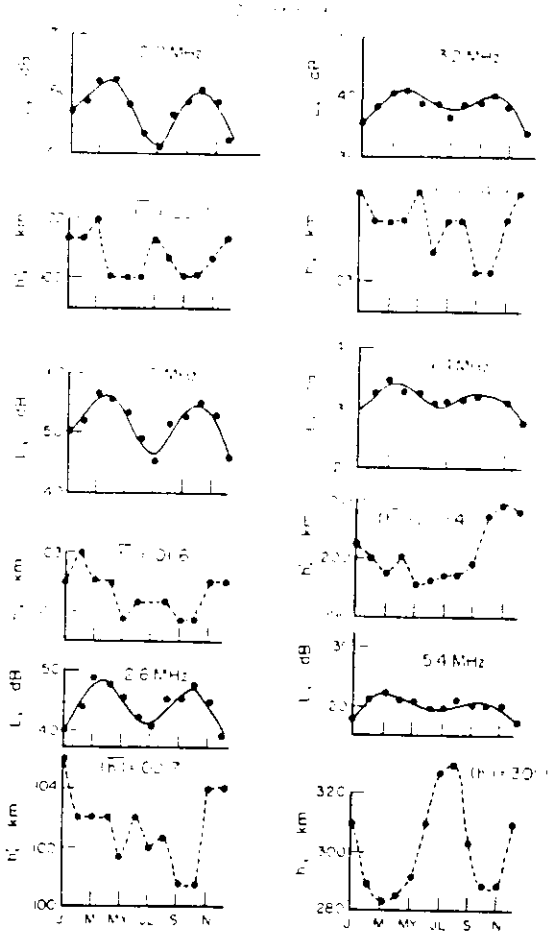

Fig. 4a

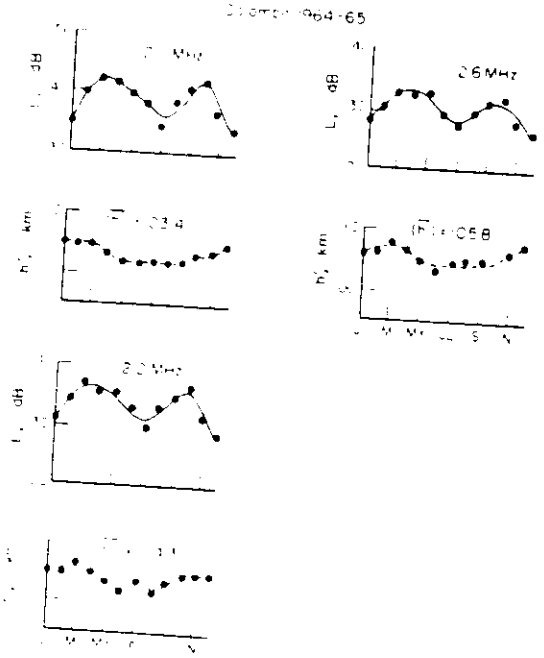

Fig. 4b

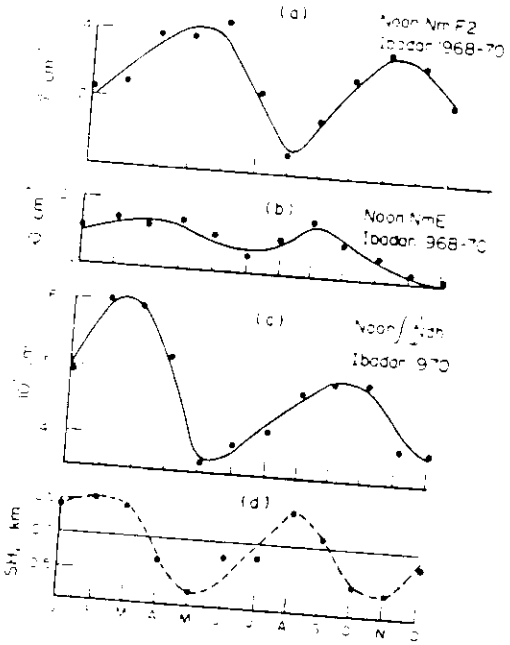

Fig. 4c

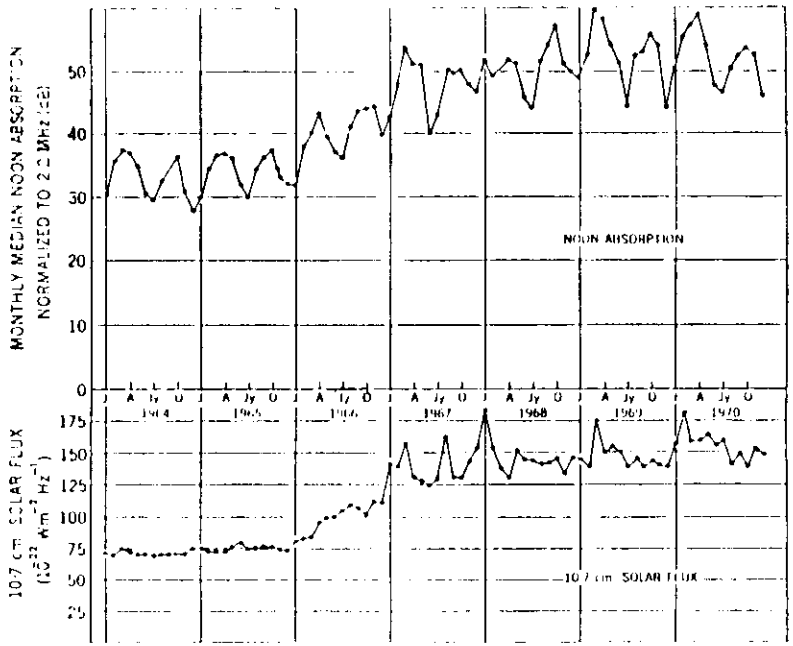
MONTHLY MEDIAN NOON ABSORPTION NORMALIZED TO 2.2 MHz (dB)
NOON ABSORPTION
10.7 cm SOLAR FLUX
10.7 cm SOLAR FLUX
1964
1965
1966
1967
1968
1969
1970

Fig. 5

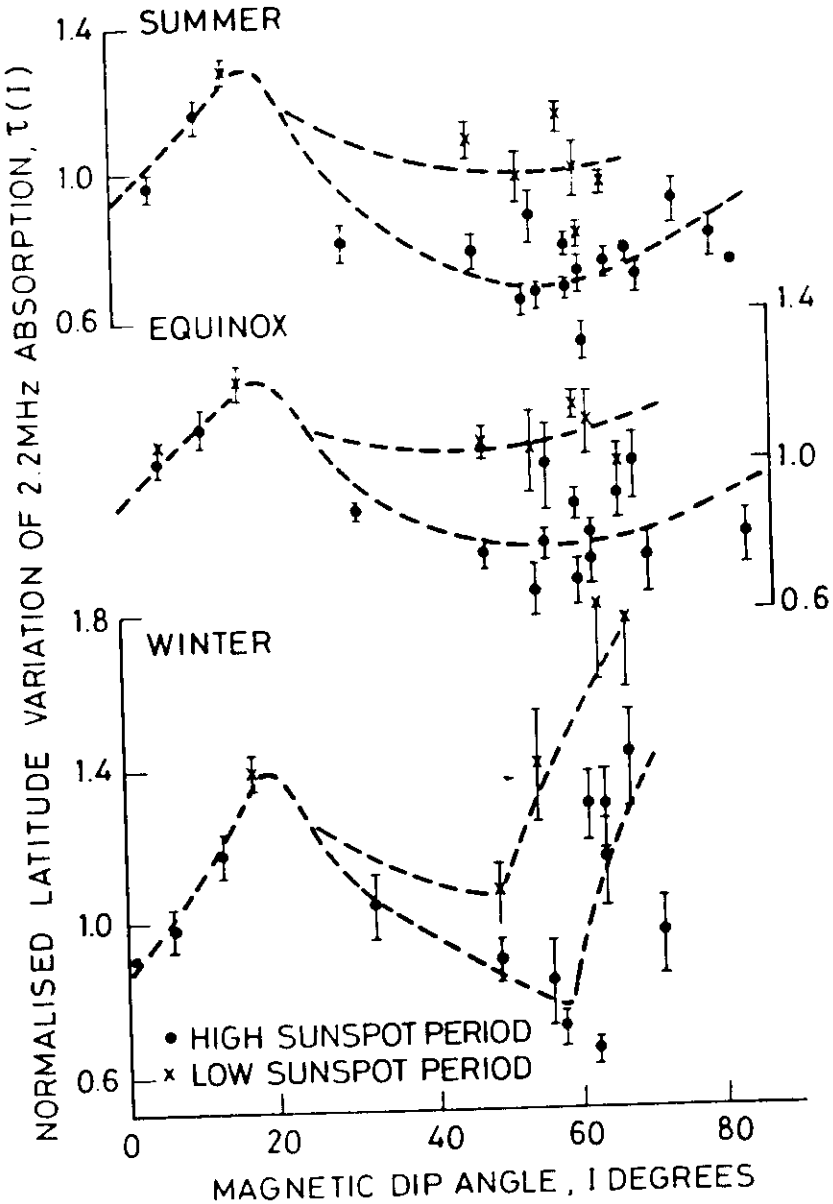
SUMMER
EQUINOX
WINTER
NORMALISED LATITUDE VARIATION OF 2.2MHz ABSORPTION, τ(I)
• HIGH SUNSPOT PERIOD
× LOW SUNSPOT PERIOD
MAGNETIC DIP ANGLE, I DEGREES

Fig. 6

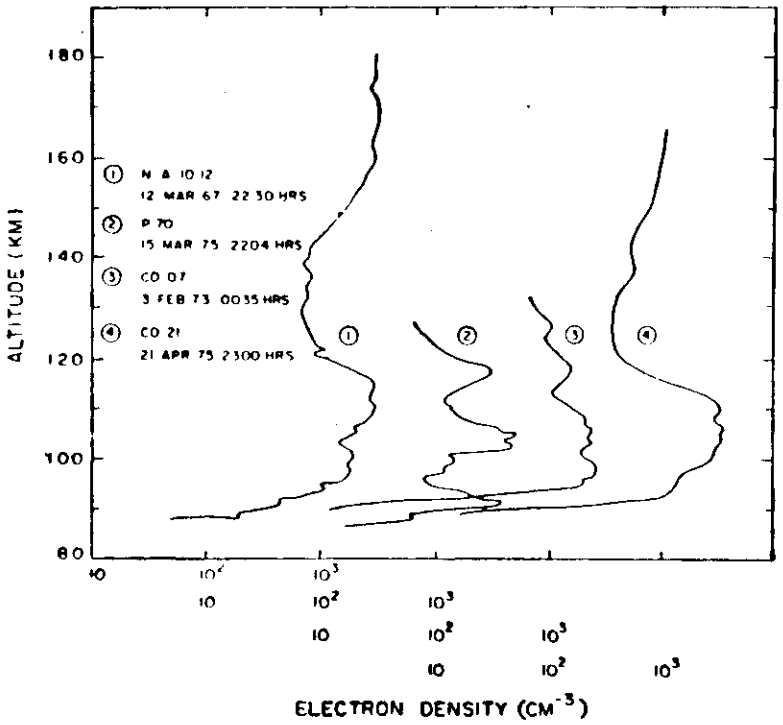
ALTITUDE (KM)
180
160
140
120
100
80
① N A 10 12
12 MAR 67 22 30 HRS
② P 70
15 MAR 75 2204 HRS
③ CO 07
3 FEB 73 0035 HRS
④ CO 21
21 APR 75 2300 HRS
10
10²
10³
ELECTRON DENSITY (CM⁻³)

Fig. 7a

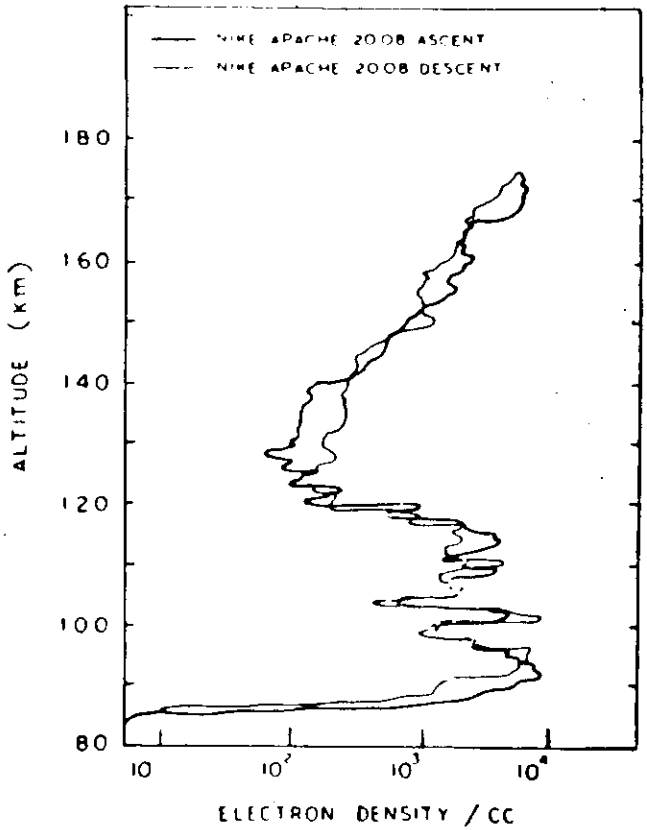
NIKE APACHE 2008 ASCENT
NIKE APACHE 2008 DESCENT
ALTITUDE (km)
180
160
140
120
100
80
10
10²
10³
10⁴
ELECTRON DENSITY / CC

Fig. 7b

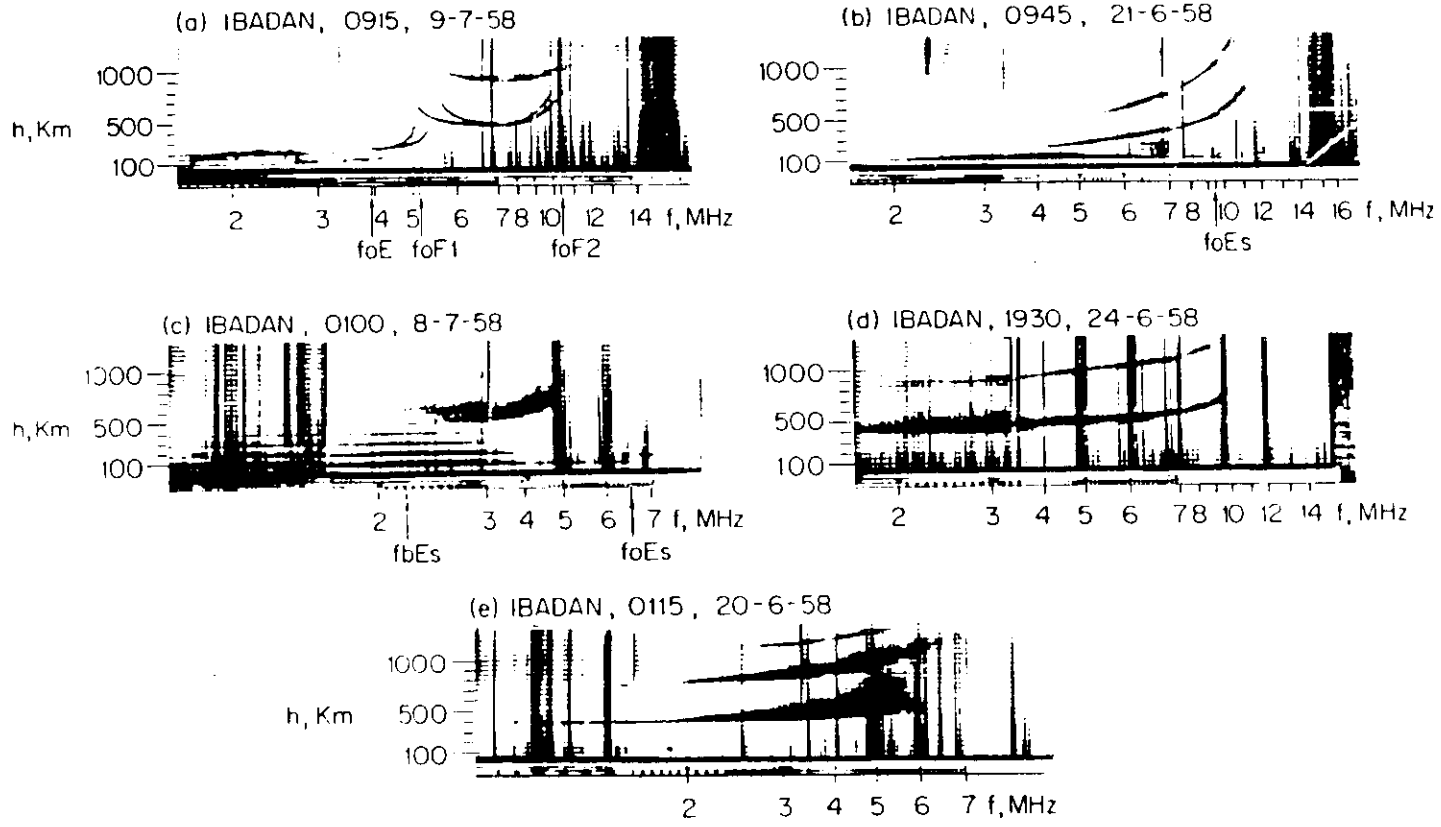

IBADAN IONOGRAMS SHOWING – (a) CRITICAL FREQUENCIES,
(b) EQUATORIAL SPORADIC E, (c) BLANKETING SPORADIC E,
(d) RANGE SPREAD F AND (e) FREQUENCY SPREAD F.

Fig. 8

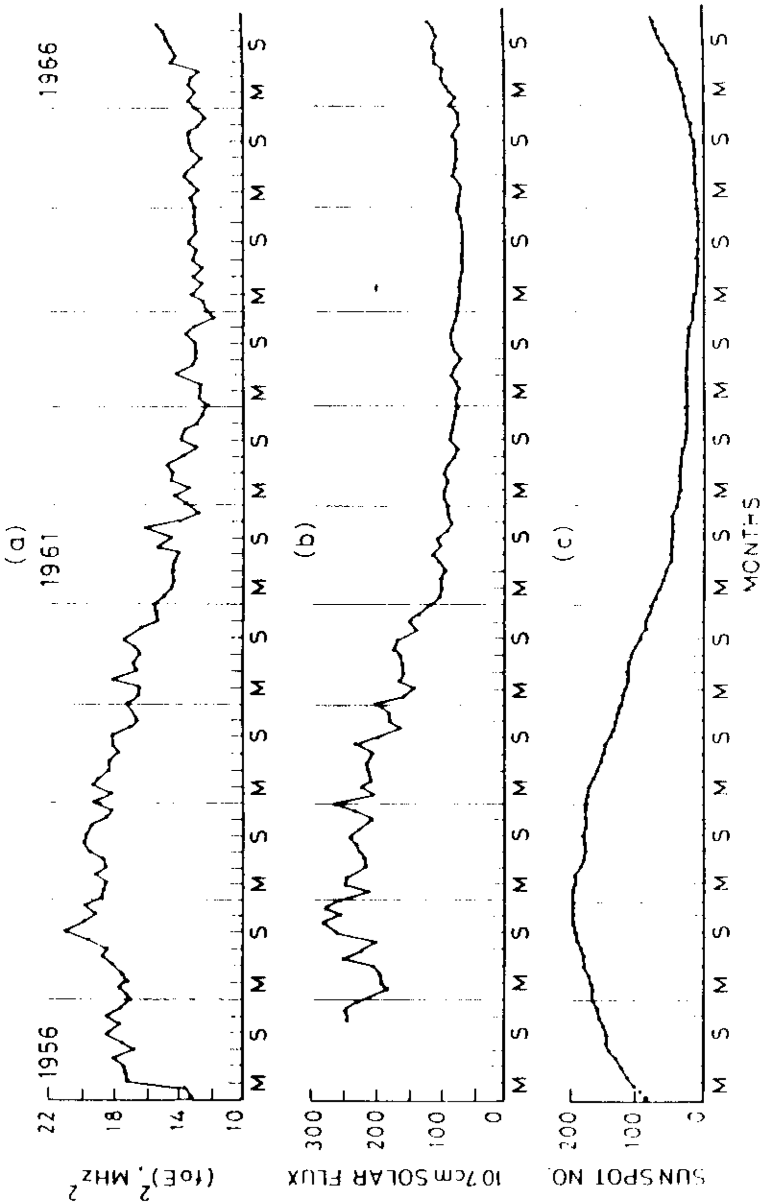

Fig. 9

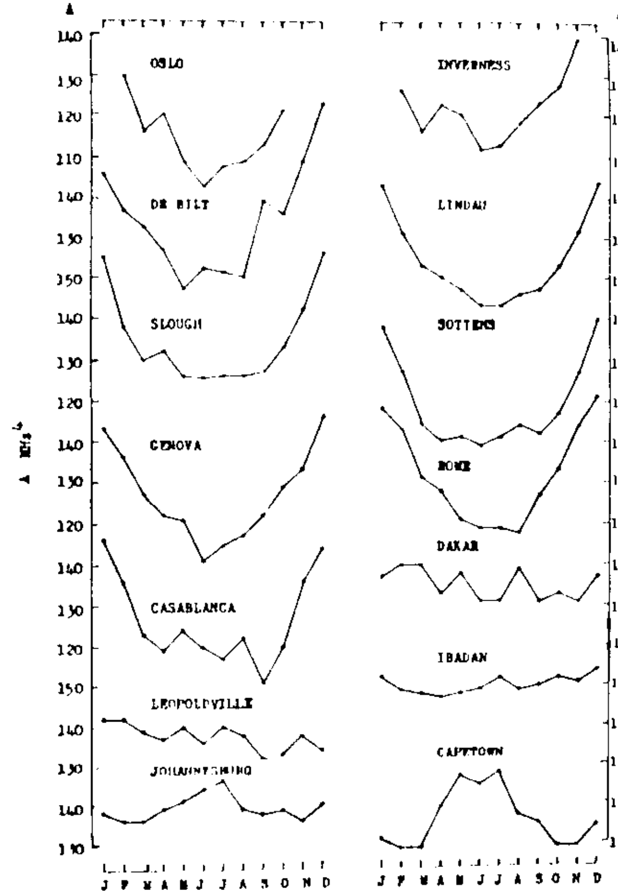

Seasonal variation of A in equation $(f_oE)^4 = A(\cos\chi)^n$, at stations in the zone centred approximately on the 5°E meridian. Data corrected for solar activity and varying Sun–Earth distance.

Fig. 10

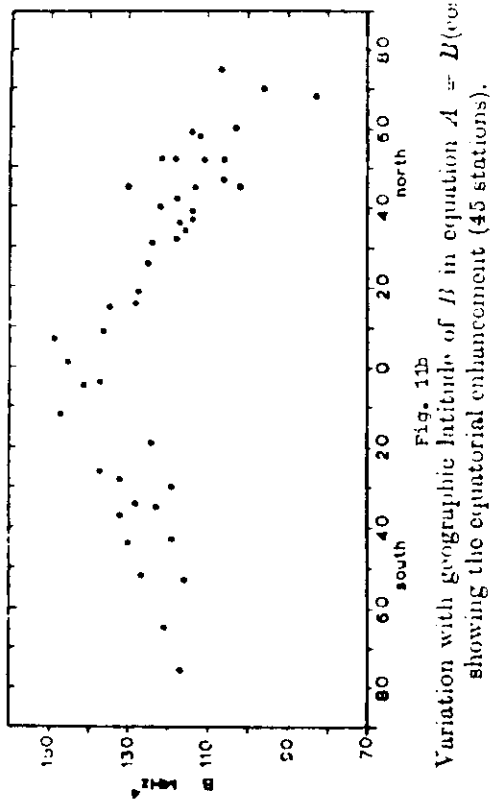

Fig. 11b
Variation with geographic latitude of B in equation $A = B(\cos \chi_{noon})^m$, showing the equatorial enhancement (45 stations).

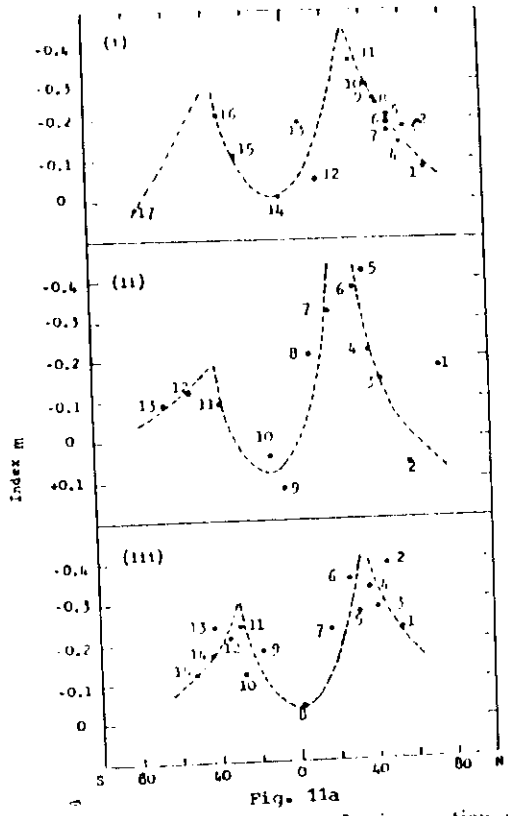

Fig. 11a

(i). Variation with geographic latitude of m in equation $A = B\ (\cos \chi_{noon})^m$ for stations centred on the 5°E meridian: (1) Tromso, (2) Kiruna, (3) Oslo, (4) Inverness, (5) De. Bilt, (6) Lindau, (7) Slough, (8) Sottens, (9) Genova, (10) Rome, (11) Casablanca, (12) Dakar, (13) Ibadan, (14) Leopoldville, (15) Johannesburg, (16) Capetown, and (17) Halley Bay.

(ii). Variation with geographic latitude for m for stations centred on the 75°W meridian: (1) Resolute Bay, (2) Churchill, (3) Ottawa, (4) Washington, (5) San Francisco, (6) White Sands, (7) Puerto Rico, (8) Panama Canal, (9) Talara, (10) Huançayo, (11) Conception, (12) Port Stanley, and (13) Port Lockroy.

(iii). Variation with geographic latitude of m for stations centred on the 150°E meridian: (1) Adak, (2) Wakkanai, (3) Akita, (4) Tokyo, (5) Yamagawa, (6) Okinawa, (7) Baguio, (8) Singapore, (9) Townsville, (10) Brisbane, (11) Wathoroo, (12) Canberra, (13) Hobart, (14) Godhoyhead, and (15) Campbell Is.

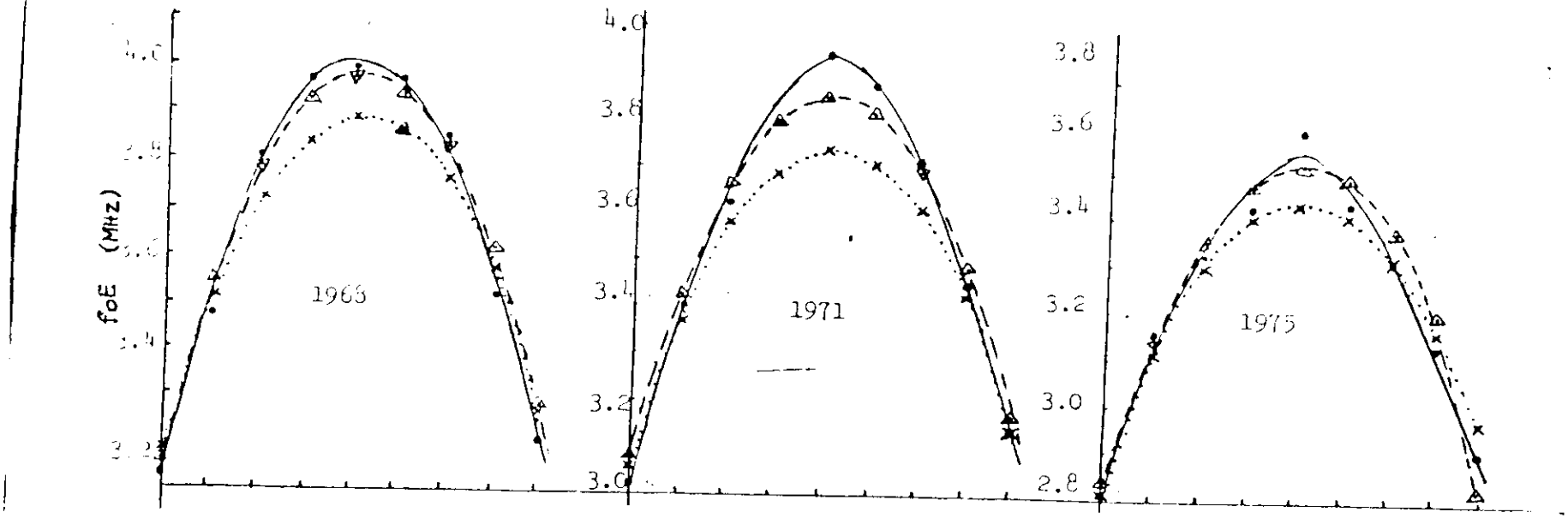

Fig. 12

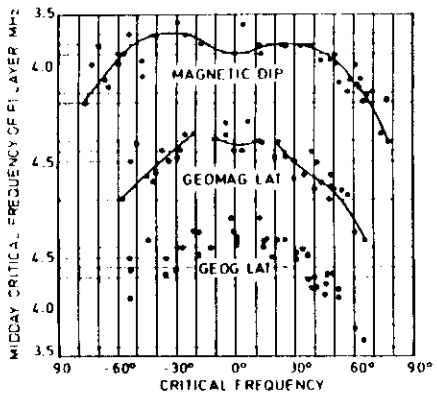

(a) VARIATION OF MIDDAY (11-13hr MEAN) CRITICAL FREQUENCY OF F1 LAYER IN MARCH 1952

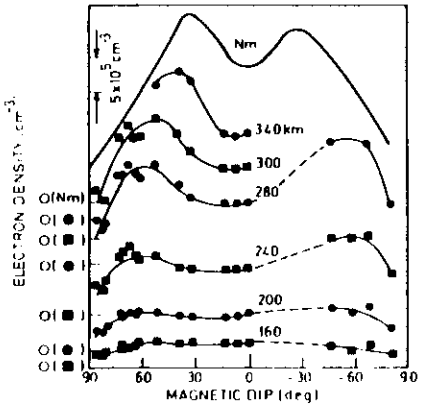

(b) VARIATION OF NmF2 AND OF ELECTRON DENSITY (ELECTRON CONCENTRATION) AT FIXED HEIGHTS WITH MAGNETIC DIP, FOR NOON ON MAGNETICALLY QUITE DAYS IN SEPTEMBER 1957. THE ZERO LEVEL FOR EACH CURVE IS INDICATED ON THE LEFT.

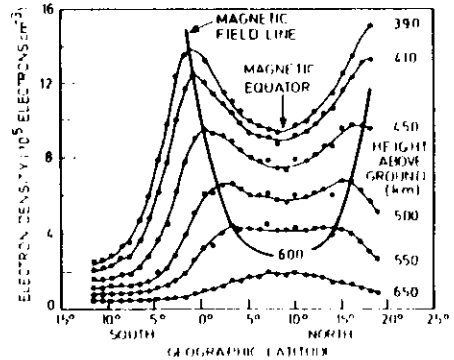

(c) LATITUDE VARIATION OF ELECTRON DENSITY (ELECTRON CONCENTRATION) AT FIXED HEIGHTS, DETERMINED BY MEANS OF THE ALOUETTE I TOPSIDE SOUNDER SATELLITE ABOVE SINGAPORE (1°N, 104°E) AT 1234 LOCAL TIME, 15 SEPTEMBER 1963. A MAGNETIC FIELD LINE IS SHOWN

Fig. 13

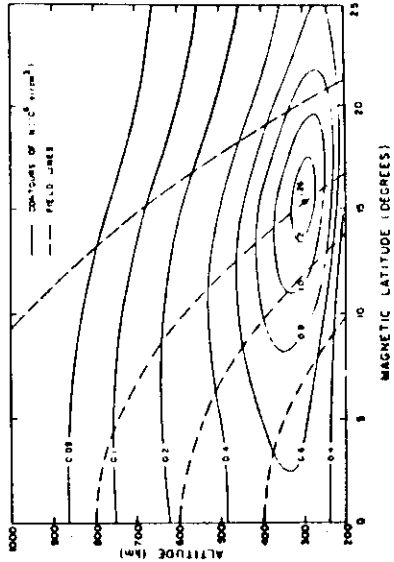

Fig. 14b

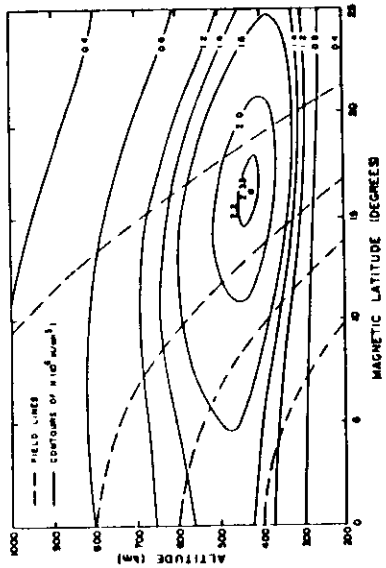

Fig. 14a

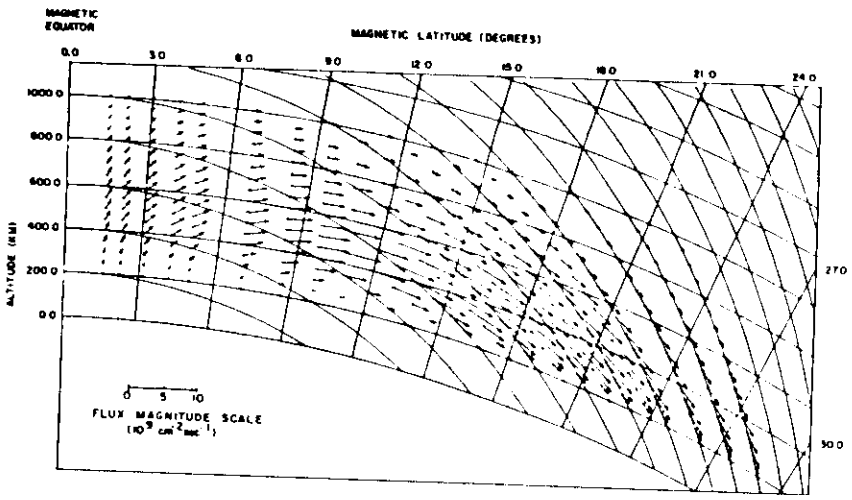

Fig. 15

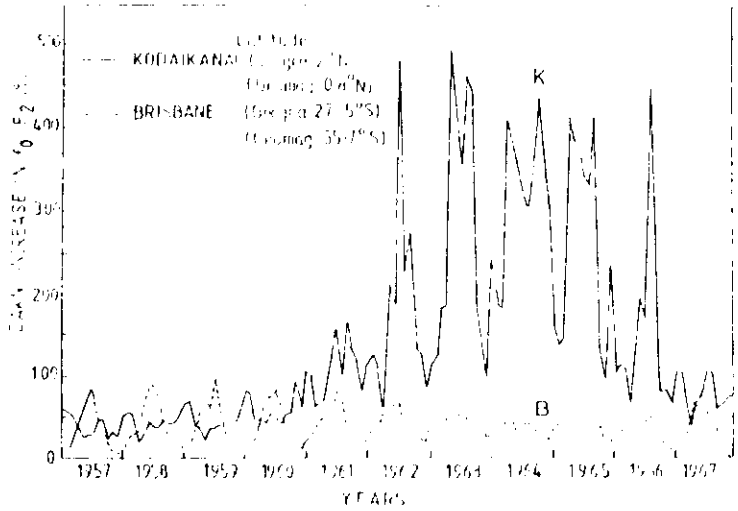

Fig. 16

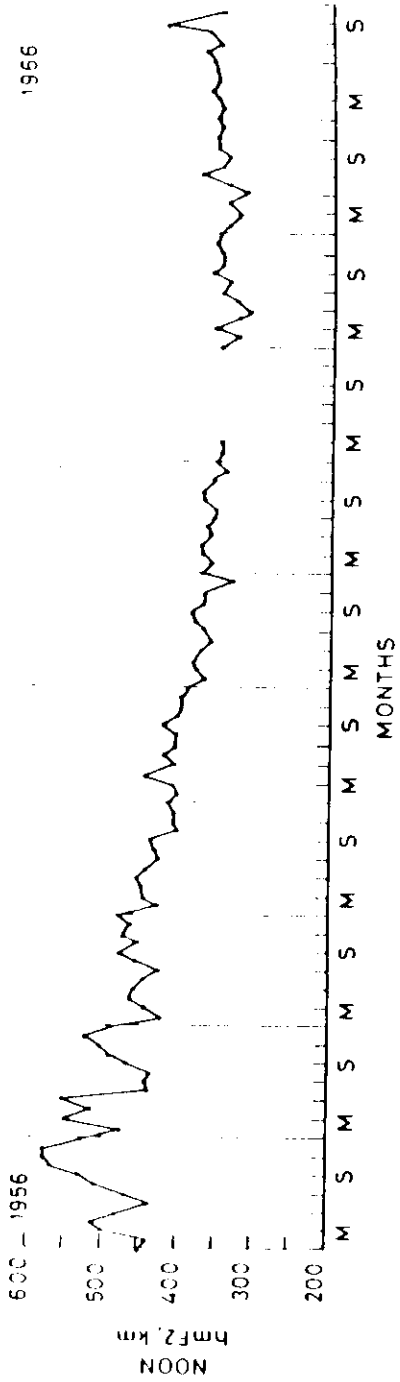

(a)

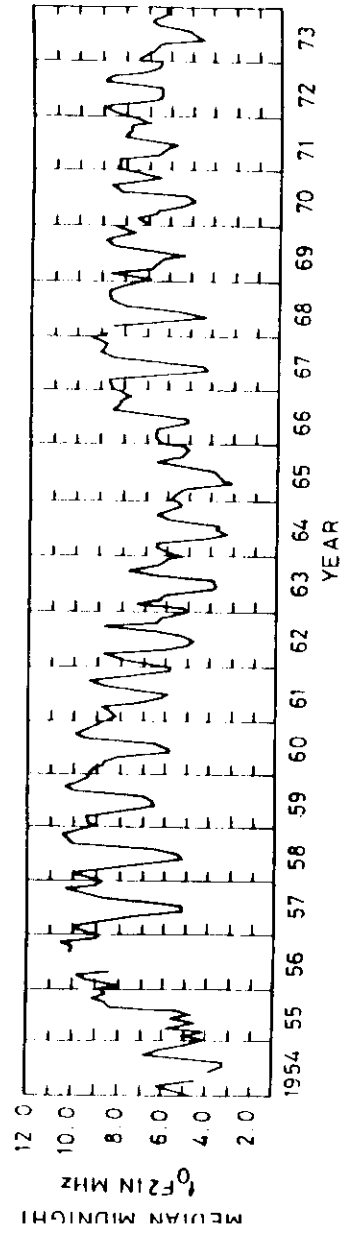

(b)

Fig. 17

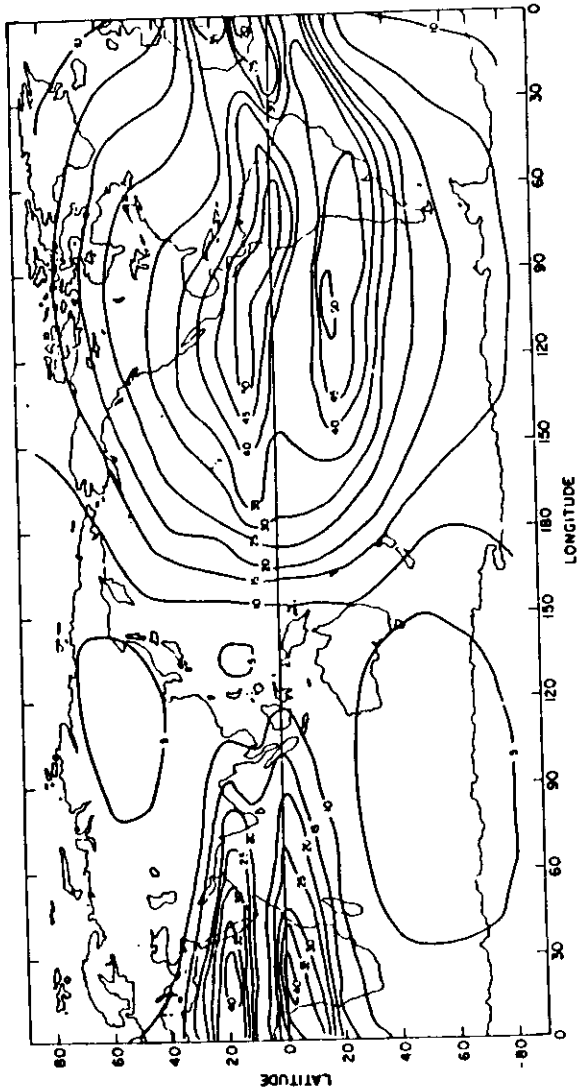

CONTOURS OF IONOSPHERIC TIME DELAY AT L1 (1575GHz) IN NANOSECONDS
MARCH 1980 ($F_{10.7}$ = 167)
2000 UT
Contours of vertical TEC, in units of 10^{16} el/m² column, for 2000 UT, March 1980.

Fig. 18

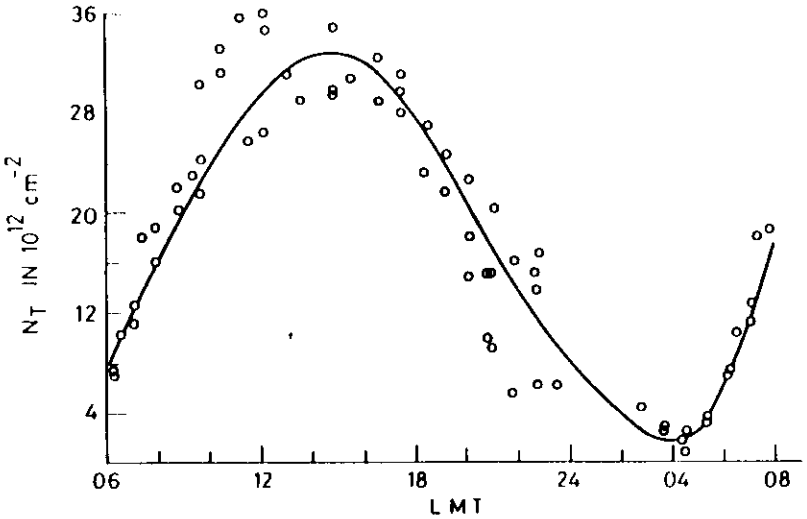

(a) DIURNAL VARIATION OF THE TOTAL ELECTRON CONTENT
MAY – JUNE, 1962

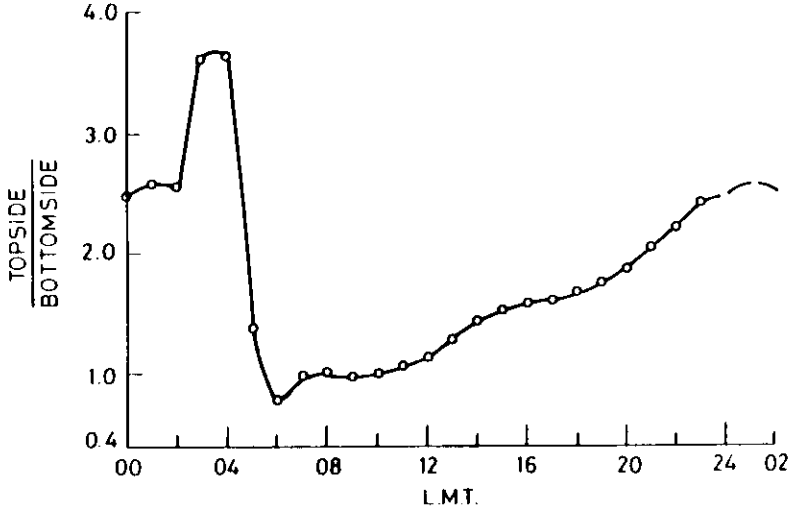

(b) TOPSIDE/BOTTOMSIDE ELECTRON CONTENT RATIO
NOVEMBER 1962 – JANUARY 1963

THE FARADAY TOTAL COLUMNAR ELECTRON CONTENT
OF THE EQUATORIAL IONOSPHERE

Fig. 19

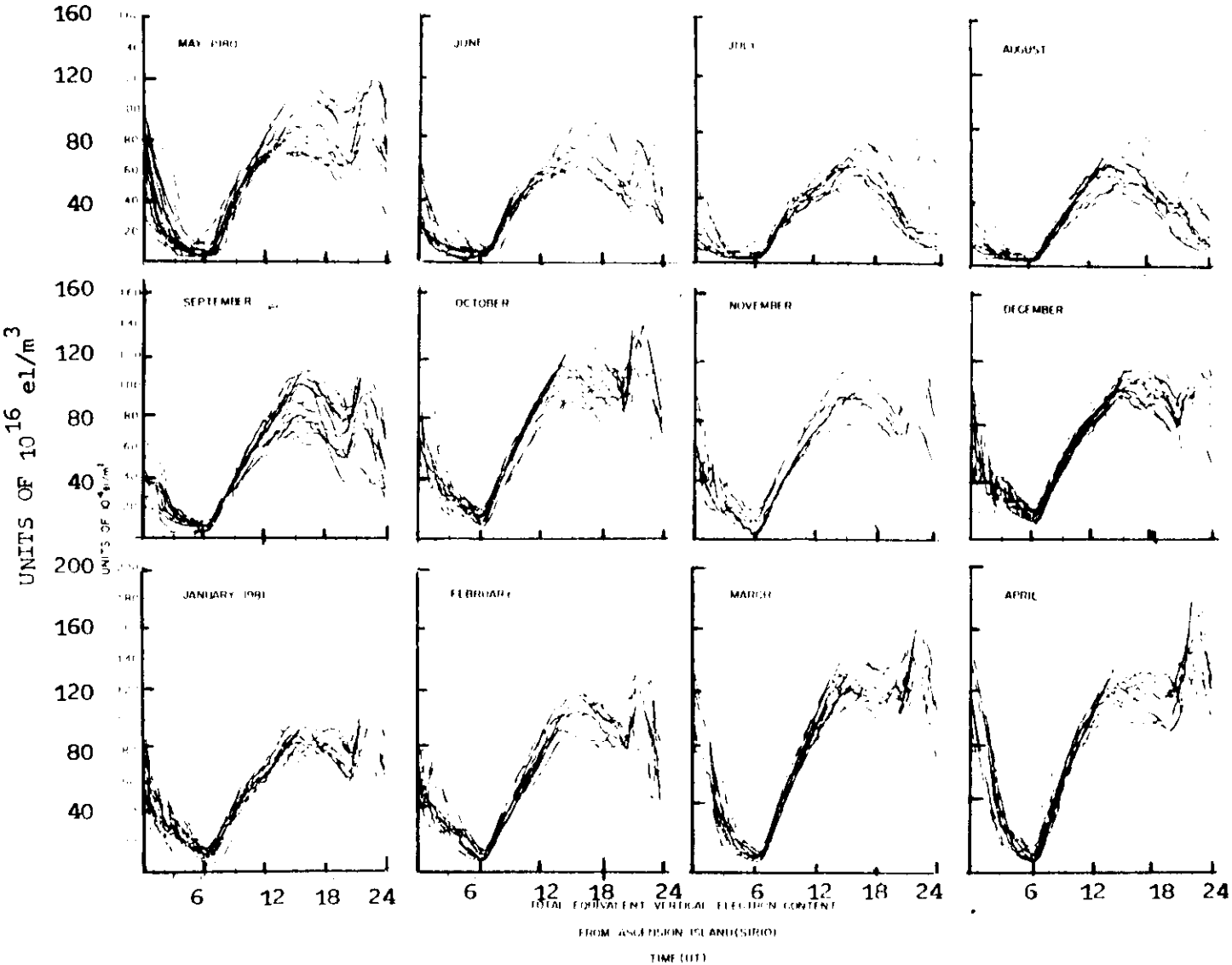

Monthly overplots of TEC diurnal curves for Ascension Island, May 1980 - April 1981.

Fig. 20

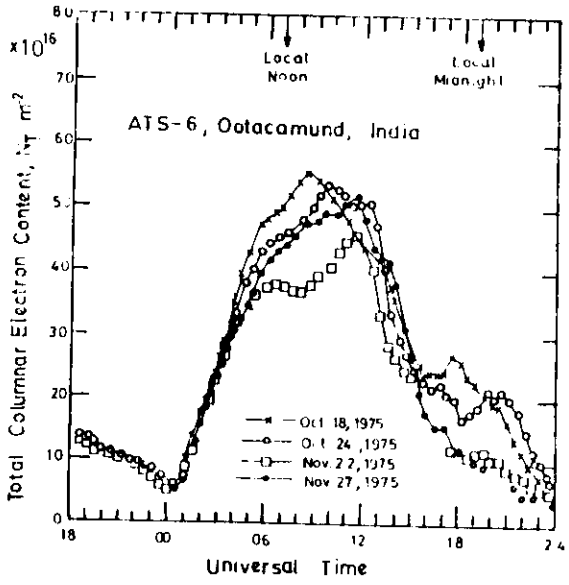

Fig. 21

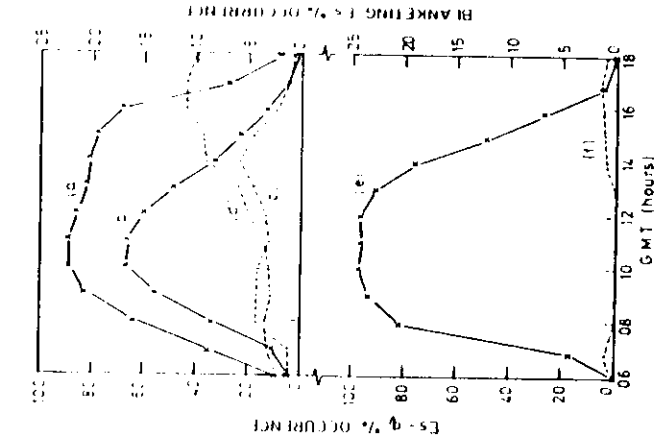

(b) THE DIURNAL VARIATION OF Es OCCURRENCE. CROSSES INDICATE THE MEAN VARIATION FOR Es-q. (a) IBADAN (1958-1959), (b) IBADAN (1963-1964), (e) ZARIA (MARCH - JUNE, SEPTEMBER - DECEMBER 1965) DOTS INDICATE THE VARIATION FOR BLANKETING Es. (c) IBADAN (1958-1959), (d) IBADAN (1963-1964), (f) ZARIA (1965).

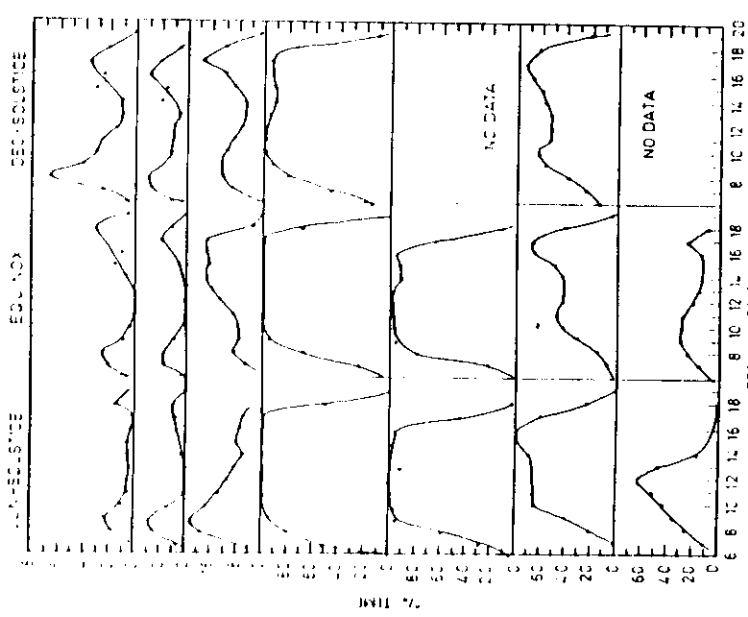

(c) DIURNAL VARIATION OF Es-q OCCURRENCE AT DIFFERENT EQUATORIAL STATIONS AND IN DIFFERENT SEASONS DURING 1958. THE EQUINOX AND JUNE - SOLSTICE CURVES FOR BOTH JULIACA AND ILO ARE BASED ON THE DATA OF MARCH - APRIL 1959 AND OF MAY 1959, RESPECTIVELY

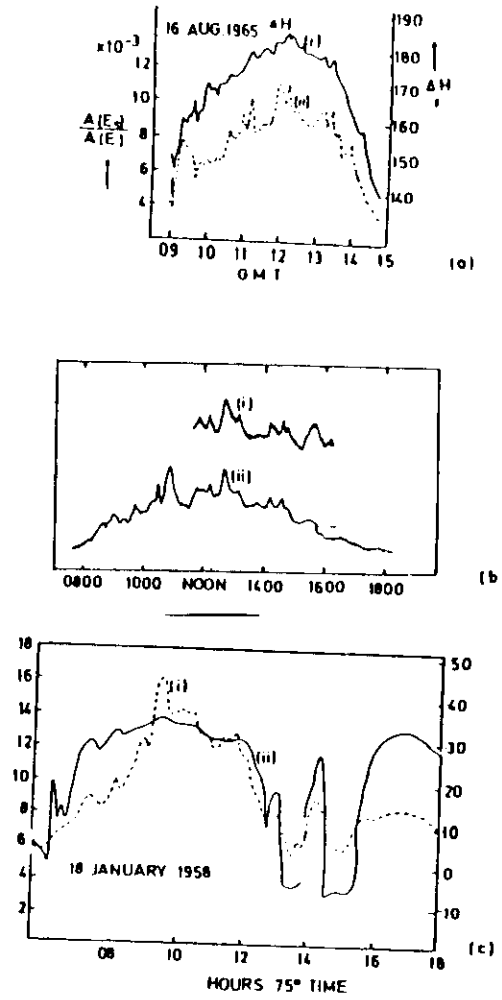

(a) Correlation of (i) HF Es reflection coefficient A(Es)/A(E) at vertical incidence with (ii) the H (arbitrary zero) trace on the magnetogram at Ibadan on 16 August, 1965. (After Lyon and Oyinloye, 1965).

(b) Correlation of (i) vertical incidence 50 MHz echo intensity with (ii) the magnetogram at Huancayo (After Bowles and Cohen, 1962)

(c) Correlation (i) of the 50 MHz forward scatter signal intensity for the Arequipa - Trujillo path with (ii) the Huancayo magnetogram for 18 January, 1958 (After Bowles and Cohen, 1962).

Fig. 23

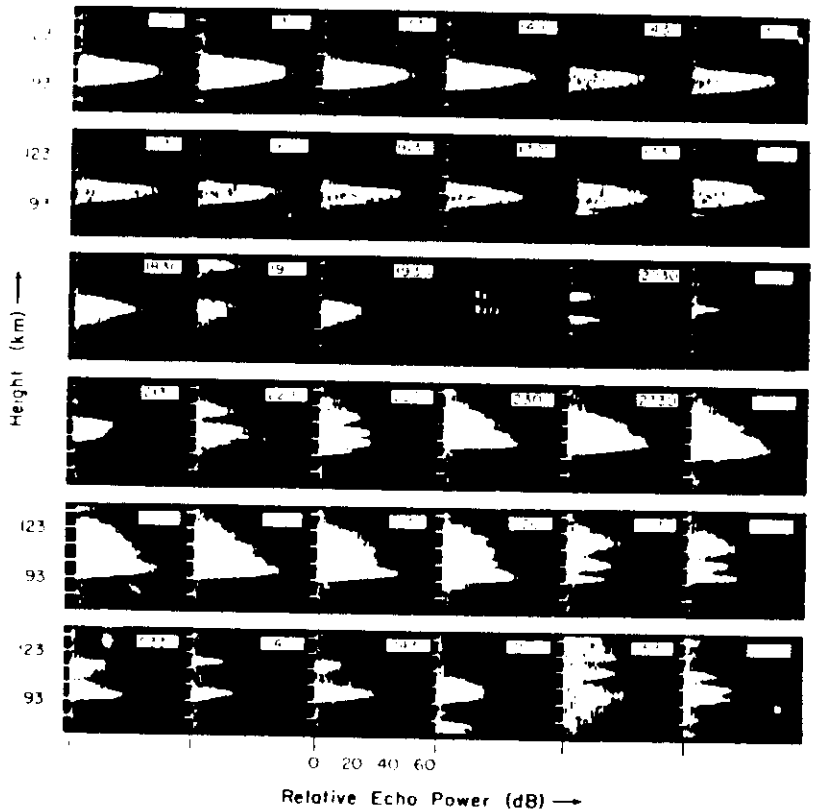

Power backscattered from the electrojet at 50 MHz. The large vertically directed incoherent scatter antenna at Jicamarca was used. Spread *F* contaminated the data between 0405 and 0550 and perhaps at 1900. The times are local times (75°W or EST).

Fig. 24

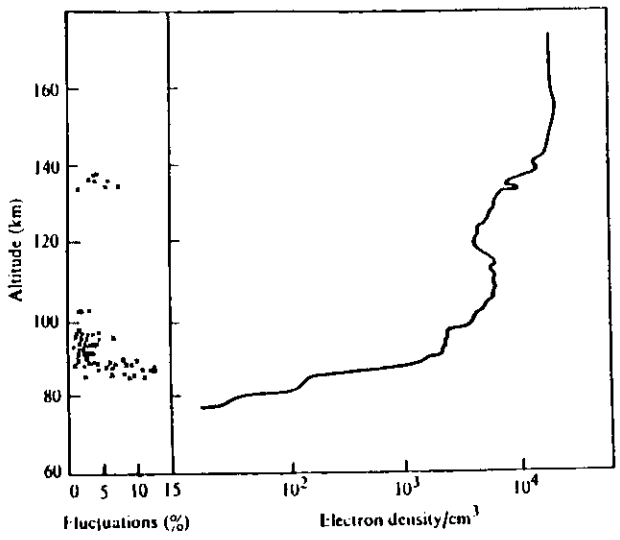

Amplitude of irregularities in scale sizes of 30-300 m observed during the ascent of flight 10.13, along with the electron density profile.

Fig. 25

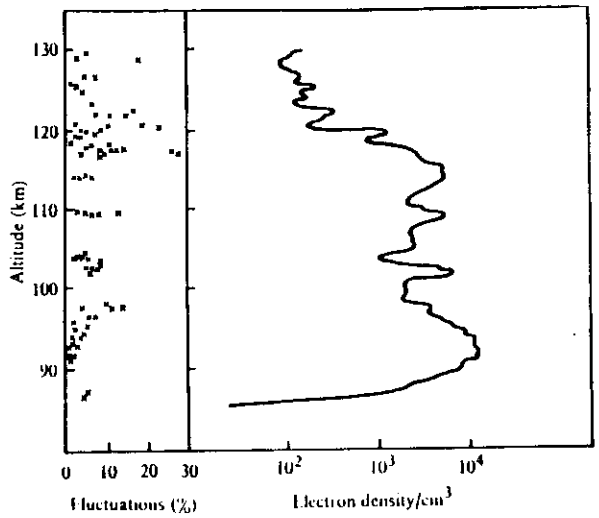

Amplitude of irregularities in scale sizes of 30-300 m during the ascent of flight 20.08, along with the electron density profile.

Fig. 26

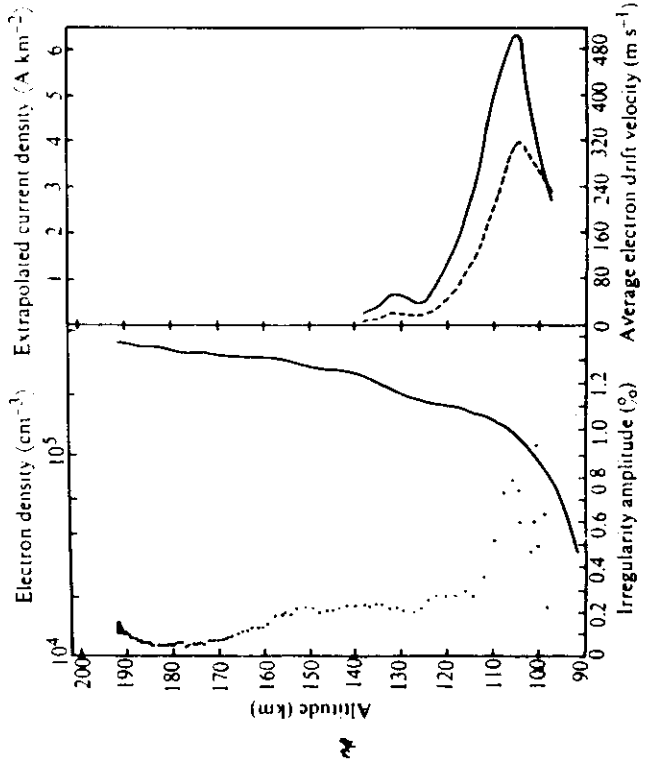

Percentage amplitude of irregularities and electron density for flight 10.38 (——, electron density; . . . , irregularity amplitude). Right side, Extrapolated electrojet current, density (——) and average electron drift velocity (- - -).

Fig. 27

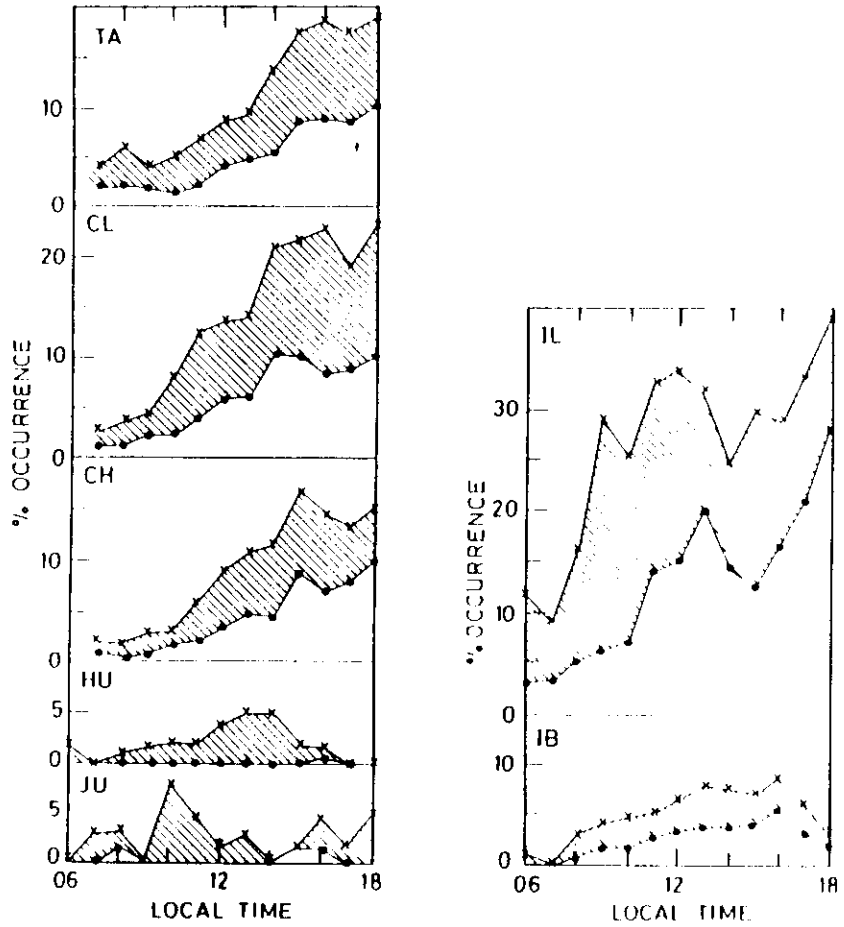

MEAN DAILY VARIATION OF THE OCCURRENCE FREQUENCY OF BLANKETING Es (a) (fbEs - foE) ≧ 0.5MHz (crosses), (b) (fbEs - foE) ≧1.0MHz (dots) AND (c) (fbEs - foE) LYING WITHIN 0.5 AND 0.9MHz (shaded portion)

Fig. 28

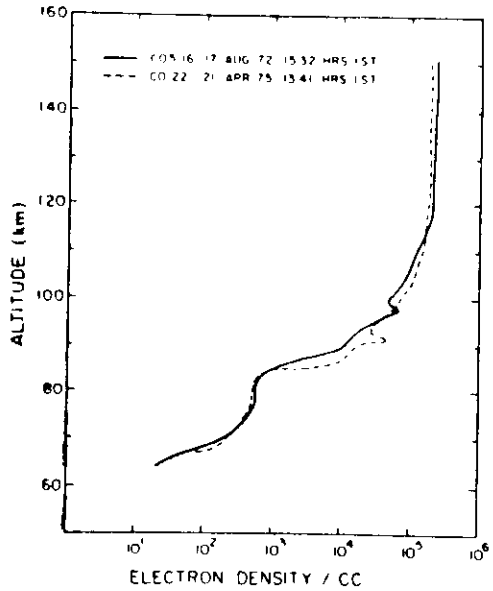

Fig. 29

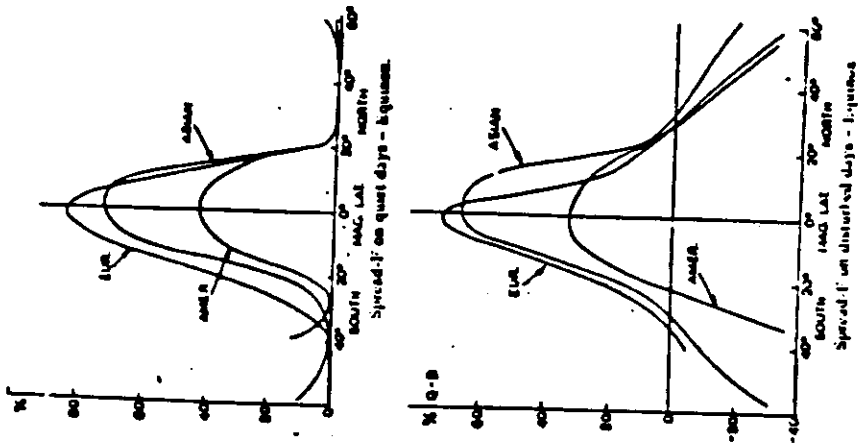

Fig. 32

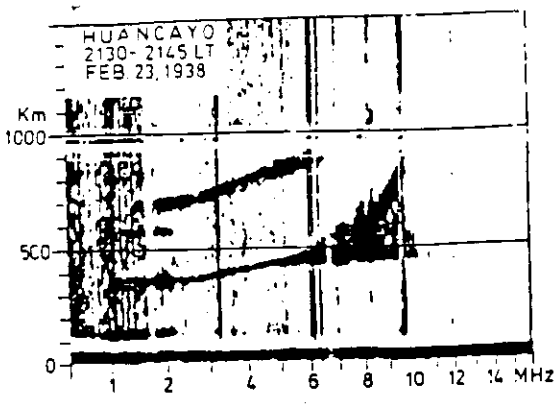

Fig. 30a

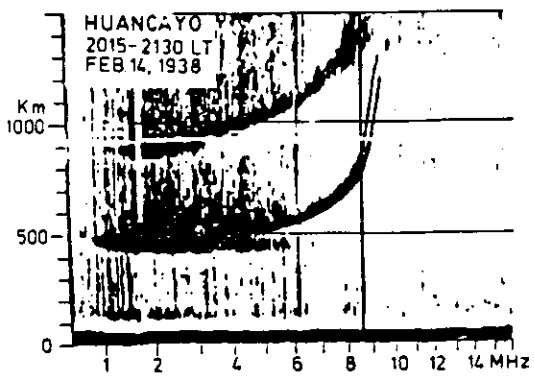

After Booker and Wells (1938)

Fig. 30b

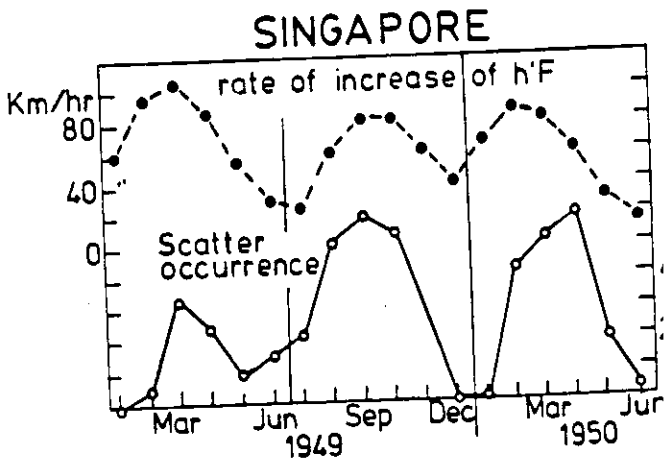

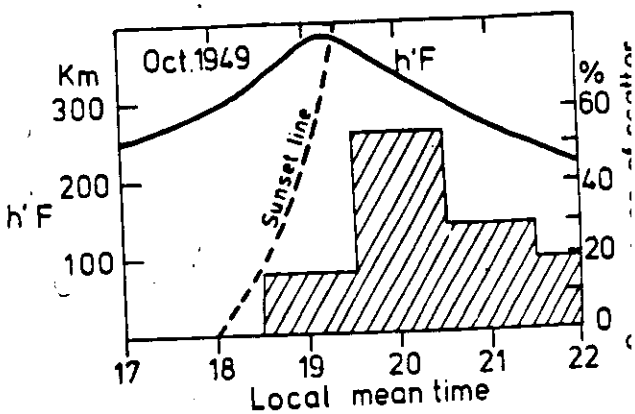

Fig. 31

The Sequence of vertical ionospheric sounding h' f records at Huancayo showing the spread F condition compared with the corresponding range intensity records of backscatter echoes of 50 MHz radar at Jicamarca. Note strong scatter on 50 MHz during range type spread-F (ref. 2200 hr) and the absence of the scatter on 50 MHz during frequency type spread F (ref. 0100 hr).

Fig. 34b

Jicamarca 2107 LT Huancayo 2100 LT
16-APRIL, 1974
INTENSITY →
FREQUENCY (MHz)
ALTITUDE (Km)

Fig. 34a

Fig. 33

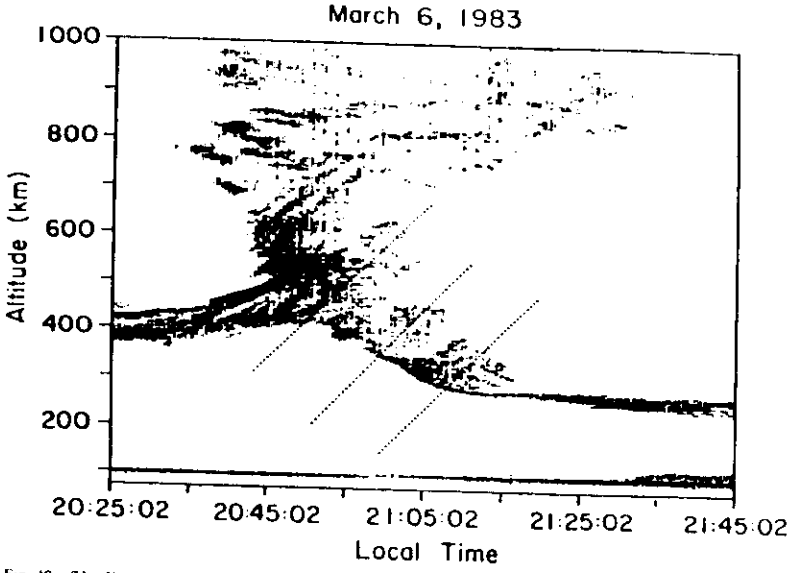

Fig. 10. The Jicamarca backscatter power map from the night of March 6, 1983, showing three prominent plume structures which erupt from the bottomside spread F as the scattering layer decends. Superposed are the relative positions of three similar structures observed using a scanning radar [*Tsunoda*, 1983].

Fig. 35

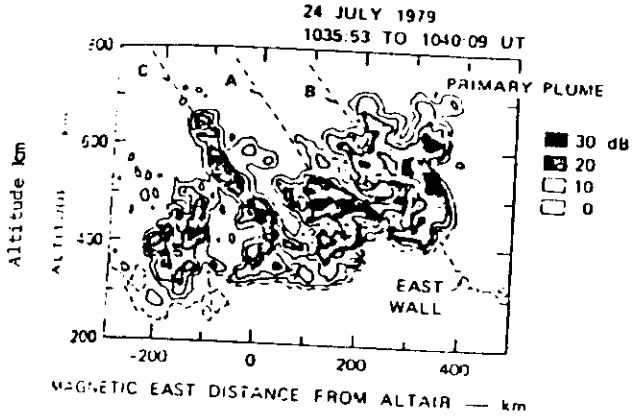

Fig. 36

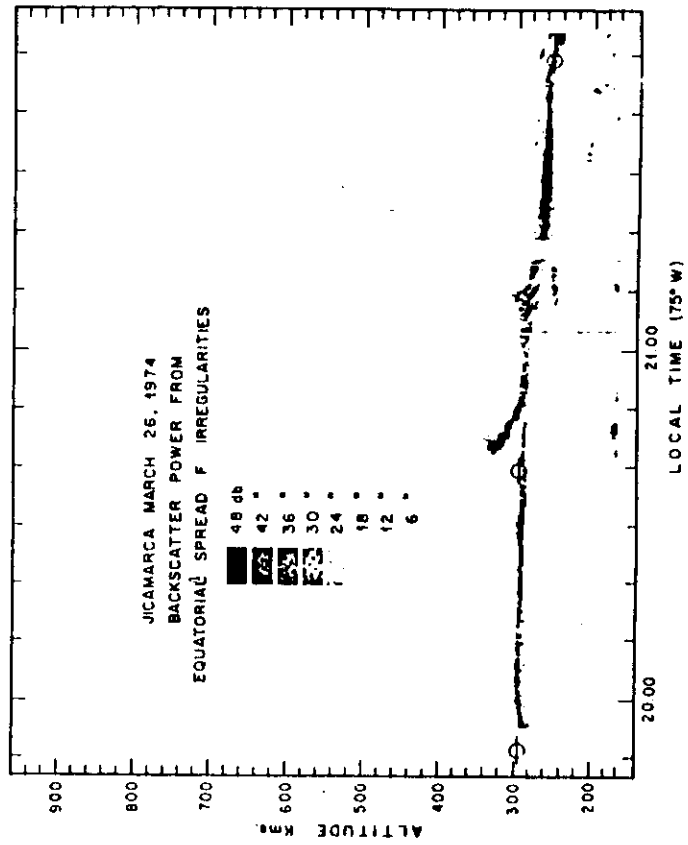

Fig. 37

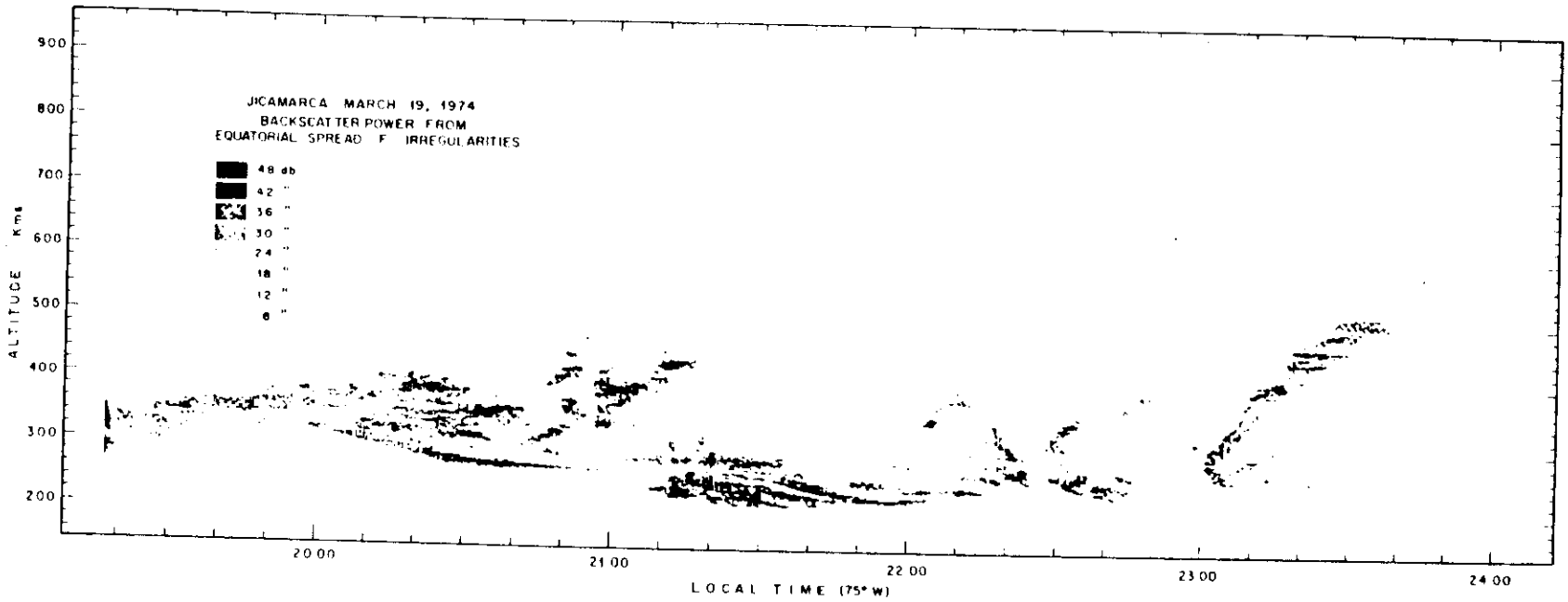
JICAMARCA MARCH 19, 1974
BACKSCATTER POWER FROM
EQUATORIAL SPREAD F IRREGULARITIES
48 db
42 "
36 "
30 "
24 "
18 "
12 "
6 "
ALTITUDE Kms
900
800
700
600
500
400
300
200
20 00
21 00
22 00
23 00
24 00
LOCAL TIME (75° W)

Fig. 38

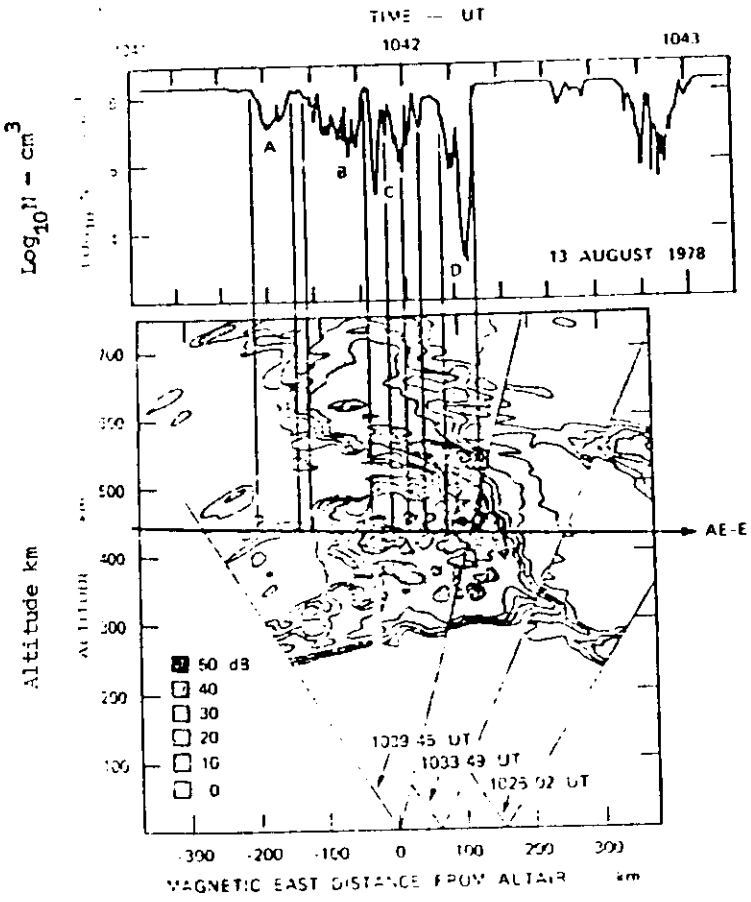

Fig. 39

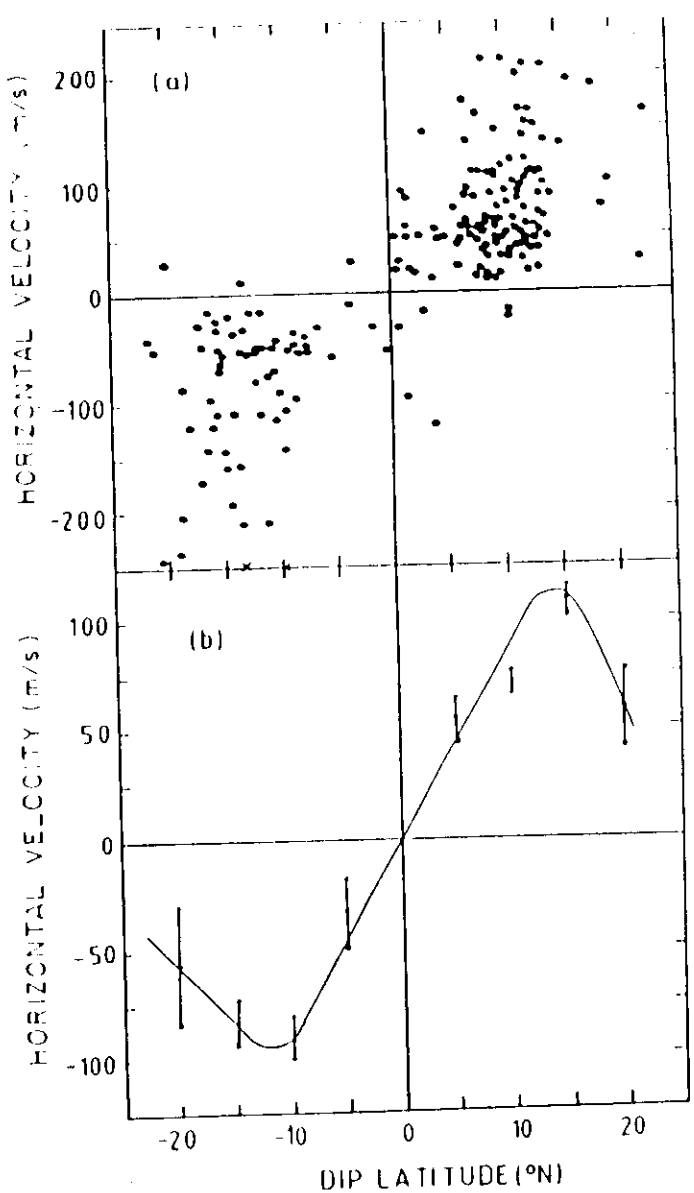

(a) Values of the north-south horizontal velocity at maximum depletion and (b) their mean variation, plotted as functions of dip latitude for bubbles with depletions of two orders of magnitude or less. In Figure b the standard error of each mean point is shown as a vertical bar.

Fig. 40.

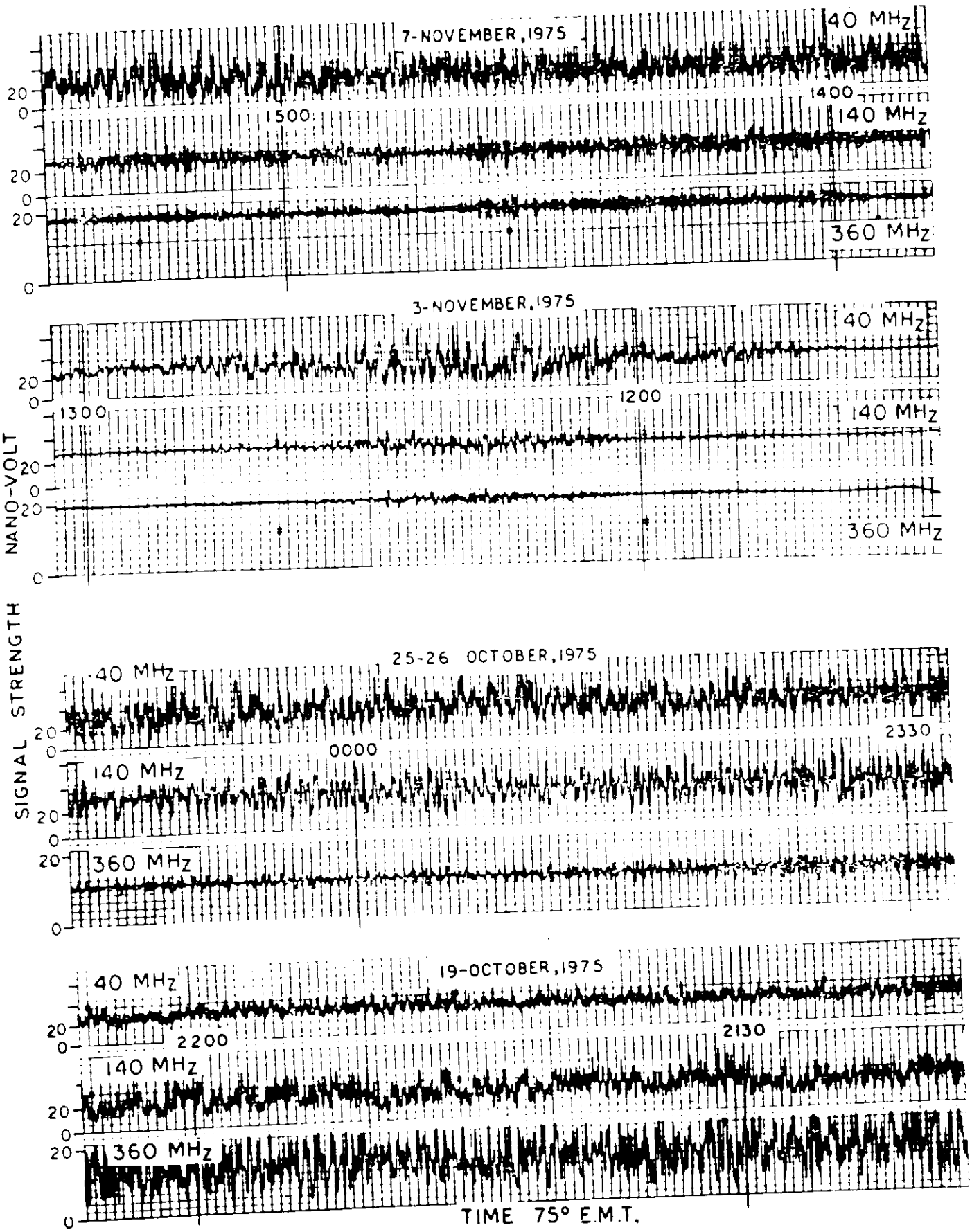

Records of amplitude scintillation of 40, 140 and 360 MHz beacon radio waves from ATS-6 satellite received at Ootacamund for the daytime hours (3 and 7 November 1975) and for the nighttime hours (19 and 25 26 October 1975). The signal strength is expressed as input voltage of the receiving aerials.

Fig. 41a

ANCON, PERU GOES 5 1694 MHz
MARCH 2, 1983

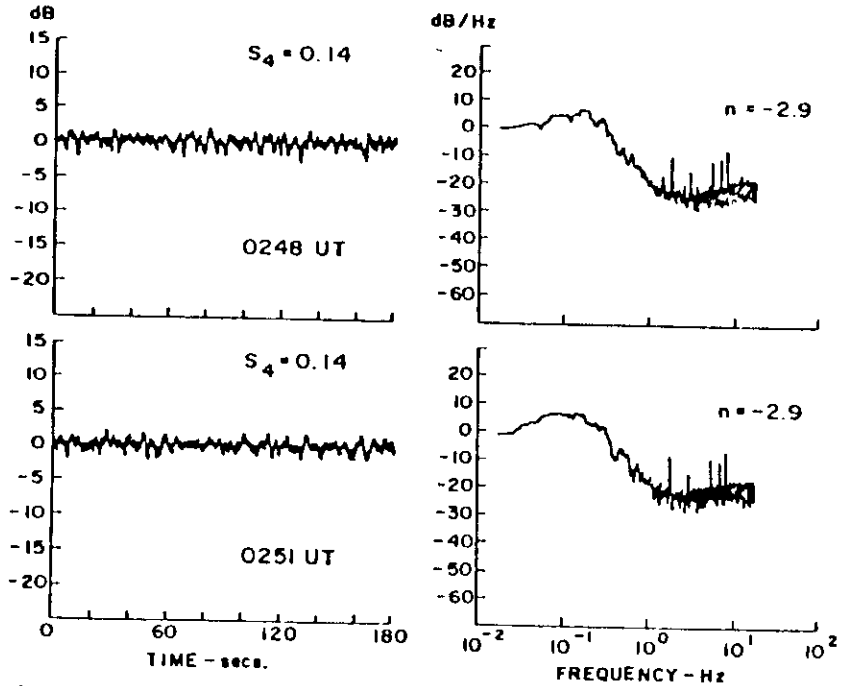

Two 3-min samples of 1694-MHz scintillation recorded at Ancon during the rocket flight on March 2, 1983 (UT date), and their FFT spectra. The spectral index n of the roll-off portions of the spectra between 0.4 and 1 Hz is indicated.

Fig. 41b

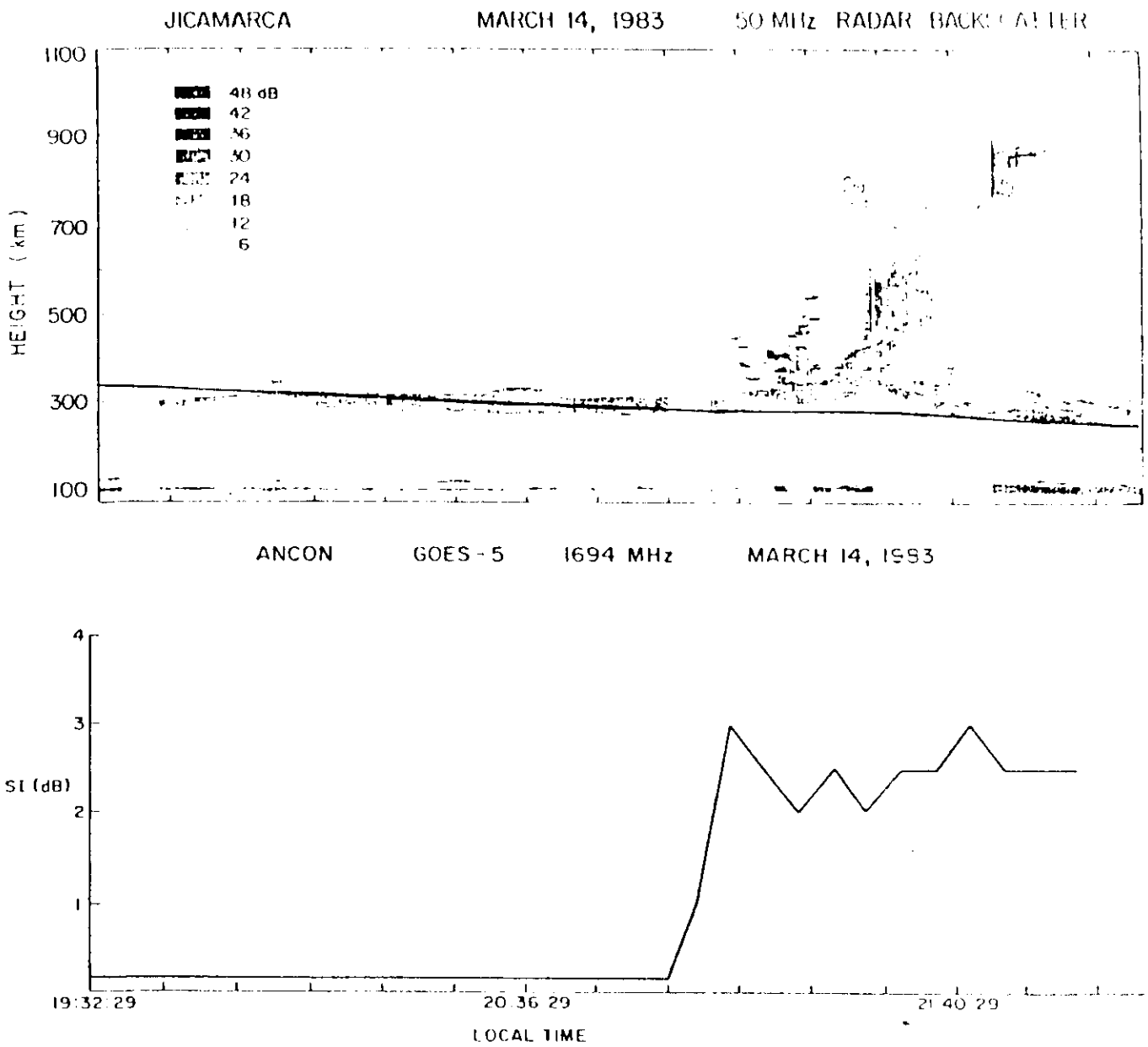

The top panel displays the Jicamarca 50-MHz backscatter power map recorded the night of March 14, 1983. The solid line indicates the altitude h_{min} as measured from the ionosonde at Huancayo. The bottom panel shows the scintillation index at 1694 MHz observed at Ancon during the same time period.

Fig. 42a

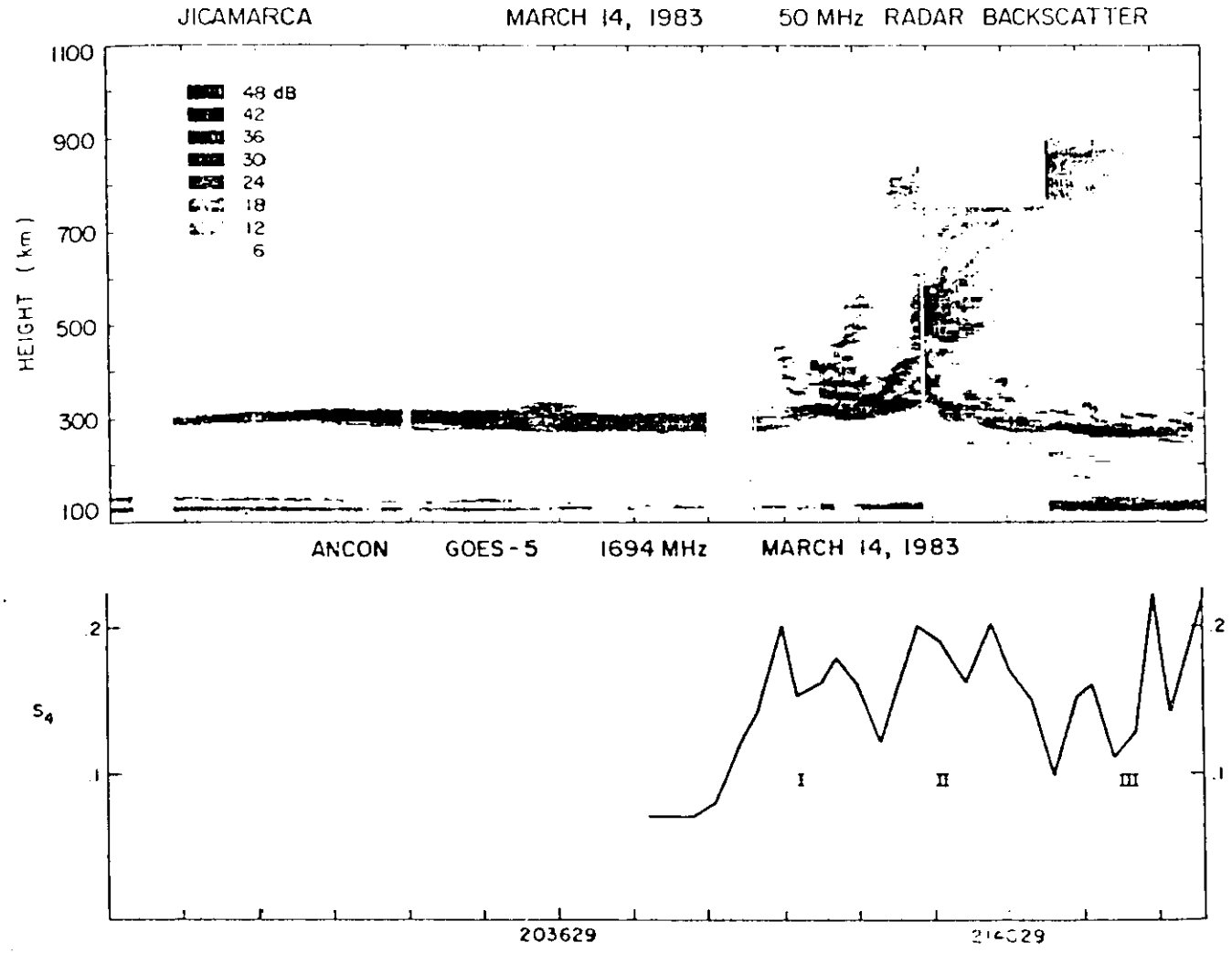
JICAMARCA
MARCH 14, 1983
50 MHz RADAR BACKSCATTER
1100
900
700
500
300
100
HEIGHT (km)
48 dB
42
36
30
24
18
12
6
ANCON
GOES-5
1694 MHz
MARCH 14, 1983
S_4
.2
.1
I
II
III
203629

Fig. 42b

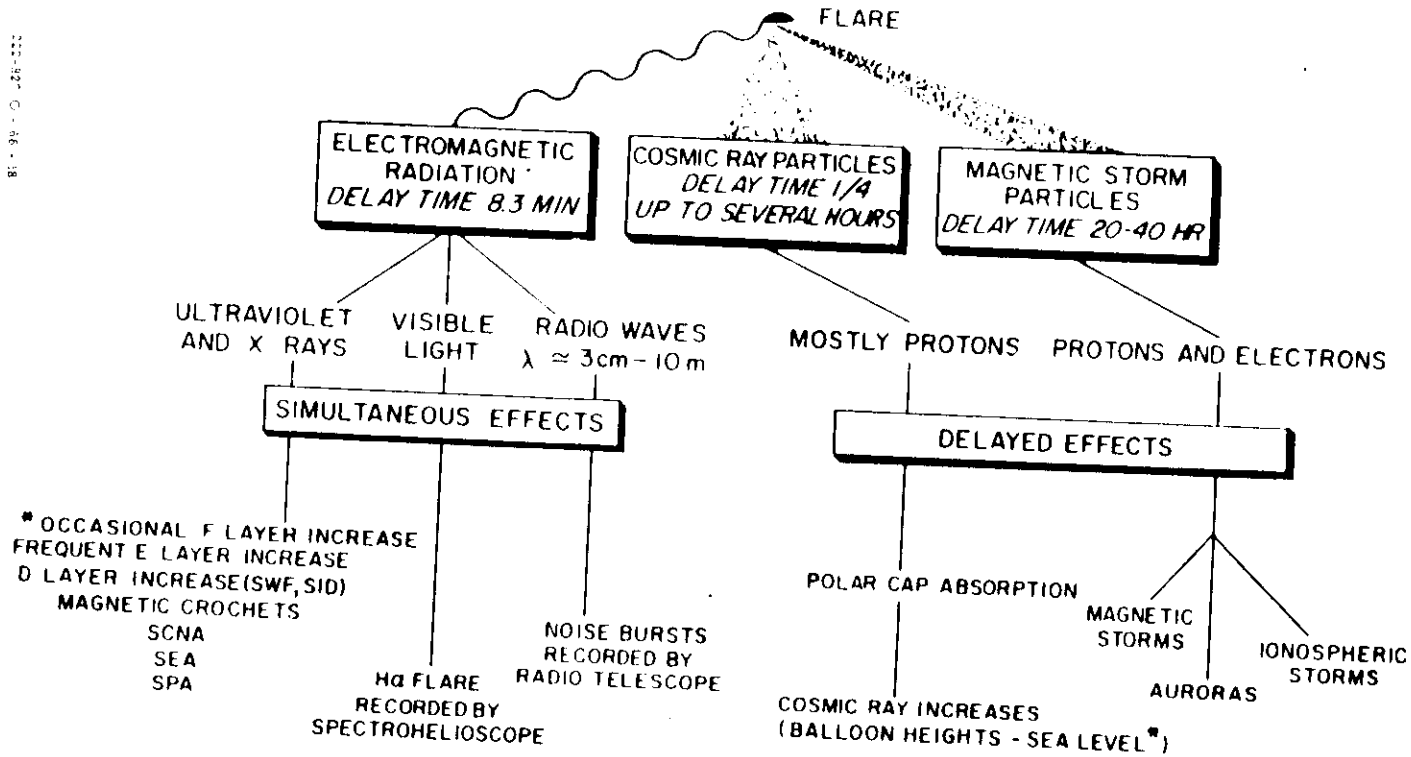

The terrestrial effects of a solar flare

(After R. W. Knecht, unpublished)

Fig. 43

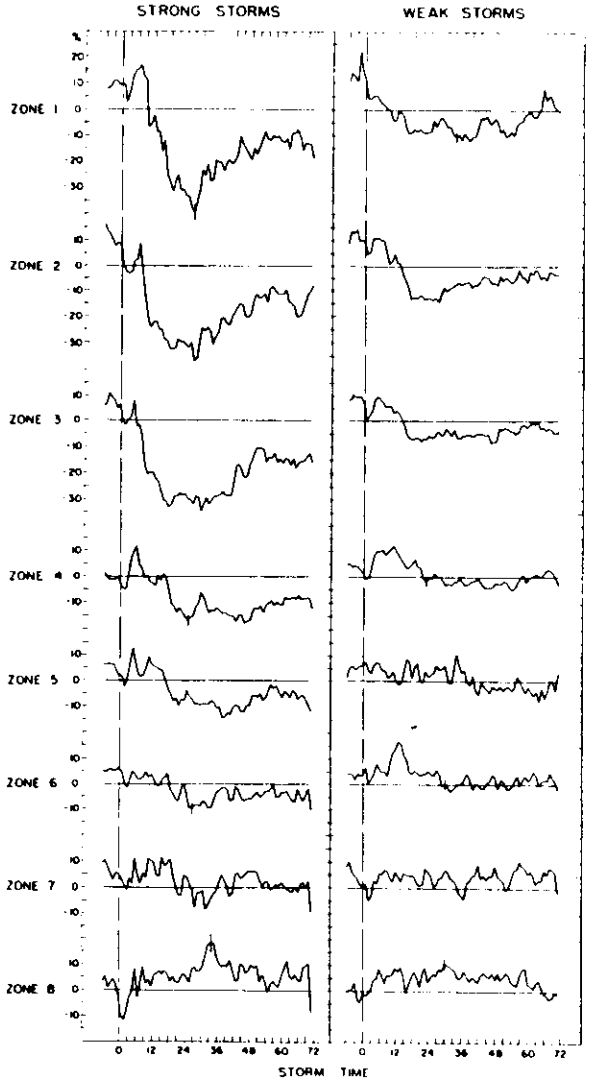
STRONG STORMS
WEAK STORMS
ZONE 1
ZONE 2
ZONE 3
ZONE 4
ZONE 5
ZONE 6
ZONE 7
ZONE 8
0 12 24 36 48 60 72
STORM TIME

Fig. 44

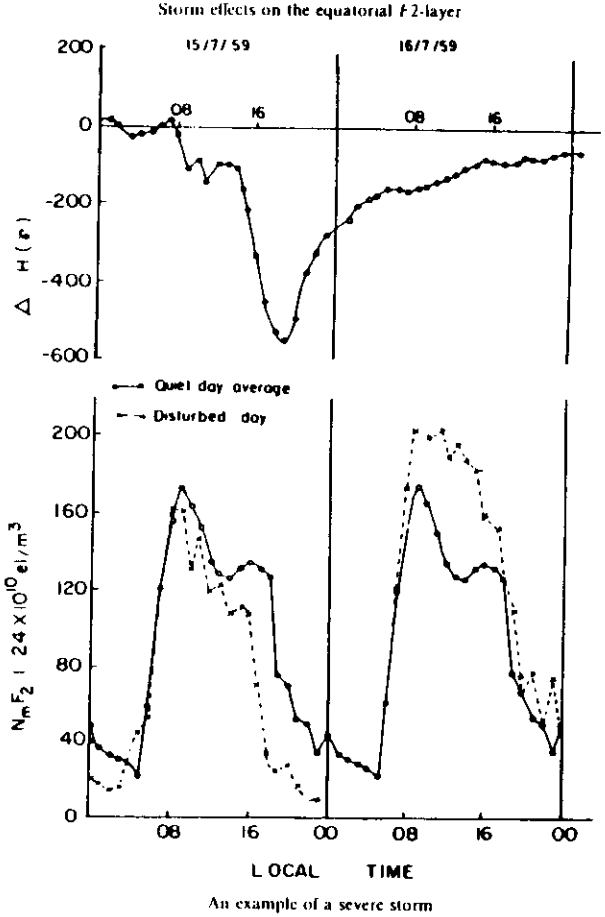
Storm effects on the equatorial F 2-layer
15/7/59
16/7/59
08
16
08
16
200
0
-200
-400
-600
Δ H (γ)
Quet day average
Disturbed day
200
160
120
80
40
0
$N_m F_2$ I 24×10^{10} el/m^3
08
16
00
08
16
00
LOCAL TIME
An example of a severe storm

Fig. 45

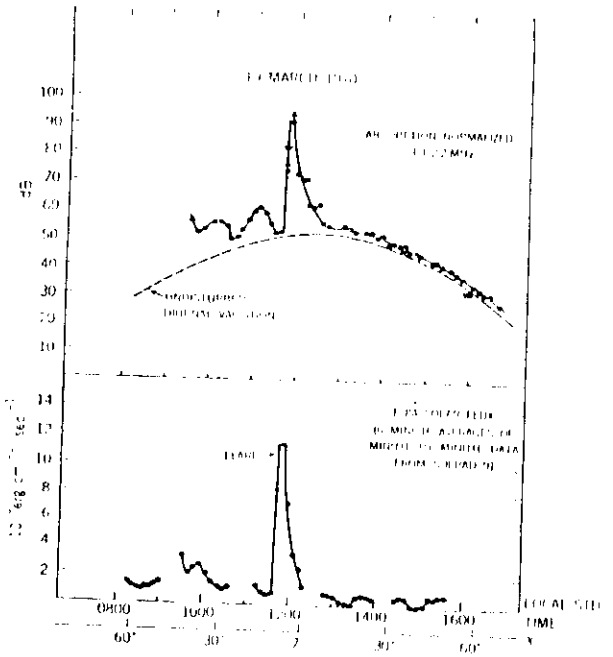

Diurnal variation on a disturbed day illustrating, in addition to the sous flare effect, the close correlation between short-term increases in equatorial orption and moderate enhancements in solar X-ray flux at large solar zenith angles.

Fig. 46a

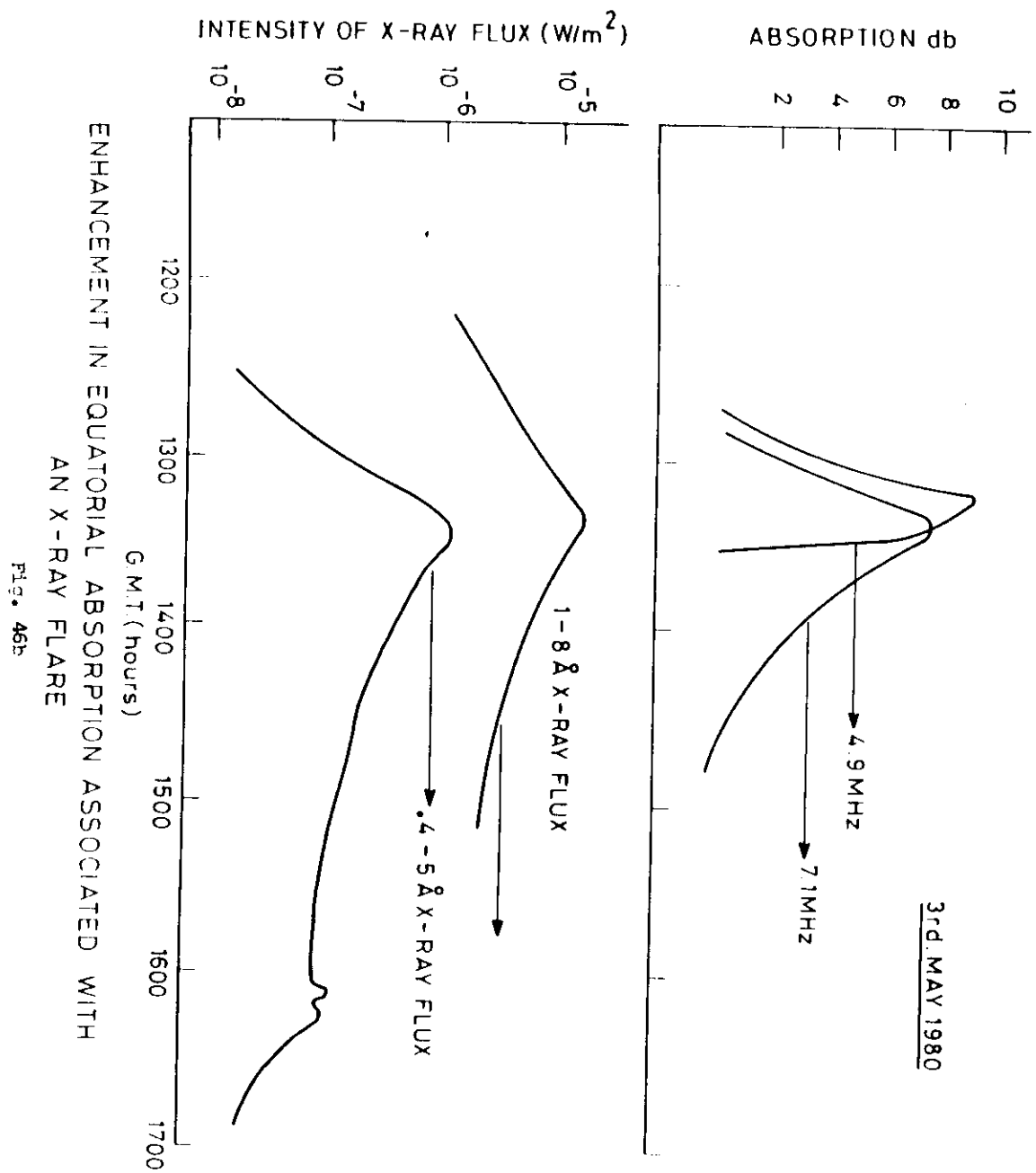

ENHANCEMENT IN EQUATORIAL ABSORPTION ASSOCIATED WITH AN X-RAY FLARE

Fig. 46b

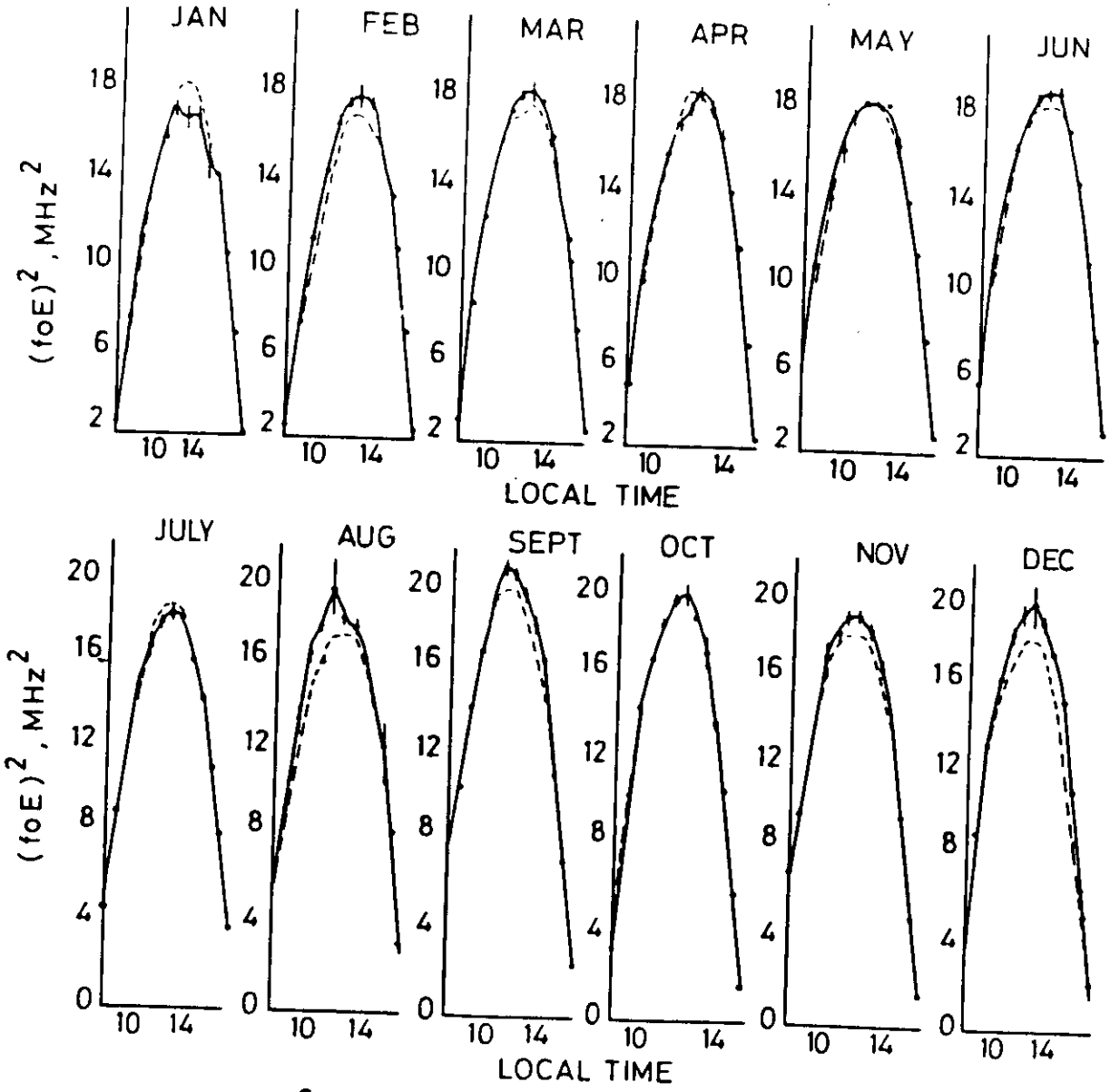

COMPARISON OF $(f_o E)^2$ ON QUIET AND DISTURBED DAYS OF THE MONTHS OF 1957

o—o—o QUIET DAYS

o--o--o DISTURBED DAYS

Fig. 47